



# **PSEUDOSPECTRAL CALCULATIONS OF HELIUM AND THE NEGATIVE HYDROGEN ION**

by Paul Eric Grabowski

---

This thesis/dissertation document has been electronically approved by the following individuals:

Wasserman, Ira M (Chairperson)

Chernoff, David Fisher (Minor Member)

Franck, Carl Peter (Minor Member)

# PSEUDOSPECTRAL CALCULATIONS OF HELIUM AND THE NEGATIVE HYDROGEN ION

A Dissertation

Presented to the Faculty of the Graduate School

of Cornell University

in Partial Fulfillment of the Requirements for the Degree of

Doctor of Philosophy

by

Paul Eric Grabowski

August 2010

© 2010 Paul Eric Grabowski

ALL RIGHTS RESERVED

PSEUDOSPECTRAL CALCULATIONS OF HELIUM AND THE NEGATIVE  
HYDROGEN ION

Paul Eric Grabowski, Ph.D.

Cornell University 2010

Calculations of helium and the negative hydrogen ion are presented using the pseudospectral method. The fundamental analytic properties, including the presence of Kato cusps and logarithmic terms of the solutions to the Schrödinger equation, are explored and their effect on the convergence properties analyzed. We find that by most measures of error the pseudospectral method converges at an exponential rate. With this method, we calculate energies and perturbations due to the finite nuclear mass and relativity and interactions with the electromagnetic field. The value calculated for the absorption oscillator strength of the  $1^1S \rightarrow 2^1P$  transition is about as accurate as the best in the literature. A general prescription is given for choosing subdomains needed for exponential convergence. With this prescription and the overall general applicability of the method, we conclude pseudospectral methods can be applied to general few-electron problems.

## BIOGRAPHICAL SKETCH

Paul Grabowski was born in New York City on April 6, 1981 to Virginia and Eric Grabowski. He joined two older sisters, Amanda and Cara. He traces his love of science back to many exciting conversations with his father, his mother enrolling and taking him to many science related extracurricular activities, and always trying to learn the material his sisters were studying. He moved to Wellesley, MA in 1992, but did not like it there very much. In 1999, he started college at Vassar, majoring in mathematics and physics. Some of his extracurriculars include being a member and eventually the leader of the Barefoot Monkeys, Vassar's juggling and circus arts group, and helping to found and later serving as co-editor-in-chief of the Vassar Daily Brew along with his now wife, Jazz Salwen-Grabowski. He fell deeply in love with Jazz and they married at the Brooklyn Botanical Gardens on July 31, 2005 amidst friends and family, a live swing band, and flourless chocolate cake. During Paul's time in Ithaca, he has very much enjoyed the local culture, which includes a mix of people from around the world, wonderful theatre productions (his favorite being Hair), and rockin' birth activists. The latter became important with the birth of his son, Peter on May 25, 2009. Fatherhood became a very enjoyable and huge responsibility during the last year of his graduate work. In his spare time, Paul loves to go hiking through the Six Mile Creek gorge and finding those magical quiet spots. After finishing his degree, he plans to move to New Mexico, where he will be working as a postdoctorate researcher at Los Alamos National Laboratory.

To Peter, who gave me the best reason to finish this work.

I love him more than words can express.

## ACKNOWLEDGEMENTS

First, I would like to thank my adviser, Professor David Chernoff, for providing me with careful guidance throughout my graduate career and for always being willing to talk for long hours about this research. He has taught me how to be a thorough and exact scientist. I have also had the help and guidance of many other professors here at Cornell, including Ira Wasserman, who helped focus me towards graduation, Cyrus Umrigar, who lent his expertise on this problem and provided good feedback on this work, Saul Teukolsky, who provided his numerical expertise, Carl Franck, who was always willing to give friendly advice and has always made physics look fun, and Veit Elser, whose teaching was an inspiration and willingness to talk about my research very helpful. I also would like to thank Harald Pfeiffer for his help with several technical questions and for his thesis work on the initial data problem in numerical relativity which inspired this work. Sharvari Nadkarni-Ghosh, my fellow graduate student, was always available to commiserate with on the trials of being a graduate student. My more senior officemates, Ali Vanderveld, Tanner Akgun, Andy Lundgren, Zach Medin, and Dave Tsang helped show the way towards graduation. But the person who deserves the most credit is my wife, Jazz Salwen-Grabowski, who gave me endless support and love, and has cared for our son through many nights and days, while I have been at work. Thank you to all of you.

## TABLE OF CONTENTS

Biographical Sketch . . . . .	iii
Dedication . . . . .	iv
Acknowledgements . . . . .	v
Table of Contents . . . . .	vi
List of Tables . . . . .	ix
List of Figures . . . . .	x
<b>1 Introduction</b>	<b>1</b>
<b>2 Background</b>	<b>3</b>
2.1 Theoretical methods for solving the nonrelativistic Schrödinger equation for two-electron atoms . . . . .	3
2.1.1 The variational method . . . . .	4
2.1.2 The finite difference method . . . . .	8
2.1.3 The pseudospectral method . . . . .	9
2.2 Experimental results for two-electron atoms . . . . .	14
2.3 Corrections to the two-electron problem . . . . .	15
2.3.1 Finite nuclear mass correction . . . . .	16
2.3.2 Relativistic corrections . . . . .	17
<b>3 Pseudospectral calculation of the wave function of helium and the negative hydrogen ion</b>	<b>19</b>
3.1 Abstract . . . . .	20
3.2 Introduction . . . . .	21
3.2.1 Variational method for two electrons and nucleus: ground state . . . . .	23
3.2.2 Variational method for excited states . . . . .	25
3.2.3 Fourier spectral expansion . . . . .	26
3.2.4 Specialized methods for two-electron systems . . . . .	26
3.2.5 Direct solution of partial differential equation for bound and continuum states . . . . .	27
3.2.6 Pseudospectral approach . . . . .	28
3.3 Setting up the problem . . . . .	30
3.4 Coordinates and the Hamiltonian . . . . .	33
3.5 The singular points in the Hamiltonian . . . . .	35
3.5.1 Two-particle coalescences . . . . .	36
3.5.2 Three particle coalescence . . . . .	39
3.5.3 Infinite separation . . . . .	41
3.5.4 Collinearity ( $B$ or $C = \pm 1$ ) . . . . .	42
3.6 The pseudospectral method . . . . .	43
3.7 Pseudospectral convergence for nonsmooth functions . . . . .	46
3.7.1 Kato cusps . . . . .	46

3.7.2	Logarithmic terms . . . . .	48
3.7.3	Conclusion . . . . .	53
3.8	Numerical domains and collocation points . . . . .	54
3.9	Boundary conditions . . . . .	57
3.9.1	Internal boundary conditions . . . . .	57
3.9.2	Symmetry and regularity conditions . . . . .	59
3.9.3	Incorporating boundary conditions into the matrix problem . . . . .	61
3.10	Matrix methods . . . . .	62
3.11	Results . . . . .	64
3.11.1	Convergence in energy . . . . .	64
3.11.2	Convergence in local energy . . . . .	70
3.11.3	Cauchy errors . . . . .	75
3.11.4	The logarithmic derivative at the triple coalescence point . . . . .	77
3.12	Conclusion . . . . .	79
<b>4</b>	<b>Pseudospectral calculation of helium wave functions, expectation values, and oscillator strength</b> . . . . .	<b>81</b>
4.1	Abstract . . . . .	82
4.2	Introduction . . . . .	83
4.3	Review of pseudospectral methods . . . . .	85
4.4	The nonrelativistic two-electron atom . . . . .	87
4.5	Review of dipole radiative transitions . . . . .	90
4.6	Methods for calculating oscillator strengths . . . . .	92
4.6.1	Approximate methods . . . . .	93
4.6.2	Perturbation theory . . . . .	94
4.6.3	Variational methods . . . . .	95
4.6.4	Miscellaneous . . . . .	96
4.7	Variables and domains . . . . .	96
4.8	Boundary conditions . . . . .	102
4.8.1	Internal boundary conditions . . . . .	102
4.8.2	The symmetry condition . . . . .	103
4.9	Matrix methods . . . . .	103
4.9.1	Quadrature . . . . .	109
4.10	Energy and oscillator strength results . . . . .	112
4.11	Corrections to the Hamiltonian . . . . .	117
4.11.1	Finite nuclear mass correction . . . . .	118
4.11.2	Relativistic corrections . . . . .	118
4.12	Mass polarization and relativistic correction calculations . . . . .	120
4.13	Expectation values . . . . .	121
4.14	Conclusions . . . . .	125

<b>5 Discussion</b>	<b>128</b>
5.1 Future work . . . . .	128
5.1.1 Continuum states . . . . .	128
5.1.2 Asymptotic forms . . . . .	129
5.2 Conclusion . . . . .	130
<b>A Setting <math>\rho_{\max}</math> for the truncated domain</b>	<b>131</b>
<b>B Fits</b>	<b>134</b>
<b>C Bhatia and Temkin Hamiltonian</b>	<b>141</b>
<b>D Calculating the oscillator strength with Bhatia and Temkin's radial functions</b>	<b>142</b>
<b>Bibliography</b>	<b>143</b>

## LIST OF TABLES

2.1	A comparison of three methods which can be used to solve quantum mechanical problems. . . . .	5
2.2	Contributions to the energy and their orders of magnitude. . . . .	16
3.1	A list of the different cases that are compared in this section. Exc refers to the first excited $S$ state. Grd refers to the ground state. $N_D$ is the number of domains. B, R, and E refer to behavioral, regularity, and excision, respectively. . . . .	65
4.1	The matrix sizes $n_m$ and number of nonzero elements $n_{NZ}$ for each resolution $n$ . . . . .	107
4.2	The fit parameters to all the convergence plots of quantities $Q$ in this section. . . . .	117
4.3	The fit parameters to all the convergence plots of quantities $Q$ in this section. . . . .	127
B.1	The convergence fits of quantities, $Q$ , displayed in figures throughout chapter 3. . . . .	134

## LIST OF FIGURES

3.1	(Color online). The logarithm base 10 of $\delta_{\text{RMS}}^N[g_1]$ (blue circles) and $\delta_{\text{RMS}}^N[g_2]$ (red crosses) with solid blue and dashed red fits, respectively. See Appendix B for fitting functions. . . . .	47
3.2	(Color online). The logarithm base 10 of the error in $f[x]$ using cardinal functions at $\rho = 10^{-6}$ (green pluses), $\rho = 10^{-1}$ (red crosses), and $\rho = 10^4$ (blue circles) with solid blue, dashed red, and dotted green fits, respectively. See Appendix B for fitting functions and method. . . . .	49
3.3	(Color online). The logarithm base 10 of the maximum error of a pseudospectral matrix. The dark blue circles are for $\alpha = 1$ and the light red crosses for $\alpha = 0$ with solid blue and dashed red fits, respectively. See Appendix B for fitting functions and method.	52
3.4	(Color online). The logarithm base 10 of the error of a pseudospectral matrix near the singularity. The dark blue circles are for $\alpha = 1$ and the light red pluses for $\alpha = 0$ with solid blue and dashed red fits, respectively. See Appendix B for fitting functions and method. . . . .	53
3.5	(Color online). This is the arrangement of grid points of the three domains at a constant value of $\rho$ in $\phi$ and $C$ coordinates. Note that the point density becomes larger at the boundary of each subdomain and that no grid points sit on the Coulomb singularities. The blue circles, red crosses, and green pluses belong to domains $D_1$ , $D_2$ , and $D_3$ , respectively. $D_1$ and $D_2$ are rectangular domains, while $D_3$ has the curved boundary in $\phi$ , $C$ coordinates but is rectangular in $\zeta$ , $B$ coordinates. The electron-proton singularity occurs on the left side (solid line at $\phi = 0$ ). The entire line corresponds to one physical point. The electron-electron singularity occurs at the lower right-hand corner (solid disk at $\phi = \pi/4, C = -1$ ). A line of symmetry falls on the right side (dashed line at $\phi = \pi/4$ where $r_1 = r_2$ ). . . . .	55
3.6	The intersection (gray) of domains $D_1$ (white) with black grid points and $D_3$ (black) with white grid points. The boundary points are depicted as black and white crosses and are connected via black and white lines to the grid points that they replace. . .	59
3.7	Barely touching domains $D_1$ (white) with black grid points and $D_2$ (black) with white grid points. The boundary points are depicted as black and white crosses and are connected via gray lines to the grid points that they replace. . . . .	60

3.8	(Color online). The convergence of the energy of $H^-$ , case A (red pluses); two non-interacting electrons in the field of a proton, case B (green stars); the ground state of He, case C (blue crosses); and its first excited S-state, case D (black circles) as a function of grid resolution $n$ , with dotted red, dot-dashed green, dashed blue, and solid black fits, respectively. See Appendix B for fitting functions and method. . . . .	66
3.9	(Color online). The convergence of the energy of, case E, $H^-$ using only one computational domain with the electron-electron interaction on (blue circles); case F, one domain with the interaction off (red crosses); and case A, three domains with the interaction on (green pluses) with dashed blue, dotted red, and solid green fits, respectively. See Appendix B for fitting functions and method. . . . .	67
3.10	(Color online). The convergence of the energy of, case H, $H^-$ doing the calculation on a finite domain (blue circles); and, case A, semi-infinite domain (red pluses) with dashed blue and solid red fits, respectively. See Appendix B for fitting functions and method. . . . .	69
3.11	(Color online). The convergence of the energy of $H^-$ using three different methods of ensuring regularity at the two-particle coalescence points: case A, relying on the regularity of the Chebyshev polynomials (green pluses); case I, using the Kato cusp condition as a regularity condition (red crosses); and case J, excising the singularity (blue circles) with green dotted, solid red, and dashed blue fits, respectively. See Appendix B for fitting functions. . . . .	70
3.12	(Color online). The convergence of the energy of $H^-$ using two different methods of ensuring regularity at the three-particle coalescence point: case A, relying on the regularity of the Chebyshev polynomials (blue circles); and case G, using the Fock condition to specify a logarithmic derivative (red pluses) with dashed blue and solid red fits, respectively. See Appendix B for fitting functions and method. . . . .	71
3.13	(Color online). The convergence of the local energy of $H^-$ at a four points in the domain: the center of the computational domain (black circles), near the triple coalescence point (blue crosses), near the proton-electron coalescence point (red pluses), and at large $\rho$ (green stars). Their geometric fits are given by the solid black, dashed blue, dotted red, and dot-dashed green lines, respectively. See Appendix B for fitting functions and method. . . . .	72

3.14	(Color online). The error in the local energy of $H^-$ as a function of $x$ with $r_1 = 2r_2$ , and $C = -1$ (the electrons are on the same side of the nucleus) at four different resolutions: $n = 5$ green dot-dashed, $n = 8$ red dotted, $n = 11$ blue dashed, $n = 14$ black solid. . . . .	73
3.15	(Color online). The error in local energy of $H^-$ plotted at different values of the angle $\theta_{12}$ with $r_1 = 2r_2$ and at resolution $n = 14$ and at $\rho = 1$ (solid black), $\rho = 0.1$ (dashed blue), $\rho = 0.01$ (dotted red), $\rho = 0.001$ (solid green), and $\rho = 0.0001$ (dot-dashed purple). . . . .	75
3.16	(Color online). The root-mean-square average Cauchy error is plotted with increasing resolution for three cases: $H^-$ with noninteracting electrons (blue circles); $H^-$ with interacting electrons (red crosses); and helium with interacting electrons (green pluses) with dashed blue, solid red, and dotted green fits, respectively. See Appendix B for fitting functions and method. . . . .	76
3.17	(Color online). Pointwise differences in the wave function evaluated at $\rho = 0$ for increasing resolution for three cases: $H^-$ with noninteracting electrons (blue circles); $H^-$ with interacting electrons (red crosses); and helium with interacting electrons (green pluses) with dashed blue, solid red, and dotted green fits, respectively. See Appendix B for fitting functions and method. . . . .	77
3.18	(Color online). The root-mean-square error in the logarithmic derivative evaluated at $\rho = 0$ with increasing resolution for three cases: $H^-$ with noninteracting electrons (blue circles); $H^-$ with interacting electrons (red crosses); and helium with interacting electrons (green pluses) with dashed blue, solid red, and dotted green fits, respectively. See Appendix B for fitting functions and method. . . . .	78
4.1	(Color online). This is the arrangement of grid points of the three domains at a constant value of $\rho$ in $\phi$ and $\theta_{12}$ coordinates for $n = 20$ . Note that the point density becomes larger at the boundary of each subdomain and that no grid points sit on the Coulomb singularities. The blue circles, red crosses, and green pluses belong to domains $D_1$ , $D_2$ , and $D_3$ , respectively. $D_1$ and $D_2$ are rectangular domains, while $D_3$ has the curved boundary in $\phi$ , $\theta_{12}$ coordinates but is rectangular in $\zeta$ , $\beta_{12}$ coordinates. The electron-proton singularity occurs on the left side (solid line at $\phi = 0$ ). The entire line corresponds to one physical point. The electron-electron singularity occurs at the lower right hand corner (solid disk at $\phi = \pi/4$ , $\theta_{12} = 0$ ). A line of symmetry falls on the right side (dashed line at $\phi = \pi/4$ where $r_1 = r_2$ ). . . . .	101
4.2	(Color online). A log-log plot of the approximate condition number $c$ of the pseudospectral matrices as a function of resolution. . . . .	108

4.3	(Color online). This is the arrangement of grid points of the three domains at a constant value of $\rho$ in $\phi$ and $\theta_{12}$ coordinates for $n = 10$ . As in Fig. 4.1, the blue circles, red crosses, and green pluses belong to domains $D_1$ , $D_2$ , and $D_3$ , respectively. Also shown are the overlap grid points in $D_1 \cap D_3$ (purple stars) and $D_2 \cap D_3$ (brown squares). The electron-electron singularity is visible at the lower right hand corner (solid disk at $\phi = \pi/4, \theta_{12} = 0$ ) as well as the line of symmetry on the right side (dashed line at $\phi = \pi/4$ where $r_1 = r_2$ ). . . . .	111
4.4	(Color online). The logarithm base 10 of the energy error of both the lowest energy S state and P state of helium. The dark blue circles are for the $1^1S$ state and the light red crosses for the $2^1P$ state with dashed blue and dotted red fits, respectively (see Tab. 4.2). . . . .	113
4.5	(Color online). The logarithm base 10 of the error in the oscillator strength of the $1^1S \rightarrow 2^1P$ transition of helium. The dark blue circles are for the length form, the light red crosses are for the velocity form, and the green pluses for the acceleration form with dashed blue, dotted red, and dot-dashed green fits, respectively (see Tab. 4.2). . . . .	114
4.6	(Color online). The logarithm base 10 of the error in the average of the length, velocity, and acceleration forms of the oscillator strength (dark blue circles) and their standard deviation (light red crosses) for the $1^1S \rightarrow 2^1P$ transition of helium, with dashed blue and dotted red fits, respectively (see Tab. 4.2). . . . .	116
4.7	(Color online). The logarithm base 10 of the error in the expectation values of operators that scale as $\rho^2$ for helium. The dark blue circles are for $\langle r_1^2 \rangle$ , the light red crosses are for $\langle r_{12}^2 \rangle$ , and the green pluses are for $\langle r_1 r_2 \cos \theta_{12} \rangle$ with dashed blue, dotted red, and dot-dashed green fits, respectively (see Tab. 4.3). . . . .	121
4.8	(Color online). The logarithm base 10 of the error in the expectation values of operators that scale as $\rho$ for helium. The dark blue circles are for $\langle r_1 \rangle$ and the light red crosses are for $\langle r_{12} \rangle$ with dashed blue and dotted red fits, respectively (see Tab. 4.3). . . . .	122
4.9	(Color online). The logarithm base 10 of the error in the expectation values of operators that scale as $1/\rho$ for helium. The dark blue circles are for $\langle 1/r_1 \rangle$ and the light red crosses are for $\langle 1/r_{12} \rangle$ with dashed blue and dotted red fits, respectively (see Tab. 4.3). . . . .	123
4.10	(Color online). The logarithm base 10 of the error in the expectation values of operators that scale as $1/\rho^2$ for helium. The dark blue circles are for $\langle 1/r_1^2 \rangle$ , the light red crosses are for $\langle 1/r_{12}^2 \rangle$ , the green pluses are for $\langle 1/r_1 r_2 \rangle$ , and the black stars are for $\langle 1/r_1 r_{12} \rangle$ with dashed blue, dotted red, dot-dashed green, and solid black fits, respectively (see Tab. 4.3). . . . .	124

4.11	(Color online). The logarithm base 10 of the error in the expectation values of delta function operators for helium. The dark blue circles are for $\langle \delta(r_1) \rangle$ and the light red crosses are for $\langle \delta(r_{12}) \rangle$ with dashed blue and dotted red fits, respectively (see Tab. 4.3). . . . .	125
4.12	(Color online). The logarithm base 10 of the error in the expectation values of the mass polarization and the orbit-orbit interaction operators for helium. The dark blue circles are for $\langle \mathbf{p}_1 \cdot \mathbf{p}_2 \rangle$ and the light red crosses are for $\langle \hat{H}_{OO} \rangle / \alpha^2$ with dashed blue and dotted red fits, respectively (see Tab. 4.3). . . . .	126
A.1	Energy error from truncation as a function of $\rho_{\max}$ with a fit to the points from $\rho_{\max} = 15$ to $\rho_{\max} = 25$ . . . . .	132
A.2	Energy error from finite resolution as a function of resolution at $\rho_{\max} = 20$ with a fit. . . . .	133

# CHAPTER 1

## INTRODUCTION

This work explores fundamental quantum mechanics. The helium atom and its isoelectronic counterparts are the most simple nontrivial Coulomb problems in quantum mechanics. They involve strong electron-electron correlations, nontrivial symmetry considerations, and single as well as double continua. Many different solution techniques have been developed and applied over the past 80 years. A thorough understanding of this simple system is important not only because of its direct relevance to experimental studies in atomic physics but also because the best methods of solution may suggest generalizations applicable to multielectron and/or multiatom systems.

Applying pseudospectral methods to this problem provides a test of the known analytic structure of the wave function, and provides an alternative high precision method to the standard variational method. It is free of explicit assumptions of the form of the solution and can give local values of the wave function and its derivatives to exponential accuracy. In chapter 3, a detailed analysis of the analytic structure and numerical errors is given. The necessity of using multiple subdomains is shown and the rate of convergence is given. This work is published in Physical Review A [73].

Many problems can be solved once one has a method for getting numerically exact wave functions. Accurately treating transitions between states due to radiation effects provides a good test of the method. This requires solving for more than one angular momentum state and constructing an accurate method of calculating matrix elements and dipole operators. These problems are solved in the first half of chapter 4.

Small effects are often treated perturbatively, including the mass polarization term (see Secs. 3.3 and 4.11.1 and relativistic corrections (see Sec. 4.11.2). In the second half of chapter 4, the leading order corrections are calculated and the convergence of their errors with respect to Drake's high precision values [45] is discussed.

Pseudospectral methods can be applied to large classes of fundamental physics problems, even if one is restricted to few-electron problems. The asymptotic form of the helium atom in the breakup limit is still an active area of research [123]. The form near the triple coalescence point is only known analytically to second order [1, 71, 72, 106]. Applying a direct numerical approach can provide verification and guidance to analytic techniques as well as in itself be a complete solution. One can also envision solving systems of two- or three-electrons which have extra terms that cannot be treated perturbatively, for example, very large magnetic fields or models of solid density matter. One can even imagine directly solving the Dirac equation, implicitly incorporating all relativistic effects up to QED corrections. Such a calculation would greatly help attempts to refine estimates of the fine structure constant.

CHAPTER 2  
BACKGROUND

## 2.1 Theoretical methods for solving the nonrelativistic Schrödinger equation for two-electron atoms

Using the infinite nuclear mass approximation, the Schrödinger equation for a two-electron atom in atomic units is

$$\left( -\frac{1}{2}(\nabla_1^2 + \nabla_2^2) - \frac{Z}{r_1} - \frac{Z}{r_2} + \frac{1}{r_{12}} - E \right) \psi = 0, \quad (2.1)$$

where  $\nabla_i^2$  is the laplacian with respect to the  $i$ th electron's coordinates,  $Z$  is the nuclear charge,  $r_i$  is the distance between the  $i$ th electron and the nucleus, and  $r_{12}$  is the electron-electron distance.

This equation has a three-three splitting (see Sec. 4.4) between the interparticle coordinates  $\{r_1, r_2, r_{12}\}$  and the coordinates giving the orientation of the particles. One important feature of this equation is the presence of physical singularities at  $r_1 = 0$ ,  $r_2 = 0$ , and  $r_{12} = 0$ . These singularities prevent complete smoothness of the wave function, a significant problem to overcome for pseudospectral methods. This problem and its solution are discussed in Secs. 3.5, 3.7, and 4.7. The solution entails carefully choosing coordinates analagous to spherical coordinates seen in Sec. 2.1.3.

There are three methods for solving this eigenvalue problem, which we will compare throughout this thesis: the variational, finite difference, and pseudospectral method. These comparisons yield insights to which method may be best for other problems. For a general problem, a variational method typically

takes the form of a spectral (linear basis) expansion

$$\psi[\mathbf{x}] = \sum_{i=1}^N c_i F^i[\mathbf{x}], \quad (2.2)$$

where  $c_i$  is an expansion coefficient and  $F^i$  is a basis function,  $\psi[\mathbf{x}]$  is the wave function,  $\mathbf{x}$  is a set of independent variables, and the summation is truncated at a finite basis size  $N$ . One changes the problem of solving for  $\psi$  to solving for the  $c_i$ 's. If the analytic properties of the basis can reproduce the analytic properties of the wave function, this method is capable of converging at an exponential rate. Finite difference methods are very different. Instead of expanding the wave function in a finite basis, the wave function is solved at a finite number of grid points. That is

$$\psi[\mathbf{x}] \rightarrow \{\psi[\mathbf{x}^1], \psi[\mathbf{x}^2], \dots, \psi[\mathbf{x}^N]\}, \quad (2.3)$$

where  $\mathbf{x}^i$  is a grid point and  $N$  is now the number of grid points. Discretizing space in this way forces one to make approximations to evaluations of derivatives by fitting polynomials of some fixed order  $m$  locally at each point on the grid. This approximation limits the method to algebraic convergence (the errors scale as  $1/N^m$ ). The pseudospectral method is a combination of the two above, it combines the exponential accuracy of a variational method (if the solution is smooth) with the grid-based technique of finite differencing. These properties are summarized in Tab. 2.1.

### 2.1.1 The variational method

In the variational method the functional

$$E_{var} = \frac{\langle \psi | \hat{H} | \psi \rangle}{\langle \psi | \psi \rangle}, \quad (2.4)$$

Table 2.1: A comparison of three methods which can be used to solve quantum mechanical problems.

Method	Type	Ideal Convergence
Variational	Spectral	Exponential
Finite Difference	Grid	Algebraic
Pseudospectral	Grid	Exponential

where  $\hat{H}$  is the Hamiltonian operator, and  $\psi$  is a trial wave function, is minimized with respect to free parameters used to describe  $\psi$ . This method gives an upper bound to the energy. This bound can approach the exact energy exponentially fast if the trial wave function is expressed as an ordered complete basis capable of representing the analytic behavior of the exact wave function. Variational methods have had enormous success solving the helium problem and many others. Many different types of bases have been used. Hylleraas [87] first recognized that S state wave functions of two-electron atoms could be written in terms of three coordinates describing the distances between particles,  $r_1$ ,  $r_2$ , and  $r_{12}$ . Since then many types of functions of these coordinates have been used to produce basis sets. Hylleraas' [87] original coordinates were

$$s = r_1 + r_2 \tag{2.5}$$

$$t = r_1 - r_2 \tag{2.6}$$

$$u = r_{12}. \tag{2.7}$$

He formed a basis with functions

$$F_A^{lmn} = s^l t^n u^m e^{-ks/2}, \tag{2.8}$$

where  $k$  is a nonlinear variational parameter. Bartlett, Gibbons, and Dunn proved that this expansion fails about the point  $r_1 = r_2 = r_{12} = 0$  [15]. This result stimulated attempts to find better bases that could represent the exact wave function. Kinoshita [94] expanded this basis by including negative powers of  $s$

$$F_B^{lmn} = s^l \left(\frac{t}{s}\right)^m \left(\frac{u}{s}\right)^n e^{-ks/2}. \quad (2.9)$$

This form had already been shown by Bartlett [14] to fail at  $s = 0$  as well, but better convergence was found. Interestingly, including half powers of  $s$ ,

$$F_C^{lmn} = s^{l+1/2} t^m u^n e^{-ks/2}, \quad (2.10)$$

which are unmotivated by any analytic calculation, improved the convergence rate more. Analytic work by Bartlett [14] and Fock [59, 60] suggested the inclusion of logarithmic terms. Frankowski and Pekeris [64] constructed a basis with functions of the form

$$F_D^{lmn} = s^l (\ln s) t^m u^n e^{-ks/2} \quad (2.11)$$

in addition to functions of the form  $F_A^{lmn}$ . This produced even better convergence, but, curiously, higher powers of the logarithm which are in Fock's expansion [59, 60] do not make further improvements [139].

Schwartz [139] tested combinations of these schemes. That is, he included functions of the form

$$F_E^{lmn} = s^{l+1/2} \left(\frac{t}{s}\right)^m \left(\frac{u}{s}\right)^n e^{-ks/2} \quad (2.12)$$

and

$$F_F^{lmn} = s^l \ln s \left(\frac{t}{s}\right)^m \left(\frac{u}{s}\right)^n e^{-ks/2}. \quad (2.13)$$

He also tried Korobov's basis [100]

$$F_K^{lmn} = e^{-\alpha_l r_1 - \beta_m r_2 - \gamma_n r_{12}}, \quad (2.14)$$

with  $\alpha_l$ ,  $\beta_m$ , and  $\gamma_n$  chosen quasirandomly within specified intervals. This basis has no analytic motivation but is extremely simple for performing calculations.

Schwartz created six different bases of these types:

$$\begin{aligned}
 A &: \{F_A^{lmn}\} \\
 B &: \{F_B^{lmn}\} \\
 C &: \{F_A^{lmn}, F_C^{lmn}\} \\
 D &: \{F_A^{lmn}, F_D^{lmn}\} \\
 K &: \{F_K^{lmn}\} \\
 E &: \{F_B^{lmn}, F_E^{lmn}\} \\
 F &: \{F_B^{lmn}, F_F^{lmn}\}
 \end{aligned} \tag{2.15}$$

These bases are listed in order of slowest convergence to fastest convergence with respect to basis size [139]. All except basis  $F$ , which appears exponential, have algebraic convergence. Having a better convergence rate for the helium problem is not needed in a practical sense (45 decimal places in the ground state energy of the infinite-nuclear mass, nonrelativistic problem are known [135], well beyond the precision of the known corrections to this number), but these tests provide some insight into the fundamental nature of the exact nonrelativistic wave function and may lead to better bases for other problems. However, the property of being able to represent the wave function by all the inter-particle distances, without those distances forming an overcomplete set, is unique to one- and two-electron atoms. Processes that ruin the overall spherical symmetry may also significantly change what is a good basis. Applying these methods to nonstandard problems may yield much worse results. Furthermore, although convergence of the wave function is guaranteed in a mean sense, local (point-wise) convergence of the wave function is not.

These bases took decades to develop for this simplest of nontrivial problems. It is inefficient to hunt for the best basis for each new problem. There is a need to have a general high precision method.

### 2.1.2 The finite difference method

The finite difference method requires an approximation for derivatives. This approximation gets better with increasing order of the scheme. However, too high an order may lead to instabilities (*i.e.* the Runge phenomenon [62]). On a grid  $\mathbf{x} = \{x^1, x^2, \dots, x^N\}$ , a first order representation of the first derivative of a one-dimensional function  $\psi$  at  $x^i$  ( $2 \leq i \leq N$ ) is

$$\left(\frac{d\psi}{dx}\right)_1 = \frac{\psi[x^i] - \psi[x^{i-1}]}{x^i - x^{i-1}}. \quad (2.16)$$

This is the slope of the line connecting  $x^i$  and  $x^{i-1}$ . If one instead fits a parabola to the three points  $x^{i-1}$ ,  $x^i$ , and  $x^{i+1}$ , one arrives at the second order approximation

$$\left(\frac{d\psi}{dx}\right)_2 = \frac{(\psi[x^{i+1}] - \psi[x^i])(x^i - x^{i-1})^2 + (\psi[x^i] - \psi[x^{i-1}])(x^{i+1} - x^i)^2}{(x^{i+1} - x^i)(x^{i+1} - x^{i-1})(x^i - x^{i-1})}. \quad (2.17)$$

If the grid is evenly spaced with spacing  $h$ , the relative difference between these two approximations simplifies to

$$\frac{\Delta\psi'}{\psi'} = \frac{(\psi[x^{i+1}] - \psi[x^i]) - (\psi[x^i] - \psi[x^{i-1}])}{(\psi[x^{i+1}] - \psi[x^i]) + (\psi[x^i] - \psi[x^{i-1}])} \approx \frac{h\psi''[x^i]}{2\psi'[x^i]}, \quad (2.18)$$

where

$$\Delta\psi' = \left(\frac{d\psi}{dx}\right)_2 - \left(\frac{d\psi}{dx}\right)_1 \quad (2.19)$$

and primes signify derivatives. The first order scheme is accurate to first order in  $h$ . In general, the  $n$ th order scheme is accurate to  $n$ th order in  $h$  (ignoring the

Runge phenomenon mentioned earlier). As  $h$  is decreased by adding more grid points, the errors usually get smaller.

Finite difference methods (FDM) [151, 12, 83, 54] have been used to solve the two-electron atom and have had some success. The most recent work [54] obtained 10 digits of accuracy in the energy of the ground state using state-of-the-art matrix and parallelization methods.

### 2.1.3 The pseudospectral method

The pseudospectral method has a long history of success in fluid dynamics [34], numerical relativity [93, 122], and quantum chemistry [65, 66, 67, 127, 74, 112, 111, 96, 84]. Some one-electron quantum mechanics problems [24, 26] have also been solved with the method.

There have not been any studies directly comparing the computational costs of pseudospectral methods to variational methods. Ideally, one must take into account both memory and time requirements. Such studies have been done with finite difference methods but for different problems. Pfeiffer *et al.* [122] directly compared a pseudospectral method to a finite difference code (Cadez), optimized to solve a nonlinear problem with a three-dimensional, infinite domain with two spherical holes. For this problem, the pseudospectral code outperformed (in terms of computing time) the finite difference code even when the latter employed Richardson extrapolation. Without Richardson extrapolation, the pseudospectral code was seven orders of magnitude better for the same runtime at the highest resolutions (the difference increased with higher resolution). Fornberg and Merrill [61] compared these two methods for convective

flow over a sphere and realized similar results. It is worthwhile to begin to explore applying the pseudospectral method to fully correlated quantum mechanical systems.

## Grid points

The pseudospectral method is a collocation method, in which the differential equation is enforced at all grid points. The grid points are chosen so that exponentially fast convergence is assured if the solution is smooth on the computational domain.<sup>1</sup> For finite nonperiodic domains, the points must be the roots (or antinodes plus endpoints) of Jacobi polynomials or a multidimensional generalization of such polynomials.

The Jacobi polynomials denoted  $P_n^{(a,b)}[x]$  with  $a, b > -1$  satisfy the orthonormality condition

$$\int_{-1}^1 (1-x)^a (1+x)^b P_n^{(a,b)}[x] P_m^{(a,b)}[x] dx = \frac{2^{a+b+1}}{2n+a+b+1} \frac{\Gamma[n+a+1]\Gamma[n+b+1]}{\Gamma[n+1]\Gamma[n+a+b+1]} \delta_{mn}, \quad (2.20)$$

where  $\Gamma$  is the gamma function. Each polynomial  $P_n^{(a,b)}$  has  $n-1$  roots on the interval  $-1 \leq x \leq 1$ , which are more closely spaced on the edges of this domain than in the center. Common choices for  $a$  and  $b$  are  $a = b = 0$  (Legendre polynomials) and  $a = b = -1/2$  (Chebyshev polynomials). The latter choice is the most common because the Chebyshev polynomials are the only Jacobi polynomials with the property

$$|P_n(a,b)[x]| \leq 1 \quad (2.21)$$

for  $-1 \leq x \leq 1$ . This property means that interpolation errors are evenly distributed.

---

<sup>1</sup>Known nonanalytic behavior can be used to provide a different choice of grid points.

Such a grid limits one to finite domains that fit within the range  $-1 \leq x \leq 1$ . This is not a strong restriction because any other domain can be scaled to fit in that range. For a finite domain given by  $-y_{min} \leq y \leq y_{max}$ , a trivial mapping is

$$x = \frac{2y - y_{min} - y_{max}}{y_{max} - y_{min}}. \quad (2.22)$$

Another possibility is a semi-infinite domain  $0 \leq r \leq \infty$ . One can then use either Laguerre polynomials or, as done here, scale by the algebraic mapping

$$x = \frac{1 - r}{1 + r}. \quad (2.23)$$

Other mappings are discussed in Ref. [25]. For any mapping employed, one must check if the solution is smooth in the transformed  $x$  coordinate.

### Differentiation matrices

For any solution method, it is essential to have a way of representing derivatives. A solution  $f[x]$  is represented by a vector  $\mathbf{f} = \{f^1, f^2, \dots, f^N\} = \{f[x^1], f[x^2], \dots, f[x^N]\}$ , where  $x^i$  is a grid point and  $N$  is the number of grid points. The  $N$ th order approximation to  $f$  is

$$f[x] \approx \sum_{i=1}^N f^i C_i[x], \quad (2.24)$$

where  $C_i[x]$  is the cardinal function

$$C_i[x] = \prod_{\substack{j=1 \\ j \neq i}}^N \frac{x - x^j}{x^i - x^j} \quad (2.25)$$

with the property

$$C_i[x^j] = \delta_i^j. \quad (2.26)$$

The differentiation matrix for the  $m$ th derivative is then defined by

$$D_i^{mj} = \left. \frac{d^m C_i[x]}{dx^m} \right|_{x=x^j}, \quad (2.27)$$

and the pseudospectral approximation to the  $m$ th derivative of  $f$  at the grid point  $x^j$  is

$$\frac{d^m f[x^j]}{dx^m} \approx \sum_{i=1}^N D_i^{mj} f^i. \quad (2.28)$$

### A simple example

The radial Schrödinger equation for the hydrogen atom is

$$-\frac{1}{2} \frac{d^2 f_{nl}}{dr^2} - \frac{1}{r} \frac{df_{nl}}{dr} + \frac{l(l+1)f_{nl}}{2r^2} - \frac{f_{nl}}{r} = E_n f_{nl}, \quad (2.29)$$

where atomic units have been used and the full solution is given by

$$\psi_{nlm}[\mathbf{r}] = f_{nl}[r] Y_{lm}[\theta, \phi], \quad (2.30)$$

where  $Y_{lm}$  is the usual spherical harmonic, with energy

$$E_n = -\frac{1}{2n^2}. \quad (2.31)$$

For simplicity, the angular momentum quantum number  $l$  will be set to zero.

With the algebraic mapping (Eq. 2.23), Eq. 2.29 turns into

$$-\frac{1}{2}(1+x)^4 \frac{d^2 f_{nl}}{dx^2} - \frac{(1+x)^3(2-x)}{1-x} \frac{df_{nl}}{dx} - \frac{1+x}{1-x} f_{nl} = E_n f_{nl}. \quad (2.32)$$

The pseudospectral approximation to this equation is

$$\sum_{i=1}^N \left[ -\frac{1}{2}(1+x^j)^4 D_i^{2j} - \frac{(1+x^j)^3(2-x^j)}{1-x^j} D_i^{1j} - \left( \frac{1+x^j}{1-x^j} + E_n \right) D_i^{0j} \right] f_{nl}^i = 0. \quad (2.33)$$

For  $N = 5$  and  $l = 0$  and a Legendre grid, this turns into the standard matrix eigenvalue problem,<sup>2</sup>

$$\begin{pmatrix} -0.049 - E_n & 0.00043 & -0.00035 & 0.00019 & -0.00054 \\ -0.045 & -0.24 - E_n & -0.012 & -0.0050 & 0.0020 \\ 0.16 & -1.0 & 0.17 - E_n & -0.31 & 0.0078 \\ -0.72 & 3.0 & -11. & 7.1 - E_n & -1.8 \\ 11. & -41. & 89. & -211. & 131. - E_n \end{pmatrix} \begin{pmatrix} f_{n0}^1 \\ f_{n0}^2 \\ f_{n0}^3 \\ f_{n0}^4 \\ f_{n0}^5 \end{pmatrix} = 0. \quad (2.34)$$

The energies of the five states that this equation gives are  $-0.501773$ ,  $-0.187408$ ,  $-0.049601$ ,  $4.770660$ , and  $134.023677$ . The exact energies are  $-0.5$ ,  $-0.125$ ,  $-0.0555556$ ,  $-0.03125$ , and  $-0.02$ . What is truly amazing is the error in the energy of the ground state is 0.35% for only five grid points. The first and second excited state energies are roughly correct while the third and fourth are very inaccurate.

In order to see how accurate the wave function is, the eigenvector must be normalized. The normalization condition is

$$\int_0^\infty r^2 |f_{nl}[r]|^2 dr = 2 \int_{-1}^1 \frac{(1-x)^2}{(1+x)^4} |f_{nl}[x]|^2 dx = 1. \quad (2.35)$$

The grid points that have been chosen are also quadrature points, so this condition becomes

$$1 = 2 \sum_{j=1}^N w_j \frac{(1-x^j)^2}{(1+x^j)^4} |f_{nl}^j|^2, \quad (2.36)$$

where the quadrature weights are  $w_0 = w_5 = 0.236927$ ,  $w_1 = w_4 = 0.478629$ , and  $w_3 = 0.568889$ . The eigenvector is then  $\{0.000156265, 0.0538214, 0.814599, 1.64433, 2.10374\}$  with the exact answer being  $\{3.00126 \times 10^{-9}, 0.0713428, 0.735759, 1.48165, 1.90395\}$ , roughly a 10% error.

---

<sup>2</sup>This matrix has been rounded to two decimal places so that it would fit on the page. All calculations were done with double precision arithmetic.

If  $N$  is increased, these errors go down exponentially fast. By the time  $N = 59$ , the energy error has dropped to machine precision. The convergence rate would have been even faster if this problem had a finite domain. At no point were any explicit assumptions about the solution made. The asymptotic form of the solution was not given at large or small  $r$ . No regularity condition was specified at the singularity. These behaviors are handled automatically by the method. The method gives the regular solution to the partial differential equation.

## 2.2 Experimental results for two-electron atoms

Spectra are powerful tools for measurements of atomic systems. These directly give the energy differences between states and if measured carefully, the relative oscillator strength of the transitions. Absolute values of both oscillator strengths and energies are more difficult to obtain.

For identical systems in the same initial state, exposed to monochromatic illumination, the absorption oscillator strength measures the fraction of transitioning systems that transition to a given final state. Comparing the brightness of two lines directly gives the relative oscillator strength, but an absolute measurement either requires measurements of all transitions or using a well-known transition to calibrate results. Oscillator strengths are more usually calculated from lifetime calculations. These measurements further suffer from cascade events, during which multiple transitions interfere with a single transition measurement. Experimental absolute oscillator strengths are not known to better than three decimal places [35], meaning finite-nuclear-mass and relativistic

effects can be ignored while comparing with theoretical calculations.

Morton *et al.* [110], reviewed the state of knowledge of energy levels of the lower part of the helium spectrum for both stable isotopes. The experimental energies are known to higher precision than theoretical calculations for most of the lowest energy states (presumably because of the difficulty in calculating the relativistic corrections), with the exception of the ground state for which the errors are comparable. The ground state energy is harder to measure because of the large gap in energy between it and the closest state. All these energies have been measured to better than 1 part in  $10^8$ . Direct comparisons between theory and experiment can be used to determine the fine structure constant. Drake [47] calculated  $\alpha^{-1} = 137.03608(13)$ , which has a precision only four times worse than  $g - 2$  experiments.

### 2.3 Corrections to the two-electron problem

There are two small parameters in which the full Hamiltonian is often expanded: the ratio of the reduced mass of the electron-nucleus pair to the nuclear mass,  $\mu/M = 1.37074563559(58) \times 10^{-4}$  [107, 108] (for  ${}^4\text{He}$ ) and the fine structure constant  $\alpha = 7.2973525376(50) \times 10^{-3}$  [107, 108]. Here, the lowest order corrections in  $\mu/M$  and  $\alpha$  are considered. For high-precision work, one needs to correct the theoretical calculations of energies and oscillator strengths perturbatively in powers of both small quantities.

A listing of the various contributions is given in Tab. 2.2. These numbers give the order of magnitudes of corrections that must be added before theoretical and experimental values can be compared. If more than eight digits of

Table 2.2: Contributions to the energy and their orders of magnitude.

Contribution (Ref. [53])	Magnitude (Ref. [53])	$-\log_{10}  \text{Magnitude} $
Nonrelativistic energy	$Z^2$	-6
Mass polarization	$Z^2\mu/M$	3.3
Second-order mass polarization	$Z^2(\mu/M)^2$	7.1
Relativistic corrections	$Z^4\alpha^2$	3.1
Relativistic recoil	$Z^4\alpha^2\mu/M$	6.9
Anomalous magnetic moment	$Z^4\alpha^3$	5.2
Lamb shift	$Z^4\alpha^3 \ln \alpha + \dots$	4.5
Finite nuclear size	$Z^4(R_N/a_0)^2$	8.8

accuracy is needed for the energy even higher order corrections should be included.

### 2.3.1 Finite nuclear mass correction

The nonrelativistic ( $\alpha^0$ ) Hamiltonian for two-electron atoms can be written

$$\hat{H}_{nr} = \hat{H}_0 + \hat{H}_{cm} + \hat{H}_{mp}, \quad (2.37)$$

where  $\hat{H}_0$  is the fixed nucleus approximation to the hamiltonian with the electron mass set to  $\mu$ ,  $\hat{H}_{cm}$  is the kinetic energy of the center of mass, and  $\hat{H}_{mp}$  is the

mass polarization term:

$$\hat{H}_0 = \frac{1}{2}(p_1^2 + p_2^2) + \hat{V} \quad (2.38)$$

$$\hat{H}_{cm} = \frac{1}{2(M + 2m_e)} p_{cm}^2 \quad (2.39)$$

$$\hat{H}_{mp} = \frac{1}{M} \mathbf{p}_1 \cdot \mathbf{p}_2, \quad (2.40)$$

where  $\hat{V}$  is the potential energy operator,  $m_e$  is the electron mass,  $\mathbf{p}_{cm}$  is the momentum operator of the center of mass, and reduced mass atomic units ( $\mu = 1$ ) are being used. The second term is removed in center-of-mass coordinates and the last term provides the dominant nontrivial correction for finite nuclear mass (the trivial one being the scaling of the energy by  $m_e/\mu$ ).

### 2.3.2 Relativistic corrections

The Schrödinger equation is a nonrelativistic approximation to the true equation of motion. The lowest order relativistic corrections enter at order ( $Z\alpha^2$ ), as summarized in Ref. [58]. The Breit-Pauli Hamiltonian encapsulates the correction

$$\hat{H}_{BP} = \hat{H}_{nr} + \hat{H}_{rel}, \quad (2.41)$$

where  $\hat{H}_{nr}$  is the usual nonrelativistic Hamiltonian used in Schrödinger's equation and  $\hat{H}_{rel}$  is the lowest order relativistic correction. The latter can be further divided into nonfine-structure (NFS) and fine-structure (FS) contributions:

$$\hat{H}_{NFS} = \hat{H}_{mass} + \hat{H}_D + \hat{H}_{SSC} + \hat{H}_{OO} \quad (2.42)$$

$$\hat{H}_{FS} = \hat{H}_{SO} + \hat{H}_{SOO} + \hat{H}_{SS}. \quad (2.43)$$

The separate contributions to the Hamiltonian are the mass-velocity (mass), two-body Darwin (D), spin-spin contact (SSC), orbit-orbit (OO), spin-orbit (SO),

spin-other-orbit (SOO), and the spin-spin (SS) terms. These are explicitly given by

$$\hat{H}_{mass} = -\frac{\alpha^2}{8} \sum_i p_i^4 \quad (2.44)$$

$$\hat{H}_D = -\frac{\alpha^2 Z}{8} \sum_i \nabla_i^2 r_i^{-1} + \frac{\alpha^2}{4} \sum_{i<j} \nabla_i^2 r_{ij}^{-1} \quad (2.45)$$

$$\hat{H}_{SSC} = -\frac{8\pi\alpha^2}{3} (\mathbf{s}_1 \cdot \mathbf{s}_2) \delta(\mathbf{r}_{12}) \quad (2.46)$$

$$\hat{H}_{OO} = -\frac{\alpha^2}{2} \left( \frac{\mathbf{p}_1 \cdot \mathbf{p}_2}{r_{12}} + \frac{\mathbf{r}_{12}(\mathbf{r}_{12} \cdot \mathbf{p}_1) \cdot \mathbf{p}_2}{r_{12}^3} \right) \quad (2.47)$$

$$\hat{H}_{SO} = \frac{\alpha^2 Z}{2} \sum_i \frac{\hat{\mathbf{l}}_i \cdot \hat{\mathbf{s}}_i}{r_i^3} \quad (2.48)$$

$$\hat{H}_{SOO} = -\frac{\alpha^2}{2} \sum_{i \neq j} \left( \frac{\mathbf{r}_{ij}}{r_{ij}^3} \times \mathbf{p}_i \right) \cdot (\mathbf{s}_i + 2\mathbf{s}_j) \quad (2.49)$$

$$\hat{H}_{SS} = \frac{\alpha^2}{r_{12}^3} \left( \mathbf{s}_1 \cdot \mathbf{s}_2 - \frac{3}{r_{12}^2} (\mathbf{s}_1 \cdot \mathbf{r}_{12})(\mathbf{s}_2 \cdot \mathbf{r}_{12}) \right), \quad (2.50)$$

where  $i$  and  $j$  can be 1 or 2,  $\mathbf{p}_i$  and  $\mathbf{r}_i$  are the momentum and position of the  $i$ th electron with respect to the nucleus, respectively,  $\mathbf{r}_{12}$  is the vector pointing from the first electron to the second, and  $\hat{\mathbf{s}}_i$  and  $\hat{\mathbf{l}}_i$  are the one-electron spin and angular momentum operators of the  $i$ th electron, respectively. The last three terms are zero for  $^1S$  states due to symmetry considerations.

CHAPTER 3  
**PSEUDOSPECTRAL CALCULATION OF THE WAVE FUNCTION OF  
HELIUM AND THE NEGATIVE HYDROGEN ION**

This chapter is material from an article published in Physical Review A (Ref. [73]).

### 3.1 Abstract

We study the numerical solution of the non-relativistic Schrödinger equation for two-electron atoms in ground and excited S-states using pseudospectral (PS) methods of calculation.

The calculation achieves convergence rates for the energy, Cauchy error in the wavefunction, and variance in local energy that are exponentially fast for all practical purposes. The method requires three separate subdomains to handle the wavefunction's cusp-like behavior near the two-particle coalescences. The use of three subdomains is essential to maintaining exponential convergence and is more computationally efficient than a single subdomain. A comparison of several different treatments of the cusps suggests that the simplest prescription is sufficient.

We investigate two alternate methods for handling the semi-infinite domain, one which involves a sequence of truncated versions of the domain and the other which employs an algebraic mapping of the semi-infinite domain to a finite one and imposes no explicit cutoffs on the wavefunction. The latter prescription proves superior.

For many purposes it proves unnecessary to handle the three-particle coalescence in a special way. The presence of logarithmic terms in the exact solution is expected to limit the convergence to being non-exponential but the only clear evidence of that is the rate of convergence of derivatives near the three-particle coalescence point. Higher resolution than achieved in this work will ultimately be needed to see its limiting effect on other measures of error.

As developed and applied here the PS method has many virtues: no explicit assumptions need be made about the asymptotic behavior of the wavefunction near cusps or at large distances, the local energy ( $\mathcal{H}\psi/\psi$ ) is exactly equal to the calculated global energy at all collocation points, local errors go down everywhere with increasing resolution, the effective basis using Chebyshev polynomials is complete and simple, and the method is easily extensible to other bound states. As the number of collocation points grows, the method achieves exponential convergence up to the resolution tested.

This study serves as a proof-of-principle of the method for more general two- and possibly three-electron applications.

## 3.2 Introduction

The nonrelativistic, two-electron atom ( $\text{H}^-$ , He,  $\text{Li}^+$ ) is the simplest “hard” problem in quantum mechanics. It involves strong electron-electron correlations, nontrivial symmetry considerations, and single as well as double continua. Many different solution techniques have been developed and applied over the past 80 years. A thorough understanding of this simple system is important not only because of its direct relevance to experimental studies in atomic physics but also because the best methods of solution may suggest generalizations applicable to multielectron and/or multiatom systems.

Our own interest in this problem arose from investigating bound-free and free-free opacity of the negative hydrogen ion  $\text{H}^-$ . As first conjectured by Wildt [150],  $\text{H}^-$  gives the greatest contribution to opacity in the atmosphere of the Sun and many other stars. The photo-absorption cross section of  $\text{H}^-$  is known to an

accuracy of a few percentage points [88] but little attention has been devoted to  $H^-$  in less-than-ideal circumstances (high density, high magnetic field, etc.) of relevance to astrophysical applications. We sought a first-principles approach that would allow “exact” calculations of initial and final states as part of these investigations and were led to reconsider this classic problem.

Ideally, there would exist a simple method capable of handling any two-electron state in the presence of a nucleus with any angular momentum whether bound or free. In practice, many individual methods have been formulated each having somewhat more specific goals. A common starting point, for example, is finding the ground-state energy for zero total angular momentum.

It is not possible in a single article, let alone an introduction, to review the full range of methods that have been developed and explored. We can briefly compare the strengths and weaknesses of a few select approaches by assessing each in terms of the generality (is it applicable to all states or just the ground state?), the capability of achieving an exact solution of the nonrelativistic Schrödinger equation in the limit of infinite nuclear mass (is it *in principle* capable of finding an exact solution [in the aforementioned sense] or are there intrinsic approximations?), the degree of tuning required (is it straightforward to apply or does it require an enlightened guess for, say, the choice of basis functions?) and, of course, the computational effort for a given level of accuracy.

The asymptotic rate of convergence of some error  $R_n$  as a function of the number  $n$  of basis functions, grid size, etc. is of central importance in evaluating a numerical method. To characterize the convergence rate the definitions of Boyd [25] are used in this article and reproduced here. The algebraic index of

convergence,  $k$  is defined as the maximum  $k$  so that

$$\lim_{n \rightarrow \infty} |R_n| n^k < \infty. \quad (3.1)$$

If  $k$  is finite then  $R_n$  converges algebraically. The simplest example of algebraic convergence is an error  $R_n \propto 1/n^k$ . If  $k$  is infinite then  $R_n$  converges exponentially. This latter category is subdivided into three cases defined by the value of

$$l = \lim_{n \rightarrow \infty} \frac{\log |R_n|}{n}. \quad (3.2)$$

If  $l$  is zero, a finite positive number, or infinite, the rate is subgeometric, geometric, or supergeometric, respectively. For example, if the error  $R_n \propto \exp(-n^m)$ , the conditions  $0 < m < 1$ ,  $m = 1$ , and  $m > 1$  correspond to subgeometric, geometric, and supergeometric convergence, respectively.

### 3.2.1 Variational method for two electrons and nucleus: ground state

The first numerical explorations of two-electron ground states adopted the approach of minimizing the global energy. Once Hylleraas determined that only three coordinates were needed to represent the wave function for  $S$  states he carried out such variational calculations (prior to the advent of computers) [87]. Pekeris and coworkers [118, 120, 64, 3] did the first high precision calculations on computers, expanding the wave function in terms of Laguerre polynomials of linear combinations of the interparticle distances times an appropriate exponential falloff. They determined the energy of  $\text{H}^-$  to eight decimal places and that of  $\text{He}$  to nine, calculations that were the gold standard for several decades.

Variational methods have been highly successful at calculating extremely precise eigenvalues of the ground state of two-electron atoms. Indeed, eigenvalue energies have been calculated to numerical accuracy—at least 42 digits—that *far* exceeds the accuracy of the underlying physical description based on nonrelativistic equations of motion [8, 46, 99, 68, 100, 48, 69, 70, 114, 115, 103]. A clear strength of the general variational approach is that intrinsic approximations to the Hamiltonian operator need not be made. The principle drawbacks are related to the difficulties inherent in the selection of the basis: it should be complete so that convergence to the exact solution is possible and efficient so that finite numbers of elements do a good job representing the wave function.

Significant progress in choice of the basis for the two-electron problem has taken place. The inclusion of new functions (e.g., logarithmic terms) typically motivated by known limiting forms of the wave function improves the rate of convergence [94, 140, 137, 64, 8, 99, 143, 63]. Furthermore, without special additions, some bases are simply incapable of representing the exact solution [15, 14]. Klahn and Morgan have shown that there are examples where the expectation value of an operator (i.e.,  $r^k$  with  $k \geq 6$ ) converges to the incorrect value or diverges even if the basis is complete. In their example the basis cannot accurately represent the derivatives of the hydrogenic solution at  $r = 0$  [95]. When employing such bases, one must always check that the physical property one is calculating is converging properly.

Schwartz [139] surveyed the convergence rate of the error in the ground-state energy eigenvalue achieved by many different strategies for basis set selection. His results for the error may be expressed as a function of  $n$ , the total number of basis functions selected according to a well-defined procedure. The

error generally converges algebraically with index,  $1.5 \leq k \leq 8.3$  ( $\propto n^{-k}$ ), depending on the basis. The range in  $k$  highlights the significance that a good choice of basis can have on the asymptotic convergence of a calculation. One basis set, which included a single power of a logarithm, appeared to converge exponentially fast as  $\sigma^{-n}$  with  $\sigma$  in the range 0.51-0.54. Such exponential behavior is often assumed of variational methods if the basis can accurately describe the behavior of the wave function everywhere. That is, the basis includes functions which have the same analytic and nonanalytic behavior as the exact solution.

Loosely speaking, even when convergence is assured, the accuracy of the variationally inferred wave function (by many different measures) is much less than that of the energy eigenvalue. Parts of the wave function that have a small effect on the total energy are not well-constrained by lowering the energy. An alternative strategy to minimizing the global energy is to minimize the variance in the local energy instead [16, 38, 145]. This approach can produce better local values of the wave function but leads to nonlinear minimization problems which are more difficult to handle numerically (minimization of the variance in local energy with respect to parameters in the trial wave function) but still tractable because one need not calculate the global energy at each step.

### **3.2.2 Variational method for excited states**

Variational methods [120, 3, 97, 98, 46] have been successful at calculating precise excitation energies. In general, variational methods extend naturally to excited, bound states whenever the variational parameters enter in a linear fash-

ion. It is then straightforward to find multiple eigenstates of the linear system. The more highly excited the state the less converged the energy is, especially if the basis was optimized in order to reproduce the features of the ground state only <sup>1</sup>.

### 3.2.3 Fourier spectral expansion

Griebel and Hamaekers [76] developed a Fourier expansion method for multidimensional quantum mechanical systems. They apply the hyperbolic cross truncation to their basis and show that for smooth solutions the exponential convergence rate is not dependent on the dimensionality of the system. They calculate the energies of several different systems including hydrogen and helium. Unfortunately, they fail to achieve exponential convergence because the cusps were not properly treated, and hence their highest resolution runs for hydrogen and helium are only good to about 2 and 10%, respectively.

### 3.2.4 Specialized methods for two-electron systems

Haftel and Mandelzweig and later other collaborators [77, 78, 79, 80, 81, 101, 102] have presented an exact treatment of two-electron atoms that begins by

---

<sup>1</sup>Drake [46] points out that alternative methods can calculate the singly excited spectrum. For high angular momentum, the system can be treated as an electron in the field of a perturbed core with higher and higher moments of the core being included for higher and higher accuracy. This calculation can be done analytically for the two-electron problem. The approximation here is that the electron correlation energy is ignored, but this is very small for such states. For large principle quantum numbers, quantum defect approximations work well. The energy is proportional to  $1/(n - \delta_l)^2$ , instead of the usual  $1/n^2$ , where  $n$  is the principle quantum number of the excited electron,  $l$  is its angular momentum, and  $\delta_l$  gives the effect of the screening due to the inner electron.

factoring out the correct cusp behavior and posing the problem in terms of the remaining part of the wave function. This piece which is continuous up to first derivatives is expanded in terms of hyperspherical harmonics yielding a set of coupled ordinary differential equations for coefficients which are functions of the hyperradius. The method fully accounts for the asymptotic behavior near coalescence points and yields results with energies good to one part in  $10^9$ . The hyperspherical harmonic expansion converges more quickly than if the cusp is not explicitly accommodated for, but remains algebraic because of the higher-order discontinuities. The method accurately determines bound excited states as well.

### **3.2.5 Direct solution of partial differential equation for bound and continuum states**

Most of the bound-state techniques mentioned thus far are unsuitable for calculating continuum-states. In fact, continuum state calculations rely on totally different variational methods. The main ones are  $R$ -matrix [31], Schwinger variational [86], and the complex Kohn variational [126] methods. Accuracy for these methods lags far behind that of bound-state calculations.

Roughly speaking, the source of some of these difficulties is related to describing the wave function over an infinite volume while simultaneously controlling the errors of greatest significance. Typically, linear variational methods are equivalent to spectral expansions of the wave function. The control one has over the accuracy of an approximate description of the wave function is indirect via the choice of the expansion. Instead, one may be motivated for both bound

and continuum problems to consider solving the partial differential equation directly on a grid where a greater degree of local control is possible.

Finite difference methods (FDM) [151, 12, 83, 54] and Finite element methods (FEM) [104, 27, 4, 141, 157, 156] represent the solution and the differential equation on a discrete grid. The FDM grid is usually evenly spaced with derivatives calculated to some small (usually second) order. FEM uses subdomains, concentrating grid points where more accuracy is needed. Recent work achieves as many as seven decimal places in the energy of the ground state but produces surprisingly nonsmooth wave functions [157, 156]. The rate of convergence of these methods is limited by the order of the representation of derivatives and is always algebraic with some small index dependent on the order used for derivatives.

### **3.2.6 Pseudospectral approach**

Some of the above considerations motivate an investigation of the pseudospectral (PS) method. Like FDM and FEM methods the PS method represents the wave function by values on a discrete grid of points rather than by coefficients of a spectral expansion. However, the points are selected in a different manner and the derivative order increases with grid resolution. Roots of Jacobi polynomials are chosen in order to make the asymptotic rate of convergence of an analytic function constant across the entire finite nonperiodic domain. Such a choice also has the advantage that exponential convergence can be lost only by nonanalytic behavior within the domain. By contrast, an equispaced grid is sensitive to singularities nearby in the complex plane and can lead to divergences

when interpolating near the endpoints (Runge phenomenon). Of all the Jacobi polynomials, Chebyshev polynomials vary the least over  $[-1, 1]$  and hence produce the smallest residual from the PS method. The mathematical theory of nonsmooth functions is not well developed and precise convergence rates are usually calculated empirically [62].

The PS method [62, 25, 124] has seen successes in many fields including fluid dynamics [34], relativistic astrophysics [23], and numerical relativity [93, 122]. When the underlying solution is smooth, the PS method typically requires less computational run time and less memory than FDM and FEM to achieve comparable precision. The method has been applied in quantum mechanics to solve the full Schrödinger equation for a single electron [55, 24, 26]. In addition, various simplifications of the multielectron Schrödinger equation have been treated, including the Hartree-Fock approximation [65, 66, 67, 127, 74, 84], Møller-Plesset perturbation theory [112], and density functional theory [111, 96].

To the authors' knowledge, no one has solved the full three-dimensional Schrödinger equation for heliumlike systems (the "exact" problem) using PS methods. This article implements the method, investigates several design choices and calculates ground and excited bound  $S$  states. The convergence rate is used as the metric to characterize different grid choices, alternative methods for handling regularity conditions and other practical considerations needed for an efficient algorithm. No attempt to reproduce the ultrahigh precision results of variational methods is made. The calculation employs a standard Chebyshev basis without any specialized tuning. The eigenvalue and eigenfunction problems are solved by a standard method. All calculations are done on a single processor with a speed of 6 GHz and 8 GB of memory.

The PS method is expected to be supergeometric on a finite computational domain if no singularities exist in the solution anywhere in the complex plane, geometric if singularities are only outside the domain, and algebraic if singularities exist within domain. If the domain is infinite or semi-infinite, subgeometric convergence is expected when no singularities are in the domain, and algebraic convergence is expected otherwise [25].

### 3.3 Setting up the problem

Let  $\mathbf{z}_i$  and  $\nabla_i^2$  be the position vector and the Laplacian of the coordinates, respectively, of the  $i$ th electron if  $i$  is 1 or 2 and of the nucleus if  $i$  is 3. The nonrelativistic Schrödinger equation for a heliumlike system is

$$\mathcal{H} = -\frac{1}{2} \left( \frac{\nabla_1^2}{m} + \frac{\nabla_2^2}{m} + \frac{\nabla_3^2}{M} \right) + \mathcal{V}, \quad (3.3)$$

where

$$\mathcal{V} = -\frac{Z}{|\mathbf{z}_1 - \mathbf{z}_3|} - \frac{Z}{|\mathbf{z}_2 - \mathbf{z}_3|} + \frac{\alpha}{|\mathbf{z}_1 - \mathbf{z}_2|}, \quad (3.4)$$

$Z$  is the nuclear charge,  $\alpha = 1$  unless the electron-electron interaction is suppressed ( $\alpha = 0$ ),  $m$  is the mass of the electron and  $M$  is the mass of the nucleus. The units are  $e = \hbar = 1/4\pi\epsilon_0 = 1$ . The Hamiltonian acts on functions of nine dimensions, i.e., three coordinate positions for each particle.

The relative and center of mass coordinates are

$$\mathbf{r}_1 = \mathbf{z}_1 - \mathbf{z}_3 \quad (3.5)$$

$$\mathbf{r}_2 = \mathbf{z}_2 - \mathbf{z}_3 \quad (3.6)$$

$$\mathbf{R} = \frac{m(\mathbf{z}_1 + \mathbf{z}_2) + M\mathbf{z}_3}{M + 2m}. \quad (3.7)$$

Define the coordinates

$$r_1 = |\mathbf{r}_1| \quad (3.8)$$

$$r_2 = |\mathbf{r}_2| \quad (3.9)$$

$$r_{12} = |\mathbf{r}_1 - \mathbf{r}_2|, \quad (3.10)$$

and rewrite the Hamiltonian

$$\mathcal{H} = \mathcal{T}_0 + \mathcal{T}_{cm} + \mathcal{T}_{mp} + \mathcal{V}, \quad (3.11)$$

where

$$\mathcal{T}_0 = -\frac{1}{2\mu}(\nabla_{r_1}^2 + \nabla_{r_2}^2), \quad (3.12)$$

$$\mathcal{T}_{cm} = -\frac{1}{2(M+2m)}\nabla_R^2, \quad (3.13)$$

$$\mathcal{T}_{mp} = -\frac{1}{M}\nabla_{\mathbf{r}_1} \cdot \nabla_{\mathbf{r}_2}, \quad (3.14)$$

$$\mathcal{V} = -\frac{Z}{r_1} - \frac{Z}{r_2} + \frac{\alpha}{r_{12}}, \quad (3.15)$$

$\mu = mM/(M+m)$  is the reduced mass of the electron and nucleus, and  $\nabla_{\mathbf{x}}$  is the gradient operator with respect to the vector  $\mathbf{x}$ .

In the center-of-mass frame  $\mathcal{T}_{cm}$  may be dropped bringing to six the number of nontrivial coordinates on which the wave function depends. Because  $m \ll M$ , the mass polarization term  $\mathcal{T}_{mp}$  is often ignored or treated perturbatively. While unnecessary for many methods including PS, we use the infinite nuclear mass approximation ( $M = \infty$ ) to facilitate comparison with previous results. In units with  $m = 1$  (atomic units) the Hamiltonian is

$$\mathcal{H} = -\frac{1}{2}(\nabla_{r_1}^2 + \nabla_{r_2}^2) - \frac{Z}{r_1} - \frac{Z}{r_2} + \frac{\alpha}{r_{12}}. \quad (3.16)$$

Atomic units are used throughout the rest of this article.

This operator is elliptic. All boundaries in physical space require specification of the function or its normal derivative or some combination of the two [7]. In the ideal problem, the physical boundary is at infinity where the wave function must be zero. The existence of the Coulomb potential's singular points at  $r_1 = 0$ ,  $r_2 = 0$ , and  $r_{12} = 0$  introduces complications in any formal and practical analysis. Before the exact nature of the Hermitian Hamiltonian operator and its spectrum was understood, Kato [91] showed that discrete eigenstates existed for the specific case of helium. In later work Kato [90] showed that the wave function must be finite at the singular points (which is also true everywhere else), and that the first derivative of the wave function on the domain excluding the singular points is bounded. This result allows discontinuities in the first derivative at the singular points, called Kato cusps. Generally, higher derivatives are not bounded at the singular points.

In any numerical treatment of the Hamiltonian operator a decision must be made about how to handle the singular points. In a formal mathematical sense, quantities at the singularities are well defined only in the limit as one approaches the singularity. This creates an effective inner boundary about such points on which additional conditions on the function and its normal derivative may be specified. Such conditions are exploited to guarantee regularity in the limit that the excised region shrinks to a point. This article assumes that it is correct to excise such a point, either explicitly or implicitly.

### 3.4 Coordinates and the Hamiltonian

The heliumlike atom is made of three particles: a nucleus and two electrons. Six coordinates are required to describe relative positions. Three coordinates describe the precise shape and size of the triangle with a particle at each vertex, and the other three describe the orientation of that triangle in space (often taken to be Euler angles). The wave function for  $S$  states is completely independent of the latter three [87]. For nonzero angular momentum one first expands the wavefunction in generalized spherical harmonics of the Euler angles. Only a finite number of terms are needed for a given total angular momentum and its  $z$  component, and the Schrödinger equation becomes a finite set of coupled partial differential equations for the remaining three variables (e.g., Refs. [21, 22]).

Two useful sets of coordinates for the triangle are  $\{r_1, r_2, r_{12}\}$  and  $\{r_1, r_2, \theta_{12}\}$ , where  $r_1$  and  $r_2$  are the proton-electron distances,  $r_{12}$  is the electron-electron distance, and  $\theta_{12}$  is the angle between the vectors pointing to the two electrons. Four additional useful sets of coordinates  $\{\rho \text{ or } x, \phi, C\}$  and  $\{\rho \text{ or } x, \zeta, B\}$  are defined by

$$r_1 = \rho \cos \phi \quad (3.17)$$

$$r_2 = \rho \sin \phi \quad (3.18)$$

$$C = -\cos \theta_{12} \quad (3.19)$$

$$\sqrt{2} \sin \zeta = \sqrt{1 + C \sin 2\phi} \quad (3.20)$$

$$B = \frac{\cos 2\phi}{\sqrt{1 - C^2 \sin^2 2\phi}} \quad (3.21)$$

$$x = \frac{1 - \rho}{1 + \rho}. \quad (3.22)$$

The ranges of these variables are given by:

$$\begin{aligned}
0 &\leq r_1, r_2, \rho < \infty \\
|r_1 - r_2| &\leq r_{12} \leq r_1 + r_2 \\
0 &\leq \theta_{12} \leq \pi \\
0 &\leq \phi, \zeta \leq \pi/2 \\
-1 &\leq x, C, B \leq 1.
\end{aligned} \tag{3.23}$$

The coordinate  $x$  maps the semi-infinite domain to a finite domain<sup>2</sup>. This simple choice works well because the wave function is exponentially small at large  $\rho$  for bound states which are the topic of interest here.

After integrating over the Euler angles the volume elements are

$$\int d^3\mathbf{r}_1 d^3\mathbf{r}_2 = 2\pi^2 \left\{ \begin{array}{l} 4 \int r_1 r_2 r_{12} dr_1 dr_2 dr_{12} \\ 4 \int r_1^2 r_2^2 \sin \theta_{12} dr_1 dr_2 d\theta_{12} \\ \int \rho^5 \sin^2 2\phi d\rho d\phi dC \\ \int \rho^5 \sin^2 2\zeta d\rho d\zeta dB \\ 2 \int \frac{(1-x)^5}{(1+x)^7} \sin^2 2\phi dx d\phi dC \\ 2 \int \frac{(1-x)^5}{(1+x)^7} \sin^2 2\zeta dx d\zeta dB. \end{array} \right. \tag{3.24}$$

The Hamiltonian for  $S$  states can be written in hyperspherical coordinates as:

$$\mathcal{H} = \mathcal{T}_\rho + \rho^{-2}(\mathcal{T}_\phi + \csc^2 2\phi \mathcal{T}_C) + \rho^{-1}\mathcal{U} \tag{3.25}$$

$$= \mathcal{T}_\rho + \rho^{-2}(\mathcal{T}_\zeta + \csc^2 2\zeta \mathcal{T}_B) + \rho^{-1}\mathcal{U}, \tag{3.26}$$

---

<sup>2</sup>One can introduce a free parameter  $L$  by defining  $x = (1 - \rho/L)/(1 + \rho/L)$  and vary  $L$  to optimize convergence but doing this led to only slight improvements. This finding is in agreement with Boyd et al. [26], who showed that  $L$  has a small effect for the hydrogen atom when using a Chebyshev basis.

where

$$\mathcal{T}_\rho = -\frac{1}{2}\partial_{\rho\rho} - \frac{5}{2\rho}\partial_\rho \quad (3.27)$$

$$= -\frac{(1+x)^4}{8}\partial_{xx} + \frac{(1+x)^3(4+x)}{4(1-x)}\partial_x \quad (3.28)$$

$$\mathcal{T}_\phi = -\left(\frac{1}{2}\partial_{\phi\phi} + 2\cot 2\phi\partial_\phi\right) \quad (3.29)$$

$$\mathcal{T}_C = -2\left((1-C^2)\partial_{CC} - 2C\partial_C\right) \quad (3.30)$$

$$\mathcal{T}_\zeta = -\left(\frac{1}{2}\partial_{\zeta\zeta} + 2\cot 2\zeta\partial_\zeta\right) \quad (3.31)$$

$$\mathcal{T}_B = -2\left((1-B^2)\partial_{BB} - 2B\partial_B\right) \quad (3.32)$$

$$\mathcal{U} = \frac{\alpha}{\sigma[C, \phi]} - Z \csc \phi - Z \sec \phi \quad (3.33)$$

$$= \frac{\alpha}{\sqrt{2} \sin \zeta} - \frac{Z\sqrt{2}}{\sigma[B, \zeta]} - \frac{Z\sqrt{2}}{\sigma[-B, \zeta]}, \quad (3.34)$$

and

$$\sigma[x, y] = \sqrt{1 + x \sin 2y}. \quad (3.35)$$

### 3.5 The singular points in the Hamiltonian

PS methods are very sensitive to discontinuous derivatives of any order. If such discontinuities exist, the method loses its exponential convergence and artificial oscillations may occur. The wave function has discontinuities only at the singular points which thus require special attention. Myers *et al* [113] discuss these singularities in detail. Here we reproduce some of their discussion for completeness.

### 3.5.1 Two-particle coalescences

There exist three lines corresponding to two-particle coalescences: two for the proton and each electron at  $\phi = 0$  and  $\phi = \pi/2$  and one for the two electrons at  $\zeta = 0$ . Only one of the proton-electron coalescence lines need appear in the numerical domain which takes advantage of the explicit symmetry of the spatial part of the wave function about  $\phi = \pi/4$ .

Kato [92] analyzed the discontinuity in the derivative of a wave function at two particle coalescence points and showed that

$$\left. \frac{\partial \hat{\psi}}{\partial r} \right|_{r=0} = \mu_{ij} q_i q_j \psi(r=0), \quad (3.36)$$

where  $\psi$  is the wave function,  $r$  is the particle-particle distance,  $\hat{\psi}$  is the limit of the average value of the wave function on a sphere centered at  $r = 0$  as its radius shrinks to zero,  $\mu_{ij}$  is the reduced mass of the two particles, and  $q_i$  and  $q_j$  are the charges of the two particles.

Pack and Byers Brown [117] extended the analysis to show that the wave function could be expanded in terms of hydrogenic solutions.

$$\psi = \sum_{lm} a_{lm} r^l Y_l^m[\theta, \phi] \left( 1 + \frac{q_i q_j \mu_{ij}}{l+1} r + O[r^2] \right), \quad (3.37)$$

where  $l \geq 0$ ,  $|m| \leq l$ ,  $a_{lm}$  is an expansion coefficient,  $\theta$  and  $\phi$  are the usual spherical angles giving the orientation of the two particles, and  $Y_l^m$  is the usual spherical harmonic.

These results describe the regularity required at the Coulomb singularities. There are three practical approaches to making sure the solution has the appropriate behavior.

## 1. Behavioral

Assume that local solutions to the Schrödinger equation that fail to satisfy Eqs. (3.36) and (3.37) are not analytic; assume that the expansion (cardinal functions) employed in the numerical treatment is incapable of representing this nonanalytic behavior. Granted these assumptions, all numerical solutions will automatically be regular at the point in question<sup>3</sup>. According to Boyd [25], in many contexts this approach is sufficient. If the solutions that do not satisfy Eqs. (3.36) and (3.37) have only weakly singular behavior, the convergence rate may be slow.

## 2. Regularity

Replace the Hamiltonian at the singular points with the Kato cusp conditions without otherwise altering the domain. The cusp conditions are

$$\left. \frac{\partial \hat{\psi}}{\partial \phi} \right|_{\phi=0} = -Z\rho\psi(\phi=0) \quad (3.38)$$

$$\left. \frac{\partial \hat{\psi}}{\partial \phi} \right|_{\phi=\pi/2} = Z\rho\psi\left(\phi = \frac{\pi}{2}\right) \quad (3.39)$$

$$\left. \frac{\partial \hat{\psi}}{\partial \zeta} \right|_{\zeta=0} = \frac{\alpha\rho}{2}\psi(\zeta=0) \quad (3.40)$$

or

$$\psi(\phi=0) = 0 \quad (3.41)$$

$$\psi\left(\phi = \frac{\pi}{2}\right) = 0 \quad (3.42)$$

$$\psi(\zeta=0) = 0, \quad (3.43)$$

where these two sets are mixed and matched while preserving the appropriate symmetry or antisymmetry. The choice depends on precisely which state one wishes to calculate.

---

<sup>3</sup>Because it is impossible to work where the potential diverges, the grid must be designed to exclude the point in question. The fact the grid does not contain the point is not a requirement of the behavioral approach.

### 3. Excision

Excise a small sphere around the singular points and impose boundary conditions on its surface that yield the correct behavior at the singularity as the sphere shrinks. From equation Eq. (3.37)

$$\psi = \sum_l b_l \rho^l \phi^l P_l[C] \left( 1 - \frac{Z\rho\phi}{l+1} + O[\rho^2\phi^2] \right) \quad (3.44)$$

$$\psi = \sum_l c_l \rho^l \tilde{\phi}^l P_l[C] \left( 1 - \frac{Z\rho\tilde{\phi}}{l+1} + O[\rho^2\tilde{\phi}^2] \right) \quad (3.45)$$

$$\psi = \sum_l d_l \rho^l \zeta^l P_l[B] \left( 1 + \frac{\alpha\rho\zeta\sqrt{2}}{2(l+1)} + O[\rho^2\zeta^2] \right), \quad (3.46)$$

where  $\tilde{\phi} = \pi/2 - \phi$ ,  $P_l$  is a Legendre polynomial of order  $l$ , and  $b_l$ ,  $c_l$ , and  $d_l$  are unknown constants. Define

$$\xi_l = \int_{-1}^1 \psi P_l[C] dC \quad (3.47)$$

$$\chi_l = \int_{-1}^1 \psi P_l[B] dB, \quad (3.48)$$

and write the conditions as

$$0 = \phi \frac{\partial \xi_l}{\partial \phi} + \left( -l + \rho\phi \frac{Z}{l+1} \right) \xi_l \quad (3.49)$$

$$= -\tilde{\phi} \frac{\partial \xi_l}{\partial \phi} + \left( -l + \rho\tilde{\phi} \frac{Z}{l+1} \right) \xi_l \quad (3.50)$$

$$= \zeta \frac{\partial \chi_l}{\partial \zeta} - \left( l + \frac{\alpha\rho\zeta\sqrt{2}}{2(l+1)} \right) \chi_l. \quad (3.51)$$

These conditions become exact as the excised volume shrinks to a point. For PS methods the volume should be reduced exponentially with increasing resolution. The changes do not increase the computational cost, but may adversely affect the condition number of the matrix.

The difficulty of implementation increases with number on the list.

### 3.5.2 Three particle coalescence

The potential is also singular when all three particles collide (i.e., when the hyperradius,  $\rho$  goes to zero). The behavior of the wave function about this point is much less well understood than two-particle coalescences and cannot be handled in the same way. Instead of simply having a discontinuity in the wave function's first derivative (the value of which is finite on both sides of the singularity), the second derivative grows logarithmically near  $\rho = 0$ . Bartlett [14] was the first to show that a simple Frobenius type expansion in powers of  $\rho$  about  $\rho = 0$  fails at second order on account of the electron-electron interaction. He suggested that logarithmic terms exist in the exact solution of helium. Fock [59, 60] introduced an expansion of the form

$$\psi = \sum_{n=0}^{\infty} \sum_{m=0}^{\lfloor n/2 \rfloor} e_{nm} \rho^n (\log \rho)^m, \quad (3.52)$$

where  $e_{nm}$  are two dimensional functions of the hyperangles  $\{\phi, C\}$  or  $\{\zeta, B\}$  determined through the recursive relationship

$$[n(n+4)+\Delta]e_{nm} = 2Ve_{n-1,m} - 2Ee_{n-2,m} - 2(n+2)(m+1)e_{n,m+1} - (m+1)(m+2)e_{n,m+2}, \quad (3.53)$$

and  $\Delta$  is the two-dimensional Laplacian over the hyperangles. All  $e_{nm}$  with  $n \leq 2$  are known analytically plus a few additional terms with higher  $n$  [1, 71, 72, 106]. Morgan proved that the series is convergent everywhere [109], and it has been shown that variational calculations converge faster when a single power of a logarithm is included in the basis [64]<sup>4</sup>.

Again, there are three basic strategies for a numerical scheme.

---

<sup>4</sup>Curiously, higher powers of the logarithm do not seem to improve the convergence rate of variational calculations [139].

### 1. Behavioral

Do nothing special and rely on the regularity of the cardinal functions. This is an imperfect approach since the exact wave function has unbounded second derivatives as  $\rho \rightarrow 0$ . If the basis set can only represent regular behavior as discussed in the case of two-particle coalescence it will not produce the exact solution. However, since the volume element scales as  $\rho^5 d\rho$  such inexactness may have negligible effect on observables calculated from the wave function.

### 2. Regularity

Impose a regularity-like condition at the singular point. For the ground state (and many other  $S$  states), the first-order solution [59, 60] to the Fock equations 3.53 is

$$e_{00} = c \tag{3.54}$$

$$e_{10} = c \left\{ -Z(\cos \phi + \sin \phi) + \frac{\alpha}{2} \sigma[C, \phi] \right\}, \tag{3.55}$$

where  $c$  is a constant given by the normalization. These solutions imply either

$$\partial_\rho \psi|_{\rho=0} = \left\{ -Z(\cos \phi + \sin \phi) + \frac{\alpha}{2} \sigma[C, \phi] \right\} \psi(\rho = 0), \tag{3.56}$$

which is valid for the ground state, or

$$\psi(\rho = 0) = 0. \tag{3.57}$$

Note that this regularity-like condition says nothing about the second derivatives. For the same reasons as above this method can never give the exact solution at  $\rho = 0$ .

### 3. Excision

Excise a small domain with  $\rho < \rho_{\min}$ , where  $\rho_{\min}$  is the cutoff. A boundary condition can be calculated on this inner surface by solving equation 3.53 to relate the wave function and normal derivative on the surface<sup>5</sup>. As the resolution increases, more terms must be calculated so that the truncation error in the Fock expansion equals the error due to having finite resolution in the numerical calculation. The basis set expansion in the bulk remains completely regular. While exact, the method is complicated and will be pursued at a later time.

### 3.5.3 Infinite separation

The domain of the ideal problem extends to infinity. The bound-state wave functions fall off exponentially. The outer boundary condition must be approximated in the numerical method. There are several approaches.

#### 1. Behavioral

Rely on the regularity of the cardinal functions to exclude exponentially growing solutions as  $\rho \rightarrow \infty$ . One must map the semi-infinite domain to a finite one to use Chebyshev collocation points or work with semi-infinite functions like Laguerre polynomials.

#### 2. Regularity

Again map the domain to a finite one but replace the Schrödinger equation at  $\rho = \infty$  by

$$\psi(\rho = \infty) = 0. \tag{3.58}$$

---

<sup>5</sup>The boundary condition is not known in analytic form (except at low order) but must be inferred by a numerical technique. Solutions to equation 3.53 can be found numerically with similar techniques as employed here for the full three dimensional problem.

Note that if one includes the endpoints using the behavioral method, this method is effectively the same as the behavioral condition because the Schrödinger equation reduces to  $E\psi = 0$  at  $x = -1$  ( $\rho = \infty$ ).

### 3. Excision

Excise the region with  $\rho > \rho_{\max}$  where  $\rho_{\max}$  is the cutoff and impose a suitable boundary condition. As in the three-particle coalescence, one may develop a more and more accurate representation at fixed  $\rho_{\max}$  and/or an approximate condition at increasing  $\rho_{\max}$ . It is easiest to set

$$\psi(\rho = \rho_{\max}) = 0 \quad (3.59)$$

or

$$\left. \frac{\partial \psi}{\partial \rho} \right|_{\rho=\rho_{\max}} = 0 \quad (3.60)$$

and vary  $\rho_{\max}$ , which is what is done in this article when using this method. In a PS numerical scheme one should vary  $\rho_{\max} \propto n^{1/2}$  for large  $n$  where  $n$  is the radial resolution (see Appendix A).

#### 3.5.4 Collinearity ( $B$ or $C = \pm 1$ )

The coefficients multiplying the second derivatives with respect to  $B$  and  $C$  at  $B, C = \pm 1$  go to zero. In ordinary differential equations this allows irregular solutions that behave as linear combinations of Legendre functions of the second kind. Regularity of the cardinal functions excludes such solutions. Since the Schrödinger equation at these points contains no infinities it does not matter if the grid includes these points. The partial differential equation is parabolic along this boundary. So no boundary conditions or regularity conditions need to be given.

### 3.6 The pseudospectral method

Boyd [25], Fornberg [62], Pfeiffer *et al* [122], and the third edition of *Numerical Recipes* [124] cover the PS method in detail. A brief review of some aspects pertinent to our work follows.

The main advantage of this method is that it provides exponentially fast convergence for smooth solutions. Unlike finite difference and finite element algorithms, all derivatives are calculated to higher and higher order with increasing resolution.

It is also noteworthy that the grid points are clustered more closely near the boundary of a domain than in its center. With this arrangement the representation of a function and its derivative is more uniformly accurate across the whole domain than is possible using an equal number of equidistant points. Finite difference and finite element methods typically use an equal-spaced grid and the derivatives are less accurate at the edge than at the center.

Let  $n_d$  be the number of coordinate dimensions and  $N_i$  the resolution in the  $i$ th dimension. The differential equation is enforced at  $n_t = \prod_{i=1}^{n_d} N_i$  collocation or grid points chosen to be the roots or extrema of a Jacobi polynomial of order  $N_i$  in each dimension. Boyd's recommendation that one use Chebyshev polynomials to generate the grid points in lieu of special circumstances is followed here [25].

The derivatives in the  $i^{\text{th}}$  direction are calculated to  $N_i^{\text{th}}$  order in terms of the function values at the collocation points. To illustrate this it is useful to define

the cardinal functions:

$$C_j^N[x] = \prod_{\substack{i=1 \\ i \neq j}}^N \frac{x - x^i}{x^j - x^i}, \quad (3.61)$$

where the  $x^i$ 's are the collocation points and  $i$  and  $j$  are superscripts not exponents. These functions have the property that

$$C_j^N[x^i] = \delta_j^i. \quad (3.62)$$

The PS representation of a function at an arbitrary  $n_d$ -dimensional position  $(x_1, \dots, x_{n_d})$  is expanded as

$$\psi \approx \psi_{N_1, \dots, N_{n_d}} = \psi^{j_1, \dots, j_{n_d}} F_{j_1, \dots, j_{n_d}}^{N_1, \dots, N_{n_d}}[x_1, \dots, x_{n_d}], \quad (3.63)$$

(using the Einstein summation convention) in terms of its grid values and the cardinal functions

$$\psi^{j_1, \dots, j_{n_d}} = \psi_{N_1, \dots, N_{n_d}}[x_1^{j_1}, \dots, x_{n_d}^{j_{n_d}}] \quad (3.64)$$

$$F_{j_1, \dots, j_{n_d}}^{N_1, \dots, N_{n_d}} = \prod_{i=1}^{n_d} C_{j_i}^{N_i}[x_i]. \quad (3.65)$$

Such an expansion is equivalent (up to an exponentially small error for smooth functions) to a spectral one,

$$\psi = s^{j_1, \dots, j_{n_d}} G_{j_1, \dots, j_{n_d}}[x_1, \dots, x_{n_d}], \quad (3.66)$$

where

$$G_{\mathbf{j}} = \prod_{i=1}^{n_d} u_{j_i}[x_i] \quad (3.67)$$

$$s^{j_1, \dots, j_{n_d}} = \int \psi G_{\mathbf{j}} \prod_{i=1}^{n_d} w[x_i] dx_i \quad (3.68)$$

$$\approx \psi^{i_1, \dots, i_{n_d}} G_{\mathbf{j}}[x_1^{i_1}, \dots, x_{n_d}^{i_{n_d}}] \prod_{k=1}^{n_d} v_{i_k}, \quad (3.69)$$

$\mathbf{j}$  means  $j_1, \dots, j_{n_d}$ ,  $u_{j_i}$  are orthonormal polynomials chosen here to be Chebyshev polynomials,  $w$  is the weight function over which they are orthonormal,

and  $v_{i_k}$  are the corresponding quadrature weights. Note, the collocation points are also quadrature points which allow exponential convergence of the quadrature. Derivatives of  $\psi$  are approximated by differentiating Eq. (3.63). To this end, it is useful to introduce differentiation matrices,

$$(D_N)_j^i = \partial_x C_j^N[x]|_{x=x^i}. \quad (3.70)$$

This method is readily applied to linear eigenvalue problems as arise from the Schrödinger equation <sup>6</sup>

$$(\mathcal{H} - E)\psi = 0, \quad (3.71)$$

where  $\mathcal{H}$  is the Hamiltonian operator,  $\psi$  is the wave function, and  $E$  is the energy eigenvalue. Discretizing on the grid gives the tensor equation

$$H_{j_1, j_2, \dots, j_{n_d}}^{i_1, i_2, \dots, i_{n_d}} \psi^{j_1, j_2, \dots, j_{n_d}} = E \psi^{i_1, i_2, \dots, i_{n_d}}, \quad (3.72)$$

where

$$H_{j_1, j_2, \dots, j_{n_d}}^{i_1, i_2, \dots, i_{n_d}} = \mathcal{H} F_{j_1, j_2, \dots, j_{n_d}} [x_1^{i_1}, x_2^{i_2}, \dots, x_{n_d}^{i_{n_d}}]. \quad (3.73)$$

Unlike finite difference methods, the tensor  $H_{j_1, j_2, \dots, j_{n_d}}^{i_1, i_2, \dots, i_{n_d}}$  is dense. Write this as  $H_{l(j_1, j_2, \dots, j_{n_d})}^{k(i_1, i_2, \dots, i_{n_d})}$  or for short  $H_l^k$ , where  $k$  and  $l$  are one-to-one functions mapping the set of  $n_d$  indices to the lowest  $n_t$  positive integers. This recasts the tensor as a large matrix so that standard matrix methods can be employed.

One way to carry out the mapping employs the Kronecker product as follows. If  $\mathcal{H}$  is given by

$$\mathcal{H} = \sum_{i_1, \dots, i_{n_d}} f_{i_1, \dots, i_{n_d}} [x_1, \dots, x_{n_d}] (\partial_{x_1})^{i_1} \dots (\partial_{x_{n_d}})^{i_{n_d}}, \quad (3.74)$$

where  $f_{i_1, \dots, i_{n_d}}$  is a function coefficient, then the matrix,  $H$  is given by

$$H_l^k = \sum_{i_1, \dots, i_{n_d}} f_{i_1, \dots, i_{n_d}} [\mathbf{x}^k] \left( \bigotimes_{j=1}^{n_d} (D_{N_j})^{i_j} \right)_l^k, \quad (3.75)$$

---

<sup>6</sup>Linearity is not required for the PS method.

where  $\mathbf{x}^k$  is the  $n_d$ -dimensional vector of coordinates with indices that map to  $k$ ,  $N_j$  is the number of grid points in the  $j^{\text{th}}$  direction,  $i_j$  is an exponent, and  $D_{N_j}$  is the differential matrix based on  $N_j$  points.

### 3.7 Pseudospectral convergence for nonsmooth functions

To make appropriate design algorithmic choices it is important to investigate how the PS method handles nonsmooth behavior of solutions. This section explores the convergence of truncated cardinal function expansions to cusps and logarithmic terms and then employs a toy model that illustrates how the triple coalescence is expected to influence the numerical results.

#### 3.7.1 Kato cusps

Consider the ground state of the hydrogen atom with wave function

$$\psi = e^{-r} = e^{-\sqrt{x^2+y^2+z^2}}. \quad (3.76)$$

In Cartesian coordinates, there is a discontinuity in the first derivative at the origin,

$$\lim_{x \rightarrow 0^+} \frac{\partial \psi}{\partial x} \Big|_{y=z=0} \neq \lim_{x \rightarrow 0^-} \frac{\partial \psi}{\partial x} \Big|_{y=z=0}. \quad (3.77)$$

In spherical coordinates no discontinuity exists for  $r \geq 0$ . All the derivatives at  $r = 0$  are well defined and a PS code has no problem exponentially converging toward the correct answer. The essence of this observation can be seen by

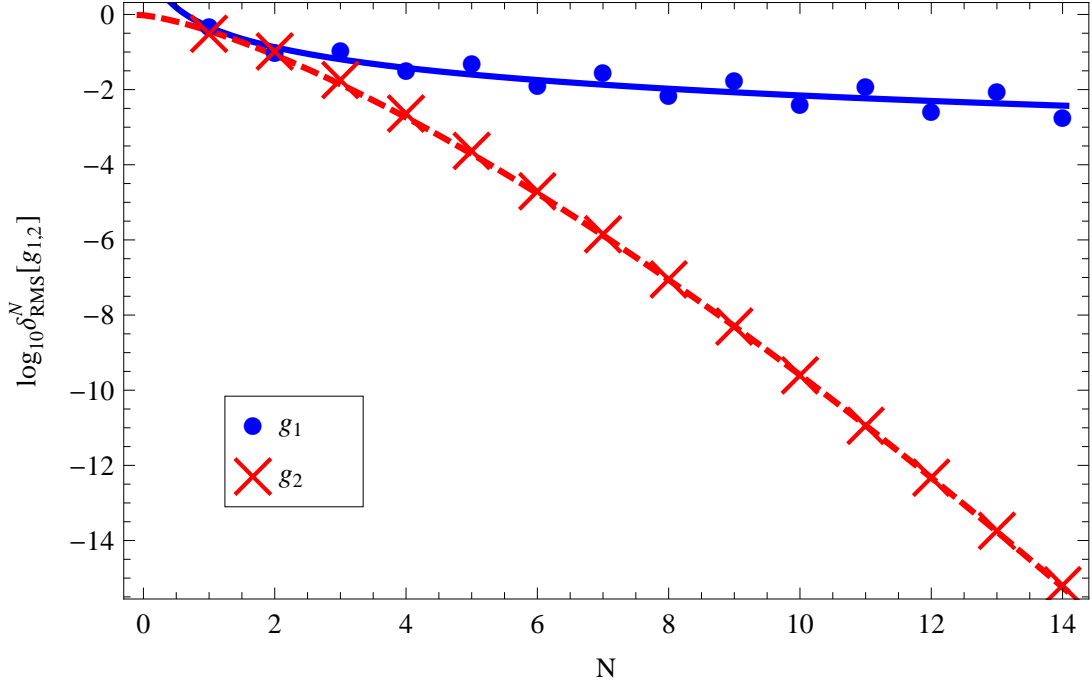


Figure 3.1: (Color online). The logarithm base 10 of  $\delta_{\text{RMS}}^N[g_1]$  (blue circles) and  $\delta_{\text{RMS}}^N[g_2]$  (red crosses) with solid blue and dashed red fits, respectively. See Appendix B for fitting functions.

considering the one-dimensional exponential functions

$$g_1[x] = e^{-|x|} \quad (3.78)$$

$$g_2[x] = e^{-(x+1)}, \quad (3.79)$$

on the domain  $-1 \leq x \leq 1$  with weight  $x^2$  (analogous to the three dimensional hydrogen atom). As a measure of error between the function  $f$  and its cardinal expansion truncated at order  $n$  define

$$\delta_{\text{RMS}}^N[f] = \sqrt{\int_{-1}^1 x^2 \left( f[x] - \sum_{i=1}^N C_i^N[x] f[x^i] \right)^2 dx}. \quad (3.80)$$

Figure 3.1 compares  $\delta_{\text{RMS}}^n[g_1]$  to  $\delta_{\text{RMS}}^n[g_2]$  as a function of  $n$ . Evidently the cusp is poorly represented compared to the smooth function at a given  $n$ . The PS

representation of the cusp converges algebraically while the representation of the smooth function converges supergeometrically (see Appendix B for fits).

The basic strategy in more complicated problems is to adopt a coordinate system with a radial-like coordinate at each cusp. For two-electron atoms no global coordinate system exists with the desired property at each of the three separate two-particle coalescences. This article uses three individual but overlapping domains to guarantee appropriate treatment near each coalescence point.

### 3.7.2 Logarithmic terms

Consider the one-dimensional function

$$f[x] = \left( 1 + \frac{1}{2}\alpha\rho[x]^2 \log[\rho[x]] \right) e^{-\rho[x]}, \quad (3.81)$$

where

$$\rho[x] = \frac{1-x}{1+x}. \quad (3.82)$$

Here  $\rho \in [0, \infty)$ ,  $x \in [-1, 1]$  and  $f$  are analogous to the hyperspherical radius, its algebraic transformation and the heliumlike wavefunction  $\psi$ , respectively. As in the full three-dimensional problem, the presence or absence of the logarithmic terms is controlled by  $\alpha$ , which can be set to 0 or 1.

There are two types of errors considered here: interpolation error and operator error. These are different sorts of error, but qualitative features (e.g., exponential or algebraic convergence) are expected to be the same.

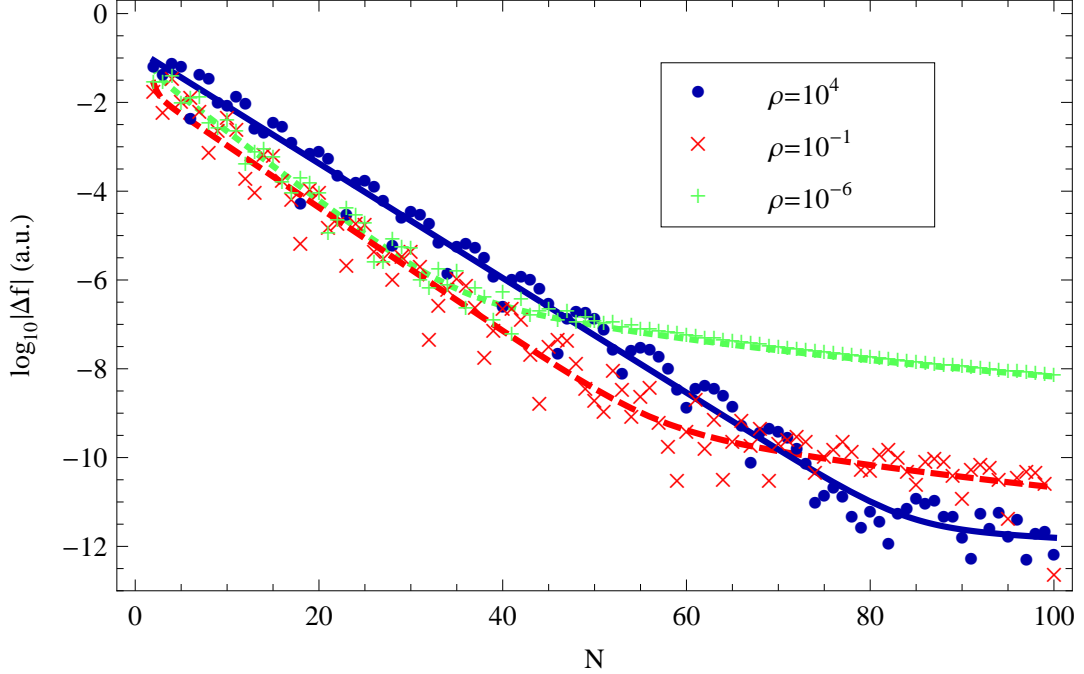


Figure 3.2: (Color online). The logarithm base 10 of the error in  $f[x]$  using cardinal functions at  $\rho = 10^{-6}$  (green pluses),  $\rho = 10^{-1}$  (red crosses), and  $\rho = 10^4$  (blue circles) with solid blue, dashed red, and dotted green fits, respectively. See Appendix B for fitting functions and method.

### Interpolation error

The pointwise error between  $f$  and its truncated expansion is

$$\Delta f = f[x] - \sum_{i=1}^N C_i^N[x] f[x^i], \quad (3.83)$$

where  $x^i$  refers to the  $i$ th grid point.

Figure 3.2 shows that the behavior of  $\Delta f$  at three different values of  $\rho$ . For each value the apparent rate of convergence starts out exponential before becoming algebraic at large  $N$ . The algebraic convergence known with the highest accuracy in Fig. 3.2 is for  $\rho = 10^{-6}$ , which asymptotically goes as  $1/N^{3.82 \pm 0.09}$

(see Appendix B). This algebraic behavior is expected when trying to represent a nonanalytic function ( $\log[\rho]$ ) with an analytic basis. Such behavior disappears if  $\alpha$  is set to zero.

The onset of algebraic convergence varies from  $N \approx 40$  to  $N \approx 80$  as  $\rho$ , moving away from the singularity, increases by 10 orders of magnitude. The error at the transition is  $< 10^{-6}$ . Typically, energy errors vary as the square of wave function errors and would already be very small compared to relativistic corrections. This calculation shows that it is possible to get precise values with apparent exponential convergence before reaching the asymptotic algebraic regime. As a practical matter, one may never reach the latter limit.

### **Operator error**

In order to estimate the error in the eigenvalue, it would help to have a one-dimensional toy eigenvalue problem with an eigenfunction similar to the function in Eq. (3.81). It is impossible to construct a one-dimensional eigenvalue problem with solutions that have logarithmic singularities without explicitly introducing such singularities into the differential operator. So here a more limited test problem is used. Instead of solving for an eigenvalue, the error in the operator is measured. This would contribute to the eigenvalue error along with the error in the wave function.

Let  $\Delta\mathcal{H}$  be the difference between the true Hamiltonian and the Hamiltonian constructed from PS differentiation matrices. The associated energy error is  $\langle\psi|\Delta\mathcal{H}|\psi\rangle$ . The aim is to construct an analog of the integrand of the energy error and use it to assess pointwise and integral errors.

Construct a differential operator  $\mathcal{D}$  similar to the full Hamiltonian  $\mathcal{H}$  [see Eq. (3.25)] but in terms of the coordinate  $x$ ,

$$\mathcal{D} = p_2[x]\partial_{xx} + p_1[x]\partial_x + p_0[x], \quad (3.84)$$

where

$$p_2[x] = -\frac{(1+x)^4}{8} \quad (3.85)$$

$$p_1[x] = \frac{(1+x)^3}{4} \left( \frac{4+x}{1-x} \right) \quad (3.86)$$

$$p_0[x] = -\frac{1}{\rho[x]}. \quad (3.87)$$

Note, the first two terms are identical to the operator  $\mathcal{T}_\rho$  and the last term is a Coulomb potential.

The corresponding matrix operator is

$$(d_N)_j^i = p_2[x^i](D_N)_k^i(D_N)_j^k + p_1[x^i](D_N)_j^i + p_0[x^i]\delta_j^i, \quad (3.88)$$

where Einstein's summation convention is used and  $\delta_j^i$  is the Kronecker delta function. The pointwise error on the grid and its maximum are

$$(\Delta H_N)^i = w[x^i] \left( (\mathcal{D}f)[x^i] - \sum_j (d_N)_j^i f[x^j] \right) \quad (3.89)$$

$$\Delta H_N^{\max} = \max_i |(\Delta H_N)^i|, \quad (3.90)$$

where

$$w[x] = \frac{(1-x)^5}{(1+x)^7} f[x] \quad (3.91)$$

The factor  $(1-x)^5/(1+x)^7$  comes from the Jacobian.

Figure 3.3 shows  $\Delta H_N^{\max}$ , the maximum error anywhere on the grid, as a function of  $n$  for  $\alpha = 0$  and  $\alpha = 1$ . The decrease appears to be exponential, not unanticipated when  $\alpha = 0$  but perhaps a surprise for  $\alpha = 1$ . The slopes

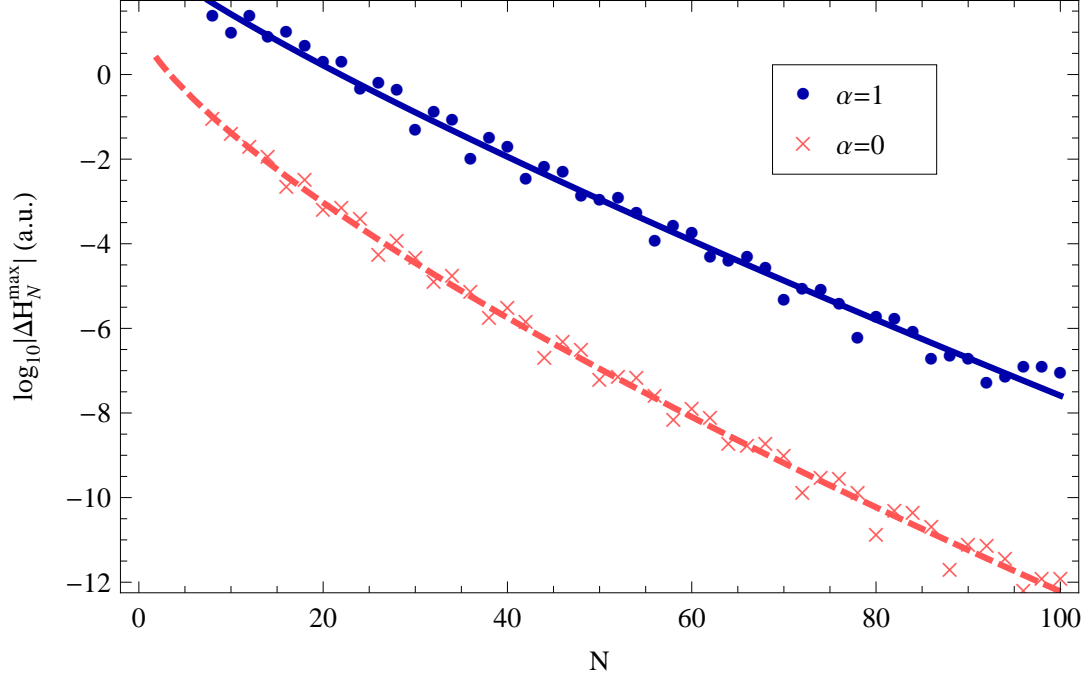


Figure 3.3: (Color online). The logarithm base 10 of the maximum error of a pseudospectral matrix. The dark blue circles are for  $\alpha = 1$  and the light red crosses for  $\alpha = 0$  with solid blue and dashed red fits, respectively. See Appendix B for fitting functions and method.

of the two curves are roughly the same and the offset is due to the variation of the magnitude of  $f$  with  $\alpha$ . An explanation is immediately suggested by Fig. 3.4 which shows the error at the grid point closest to the singularity  $(\Delta H_N)^{i^*}$  (here  $i^*$  refers to that point). The data for  $\alpha = 1$  is well fit by an algebraic rate of convergence  $(1/N^{10.36 \pm 0.08})$  at large  $N$  while  $\alpha = 0$  has an approximately exponential fall-off (the convergence is subgeometric because the calculation is done on a semi-infinite domain). The log term *does* spoil the method's exponential convergence. Assuming that the effect is greatest at  $i = i^*$ , the maximum error is dominated by the log term when  $N$  is greater than about 200 and the error is *very* small. This is exponential convergence "for all practical purposes."

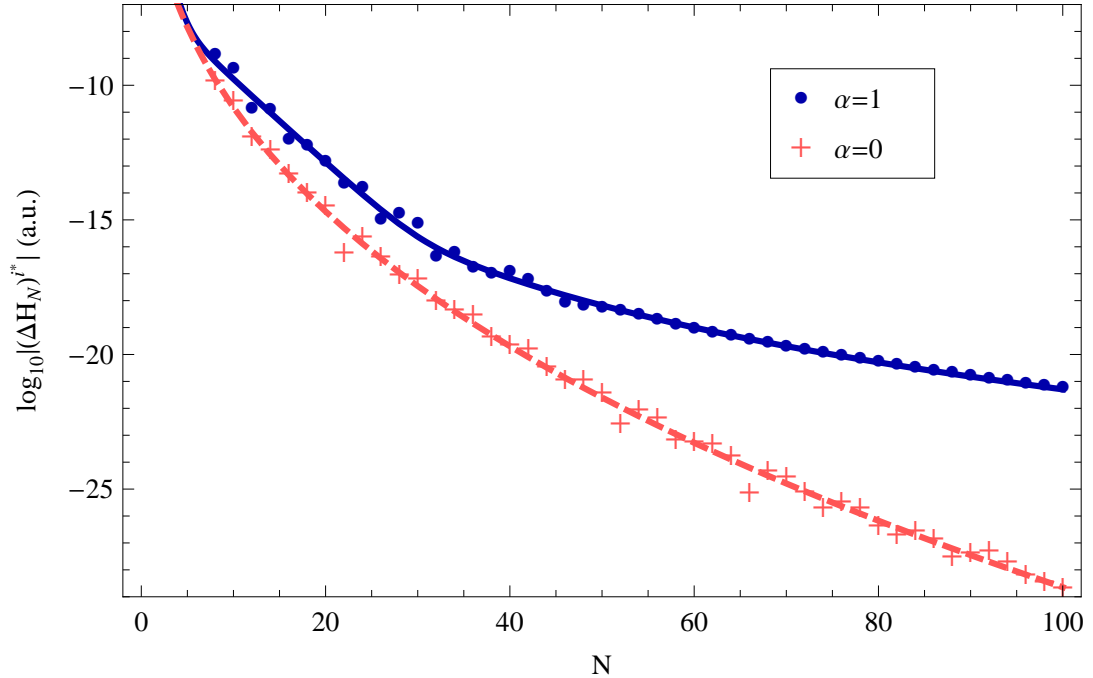


Figure 3.4: (Color online). The logarithm base 10 of the error of a pseudospectral matrix near the singularity. The dark blue circles are for  $\alpha = 1$  and the light red pluses for  $\alpha = 0$  with solid blue and dashed red fits, respectively. See Appendix B for fitting functions and method.

### 3.7.3 Conclusion

For the interpolation and operator errors, the logarithmic term does not slow convergence unless one is at high resolution or interested in small values of  $\rho$ . For those cases, one would need to apply the excision method about the triple coalescence point in order to retain exponential convergence. For most applications the level of precision needed is obtained before the algebraic behavior becomes apparent.

### 3.8 Numerical domains and collocation points

Because the two electrons are identical particles the full wave function is anti-symmetric. In the ground state, the spins are antisymmetric and the spatial part is symmetric. The spatial domain may be taken as  $\phi < \pi/4$  and  $B > 0$ . The complete numerical domain is

$$\begin{aligned}
 D_0 : \quad & -1 \leq x \leq 1 \quad 0 \leq \phi \leq \frac{\pi}{4} \quad -1 \leq C \leq 1 \\
 & \text{or} \\
 D_0 : \quad & -1 \leq x \leq 1 \quad 0 \leq \zeta \leq \frac{\pi}{2} \quad 0 \leq B \leq 1.
 \end{aligned} \tag{3.92}$$

A single domain does not allow the proper treatment of the two-particle coalescences. Therefore, introduce three subdomains to cover  $D_0$  using two different sets of variables:

$$\begin{aligned}
 D_1 : \quad & -1 \leq x \leq 1 \quad 0 \leq \phi \leq \frac{1}{2} \quad -1 \leq C \leq 1 \\
 D_2 : \quad & -1 \leq x \leq 1 \quad \frac{1}{2} \leq \phi \leq \frac{\pi}{4} \quad -\frac{2}{3} \leq C \leq 1 \\
 D_3 : \quad & -1 \leq x \leq 1 \quad 0 \leq \zeta \leq \frac{1}{2} \quad 0 \leq B \leq 1.
 \end{aligned} \tag{3.93}$$

For calculations done on a finite domain, the condition  $-1 \leq x \leq 1$  is replaced by  $0 \leq \rho \leq \rho_{\max}$ . Cross sections of these domains at fixed  $\rho$  are shown in Fig. 3.5. An electron-proton singularity lies in  $D_1$ , while the electron-electron singularity lies in  $D_3$ . The radial-like coordinates in  $D_1$  ( $\phi$ ) and  $D_3$  ( $\zeta$ ) accommodate the cusps just like the usual radial coordinate does in the hydrogen atom.  $D_2$  fills in the remaining volume. All three domains have boundaries that touch the triple coalescence point (not pictured).

Consideration of the electron-electron singularity shows why the single domain  $D_0$  is inadequate. Byers Brown and White [30] showed that the wavefunction can be expanded in powers of  $r_{12}$  about  $r_{12} = 0$ . Using such a coordinate

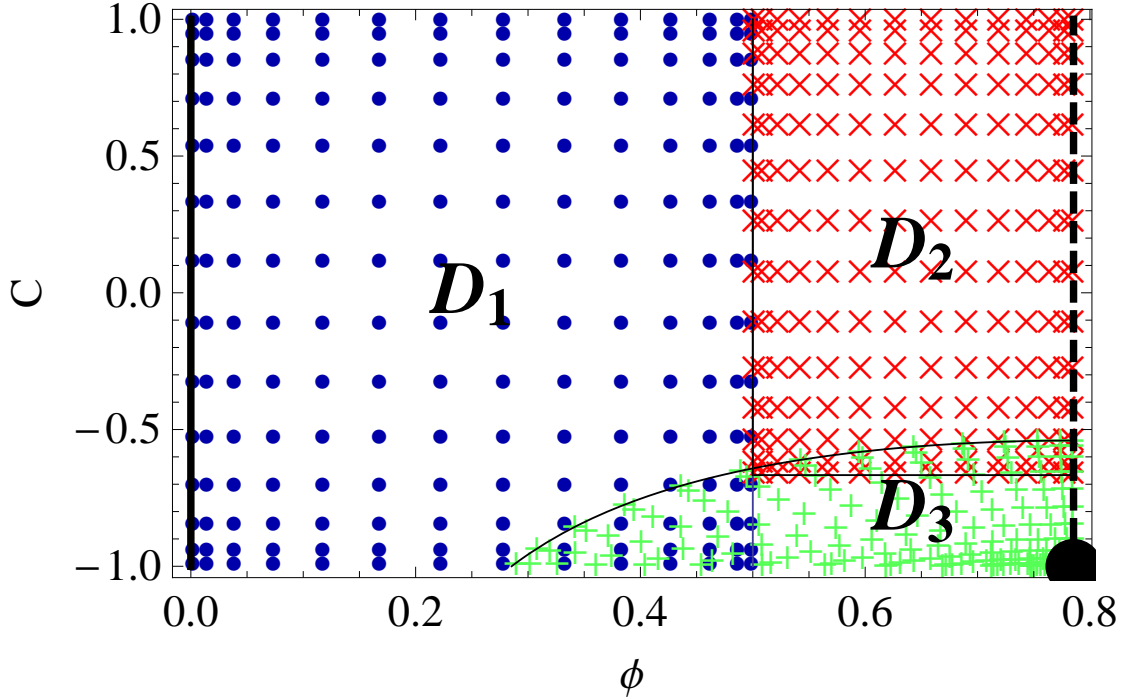


Figure 3.5: (Color online). This is the arrangement of grid points of the three domains at a constant value of  $\rho$  in  $\phi$  and  $C$  coordinates. Note that the point density becomes larger at the boundary of each subdomain and that no grid points sit on the Coulomb singularities. The blue circles, red crosses, and green pluses belong to domains  $D_1$ ,  $D_2$ , and  $D_3$ , respectively.  $D_1$  and  $D_2$  are rectangular domains, while  $D_3$  has the curved boundary in  $\phi, C$  coordinates but is rectangular in  $\zeta, B$  coordinates. The electron-proton singularity occurs on the left side (solid line at  $\phi = 0$ ). The entire line corresponds to one physical point. The electron-electron singularity occurs at the lower right-hand corner (solid disk at  $\phi = \pi/4, C = -1$ ). A line of symmetry falls on the right side (dashed line at  $\phi = \pi/4$  where  $r_1 = r_2$ ).

accurately treats the cusp away from the triple coalescence point. The expansion in powers of  $\zeta$  is very similar [see Eq. (3.46)] or equivalently powers of  $\sqrt{2} \sin \zeta = \sqrt{1 + C \sin 2\phi}$ <sup>7</sup>. Re-expanding in  $\phi$  and  $C$  coordinates gives derivatives of  $\sqrt{1 + C \sin 2\phi}$  with respect to  $C$  and  $\phi$ , terms that are either infinite or undefined at  $\phi = \pi/4$  and  $C = -1$ . This is why the PS method fails to converge rapidly using  $D_0$  alone.

Within each domain, grid points are set as follows. Let the  $i$ th dimension extend from  $x_{i,\min}$  to  $x_{i,\max}$  and have  $N_i$  collocation points. These points are the roots or antinodes plus endpoints of the  $N_i^{\text{th}}$  order Chebyshev polynomial<sup>8</sup> stretched to fit length  $\Delta x_i = x_{i,\max} - x_{i,\min}$ . The  $j$ th point (for  $j = 1, 2, \dots, N_i$ ) of dimension  $i$  is

$$x_i^j = \frac{\Delta x_i}{2}(y_i^j + 1), \quad (3.94)$$

where

$$y_i^j = \cos \left[ \frac{(N_i - j + \lambda)\pi}{N_i} \right] \quad (3.95)$$

and  $\lambda$  is 0 or 1/2 for nodes or antinodes plus endpoints, respectively<sup>9</sup>. In this article, nodes are generally used except when explicit boundary conditions are needed at both endpoints,  $x_{i,\min}$  and  $x_{i,\max}$ .

Potentially each dimension and domain could have its own  $N_i$  but in this paper the  $x$  direction is set to be twice as large as the other two dimensions and all are varied in lockstep. That is,  $\{N_x, N_C, N_\phi\} = \{2n, n, n\}$  in domains  $D_1$  and  $D_2$  and  $\{N_x, N_B, N_\zeta\} = \{2n, n, n\}$  in domain  $D_3$ . The total number of grid

---

<sup>7</sup>The radius of convergence of the Byers Brown and White expansion is unknown to the authors but is clearly invalid at  $\rho = 0$ , the location of the triple coalescence point. Here only the effect of the double coalescence point is being considered.

<sup>8</sup>When the excision method is used near the two-particle coalescence points, the nodes of Legendre polynomials are used in the  $B$  and  $C$  directions. This choice makes it easier to apply Eq. (3.49) with a simple quadrature.

<sup>9</sup>It is also possible to use the so called Chebyshev-Randau points, which include one endpoint on one side of the domain but not the other.

points is  $n_t = 3 \times (2n \times n \times n) = 6n^3$  points. Twice as many points were used in the  $x$  dimension, an arbitrary choice but one motivated by the semi-infinite range of the hyperspherical coordinate and by the wave function's logarithmic dependence on the hyperspherical radius near the triple coalescence point.

## 3.9 Boundary conditions

### 3.9.1 Internal boundary conditions

It is necessary to ensure continuity of the wave function and its normal derivative at internal boundaries. There are two ways in which the subdomains can touch: they can overlap or they can barely touch. For clarity, consider a one-dimensional problem with two domains. Let the first domain be domain 1 and the second be domain 2 with extrema  $x_{1,\min} < x_{2,\min} \leq x_{1,\max} < x_{2,\max}$ , where the 1 and 2 now refer to domain number. The first case corresponds to  $x_{2,\min} < x_{1,\max}$  and the second to  $x_{2,\min} = x_{1,\max} \equiv x_*$ . For both cases, exactly two conditions are need to make the wave function and its derivative continuous. The simplest choice for the first case is

$$\psi_1[x_{1,\max}] = \psi_2[x_{1,\max}] \quad (3.96)$$

$$\psi_1[x_{2,\min}] = \psi_2[x_{2,\min}], \quad (3.97)$$

and for the second case is

$$\psi_1[x_*] = \psi_2[x_*] \quad (3.98)$$

$$\frac{d}{dx}\psi_1[x_*] = \frac{d}{dx}\psi_2[x_*]. \quad (3.99)$$

For multidimensional grids, the situation is analogous. The conditions are applied on surfaces and the derivatives are normal derivatives at the surface. On a discrete grid, a finite number of conditions are given which, in the limit of an infinitely fine mesh, would cover the entire surface. There is a great deal of freedom in the selection of the points but in this article the edge of a domain has one constant coordinate so there is a natural choice. Conditions are imposed at the points of the finite mesh formed by varying all the other coordinates (in general, these are not collocation points). In other words, the matching points lie at the intersection of the coordinate lines normal to the surface with the surface itself. The positions of the crosses in Figs. 3.6 and 3.7 illustrate where the matching occurs when the domains overlap and when they just touch.

For touching domains, the black and white crosses in Fig. 3.7 are used. Note that four (three) crosses are defined by the coordinate lines in  $D_2$  ( $D_1$ ). At the set of four crosses, function values are equated, and at the set of three crosses, normal derivatives are equated. In general, function values (derivatives) are equated at points stemming from the subdomain with a greater (lesser) density of points along the boundary.

For overlapping domains, the function values are equated at the black and white crosses in Fig. 3.6 which lie on two separate surfaces. The points are selected in a manner similar to that of touching domains, i.e. in terms of the intersection of the coordinate lines in  $D_1$  and  $D_3$  with the surface.

In all cases, values and derivatives at all points are calculated using Eq. (3.63) and are ultimately linear combinations of the grid point values.

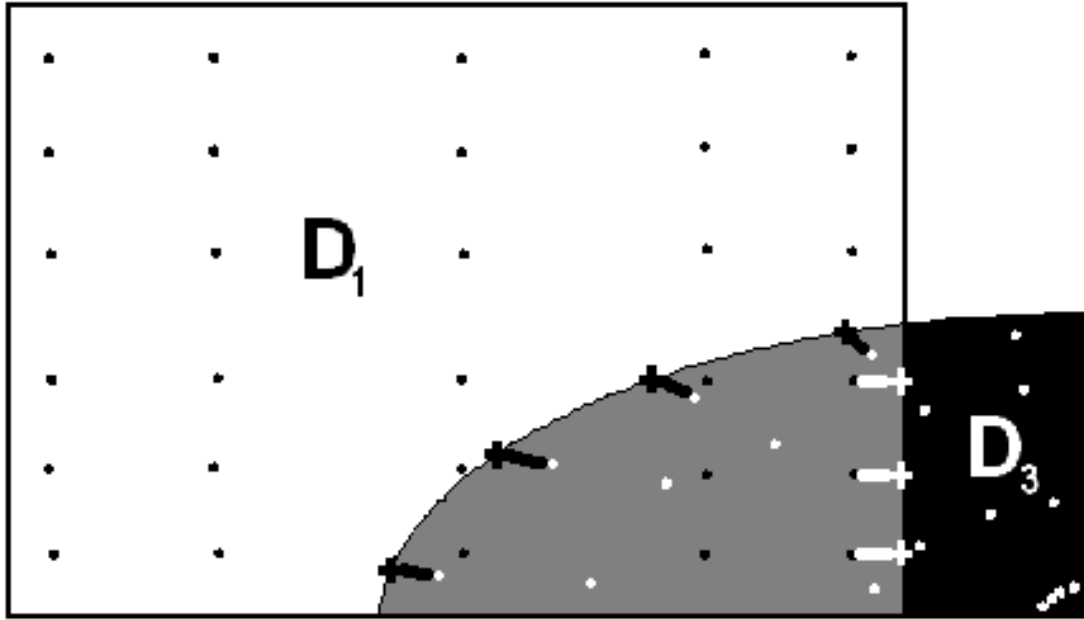


Figure 3.6: The intersection (gray) of domains  $D_1$  (white) with black grid points and  $D_3$  (black) with white grid points. The boundary points are depicted as black and white crosses and are connected via black and white lines to the grid points that they replace.

### 3.9.2 Symmetry and regularity conditions

For this problem there are two types of boundary conditions on the boundary of the numerical domain: the symmetry condition from electron exchange and the regularity conditions imposed near singular points.

The symmetry condition is related to the total spin of the two electrons,  $S$ . If  $S = 0$  ( $S = 1$ ) the wave function is symmetric (antisymmetric) about  $\phi = \pi/4$  or  $B = 0$  and the normal derivative (value) of the wave function is equal to zero. This condition is enforced at all the points on the boundary that have the same  $\rho$  and  $C$  coordinates as grid points in  $D_2$  or the same  $\rho$  and  $\zeta$  coordinates in  $D_3$ . This gives  $2 \times 2n \times n = 4n^2$  boundary conditions.

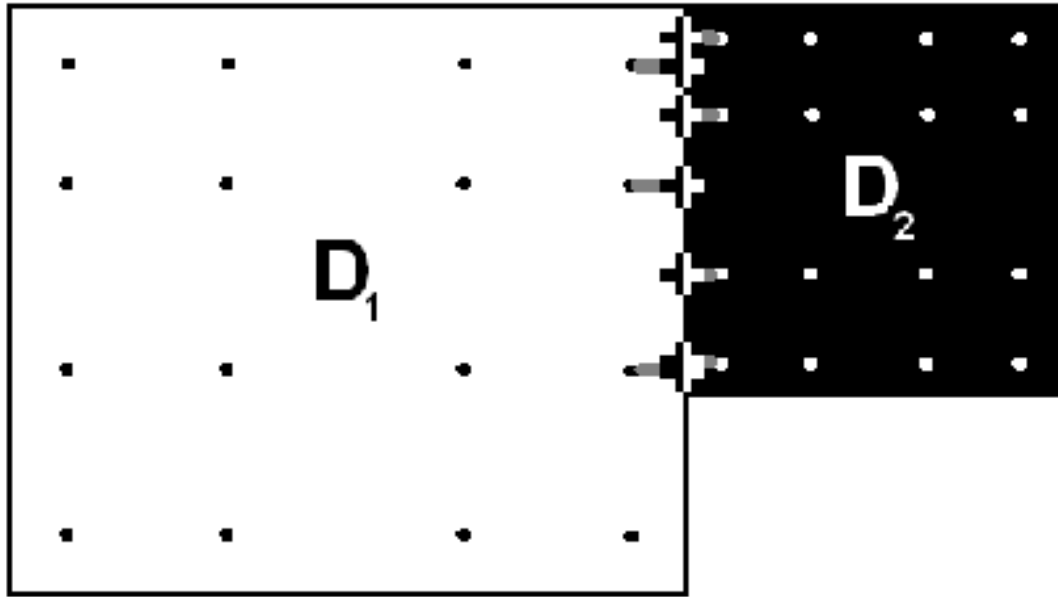


Figure 3.7: Barely touching domains  $D_1$  (white) with black grid points and  $D_2$  (black) with white grid points. The boundary points are depicted as black and white crosses and are connected via gray lines to the grid points that they replace.

Regularity conditions are imposed as boundary conditions at four two-dimensional surfaces:  $\rho = 0$ ,  $\rho = \infty$ ,  $\phi = 0$ , and  $\zeta = 0$ . These are similar in form to the symmetry condition except involve linear combinations of derivative and value. Depending on which type of conditions are given at singular points (behavioral versus regularity or excision) are used, there are 0 to  $10n^2$  conditions. These conditions replace an equal number of equations. The particular equation replaced is the one that stems from enforcement of the discretized Schrödinger equation at the collocation point nearest to the boundary at which the condition applies.

The most complicated type of boundary condition arises when a region is excised about a two-particle coalescence. First, one must project out terms proportional to each Legendre polynomial by performing an integral over  $C$  or  $B$ .

This can be done by quadrature over the grid points in those dimensions. For example, Eq. (3.47) turns into

$$\xi_l[\rho^i, \phi^j] = \sum_k w_k P_l[C^k] \psi[\rho^i, \phi^j, C^k], \quad (3.100)$$

where  $w_k$  are the quadrature weights. Then Eq. (3.49) becomes for  $j = 1$  (the excision boundary)

$$0 = \left( \phi^j (D_{N_\phi})_k^j + \left( -l + \frac{\rho^i \phi^j Z}{l+1} \right) \delta_k^j \right) \xi_l[\rho^i, \phi^k], \quad (3.101)$$

which is  $N_\rho N_C$  conditions ( $0 \leq l \leq N_C - 1$  and  $1 \leq i \leq N_\rho$ ).

### 3.9.3 Incorporating boundary conditions into the matrix problem

All of the above boundary conditions are expressed as a linear combination of the function values at the grid points equal zero. In matrix form

$$\underbrace{n_b \{ (B_1 B_2) \}}_{n_b + n_i} \begin{pmatrix} \psi_1 \\ \psi_2 \end{pmatrix} \begin{matrix} \} n_b \\ \} n_i \end{matrix} = 0, \quad (3.102)$$

where  $\psi_1$  ( $\psi_2$ ) is a vector of the  $n_b$  ( $n_i$ ) wave function values at all the boundary (interior) points, the boundary condition matrix has been broken into an  $n_b$  by  $n_b$  matrix  $B_1$  and an  $n_b$  by  $n_i$  matrix  $B_2$ , and  $n_b + n_i = n_t$ . For the case where an endpoint is not a collocation point, the grid point nearest to the boundary, at which an explicit boundary condition is given, is considered as a boundary point. All the points near where behavioral boundary conditions are given are not included in this definition. These points are the ones that give rise to the first  $n_b$  rows in Eqs. (3.102) and (3.103). Note, that this ordering was chosen for clarity in this section.

There is also the Hamiltonian matrix equation

$$\begin{matrix} n_b \{ \\ n_i \{ \end{matrix} \underbrace{\begin{pmatrix} H_{11} - E & H_{12} \\ H_{21} & H_{22} - E \end{pmatrix}}_{n_b+n_i} \begin{pmatrix} \psi_1 \\ \psi_2 \end{pmatrix} = 0, \quad (3.103)$$

where the Hamiltonian matrix has also been divided into four matrices:  $H_{11}$ ,  $H_{12}$ ,  $H_{21}$  and  $H_{22}$ .

So there are  $n_t + n_b$  equations and  $n_t$  unknowns ( $\psi_1$  and  $\psi_2$ ) as well as the eigenvalue. One could approximately solve these equations with singular value decomposition [124], but it is much faster to simply discard the first  $n_b$  rows of the Hamiltonian matrix and incorporate the boundary conditions into the remaining eigenvalue problem:

$$(H_{22} - H_{21}B_1^{-1}B_2 - E)\psi_2 = 0, \quad (3.104)$$

where  $B_1$  has an inverse because all of its rows are linearly independent (otherwise more than one boundary condition would have been specified for a given boundary point). Calculating the inverse is not too computationally expensive because  $n_b \ll n_t$ . Then solve for  $\psi_1$  afterwards with

$$\psi_1 = -B_1^{-1}B_2\psi_2. \quad (3.105)$$

### 3.10 Matrix methods

In one dimension the Hamiltonian matrix for the PS method is dense but in three dimensions with three domains the number of nonzero elements scales as  $24n^4$  out of a possible  $36n^6$ . The boundary condition matrix is also sparse with  $8n^4$  non-zero elements out of  $48n^5$  (for the simplest case where behavioral

conditions are used whenever possible). Therefore, any attempt to solve these equations should take advantage of these memory savings.

Equation (3.104) is solved by the method of inverse iteration [124] after shifting the eigenvalue with an approximately known value. In cases where the exact eigenvalue is not known *a priori*, one solves the full eigenvalue problem for a low resolution case first and then at each successive iteration shifts the eigenvalue using the result of the previous iteration. Because the Hamiltonian matrix is not symmetric, a complex eigenvalue may occur. There is no theoretical reason prohibiting the numerical eigenvalue from containing an imaginary part at finite resolution but, in fact, none were generated for  $n > 5$ . Of course, the imaginary part contributes to the error which must converge to zero.

The above solution method can yield highly oscillatory wave functions which appear to diverge on the boundaries of the computational domain. These nonphysical wave functions do not satisfy the first  $n_b$  rows of Eq. (3.103) and arise as an artifact of solving a subset of equations of the overdetermined system. They are easily identified and rejected and in no way affect the true solution.

The entire calculation for  $n = 14$  took only about 20 minutes on a 6-GHz machine. Memory needed to solve the linear equations was the limiting factor because inverting the equation has requirements scaling as  $n^6$ . The generalized *minimal residual* (GMRES) algorithm [13] might reduce the memory requirements of the solution of the linear equations that arise in the inverse iteration.

For simplicity of coding, the above calculations were done using *Mathematica* [152]. Care was taken to use predefined functions whenever such choice was

more efficient.

### 3.11 Results

This article is an exploration of the PS method as applied to heliumlike systems, not an attempt to improve the energy eigenvalues for bound states. That has already been done to a higher precision than will ever be needed [8, 46, 99, 68, 100, 48, 69, 70, 114, 115, 103]. The focus here is on showing the PS method works in a new application and assessing its convergence properties.

Table 3.1 gives a list of runs used in this section to discuss the effects of the Coulomb terms, energy level (ground or excited), computational domains and numerical methodology on the convergence of the solution to the two-electron problem.

#### 3.11.1 Convergence in energy

In this section, the energy error means the difference between the numerical energy eigenvalue at finite resolution and the exact energy eigenvalue of the nonrelativistic infinite-mass-nucleus Hamiltonian. When no analytic value exists, highly precise variationally calculated values are used [8, 46, 99, 68, 100, 48, 69, 70, 114, 115, 103].

The energy errors for  $H^-$ ,  $H^-$  with the electron-electron interaction turned off, the ground states of Helium, and the first excited  $S$  State of helium (cases A,B,C, and D) are shown in Fig. 3.8. The first important result is that the energies

Table 3.1: A list of the different cases that are compared in this section. Exc refers to the first excited  $S$  state. Grd refers to the ground state.  $N_D$  is the number of domains. B, R, and E refer to behavioral, regularity, and excision, respectively.

Case	Potential		State	Domains	Boundary Conditions		
	$Z$	$\alpha$	Exc/Grd	$N_D$	$\rho = 0$	$\phi, \zeta = 0$	$\rho = \infty$
A	1	1	Grd	3	B	B	B
B	1	0	Grd	3	B	B	B
C	2	1	Grd	3	B	B	B
D	2	1	Exc	3	B	B	B
E	1	1	Grd	1	B	B	B
F	1	0	Grd	1	B	B	B
G	1	1	Grd	3	R	B	R
H	1	1	Grd	3	R	B	E
I	1	1	Grd	3	B	R	B
J	1	1	Grd	3	B	E	B

appear to converge in an approximate exponential fashion. Since these are not variational calculations there is no reason to expect monotonically decreasing energy errors. Detailed inspection of the solutions suggests that the kinks in the graphs are discreteness effects. That is, the precise positioning of the grid points has a large effect on the magnitude of the error.

A potentially significant issue is the impact on convergence of logarithmic terms present in the Fock expansion. Prior authors have been able to calculate very accurate energies without adverse effects of the infinite second derivative at  $\rho = 0$ , but the PS method is sensitive to singularities anywhere within the

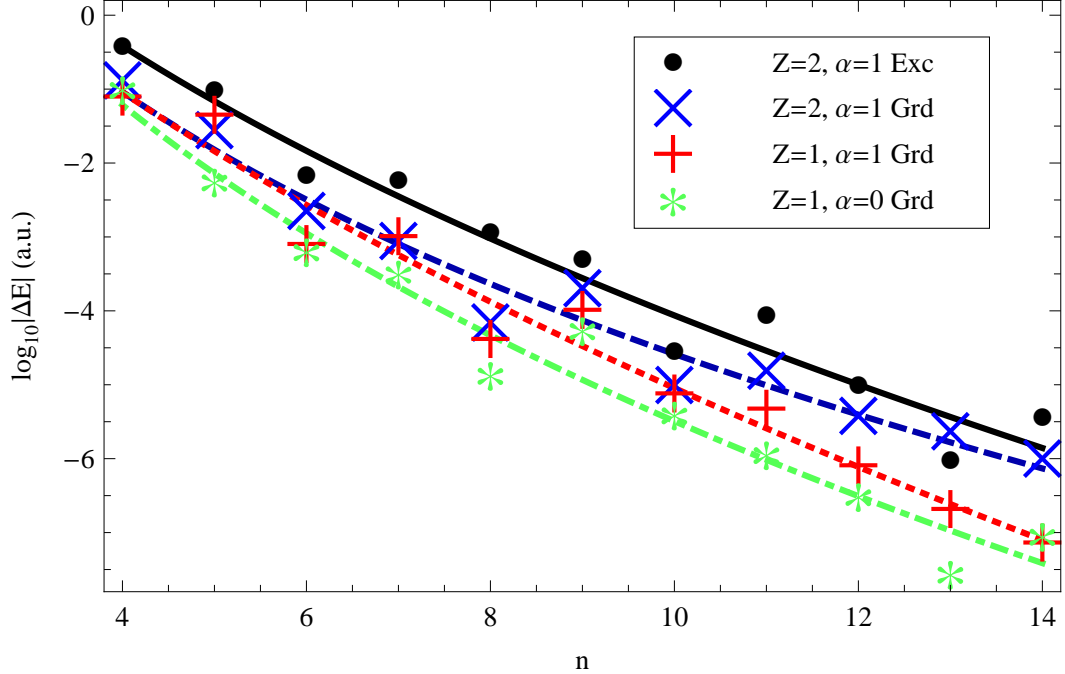


Figure 3.8: (Color online). The convergence of the energy of  $\text{H}^-$ , case A (red pluses); two non-interacting electrons in the field of a proton, case B (green stars); the ground state of He, case C (blue crosses); and its first excited S-state, case D (black circles) as a function of grid resolution  $n$ , with dotted red, dot-dashed green, dashed blue, and solid black fits, respectively. See Appendix B for fitting functions and method.

domain. Figure 3.8 includes a calculation of the  $\text{H}^-$  system with the electron-electron interaction turned off, altering the exact solution and removing the logarithmic term. The rate of convergence is comparable in all cases suggesting that the influence of the logarithmic term on convergence is subdominant for  $n \leq 14$ . This conclusion agrees with the analysis in subsection 3.7.2.

Ideally, the numerical method should handle states other than the ground state. Figure 3.8 shows the convergence of energies for the ground state and the first excited S state of helium. The important result is that the convergence of both calculations is approximately exponential with a similar rate.

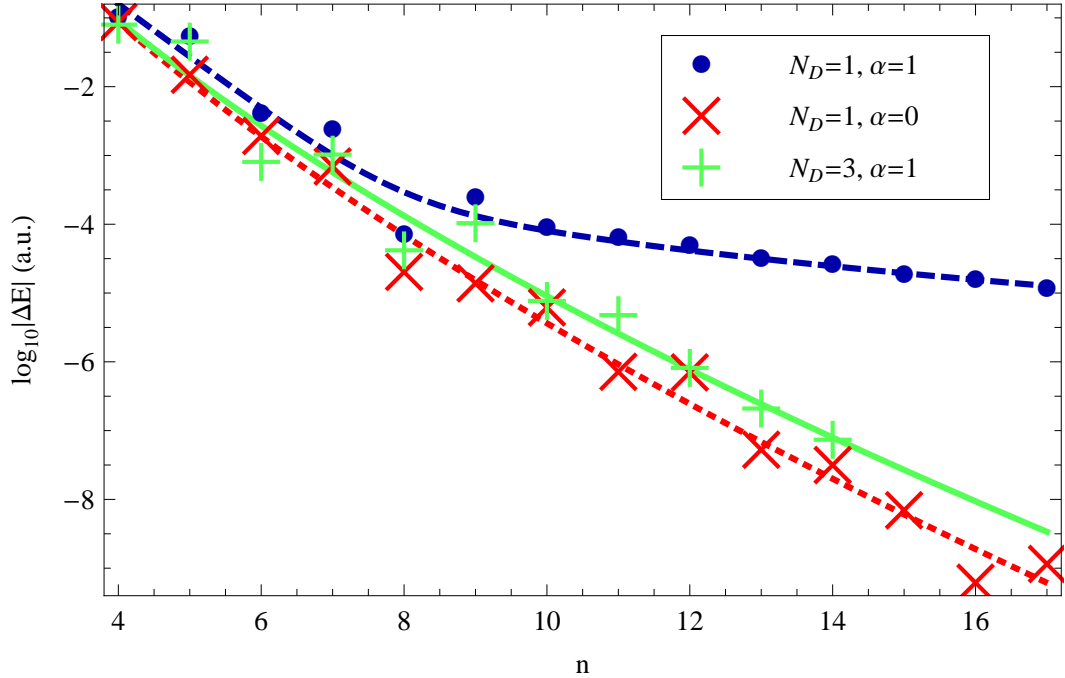


Figure 3.9: (Color online). The convergence of the energy of, case E,  $H^-$  using only one computational domain with the electron-electron interaction on (blue circles); case F, one domain with the interaction off (red crosses); and case A, three domains with the interaction on (green pluses) with dashed blue, dotted red, and solid green fits, respectively. See Appendix B for fitting functions and method.

The relative sizes of the magnitude of the error at fixed grid size for  $H^-$ , He and excited He are roughly consistent with the general expectation set by the difficulty in resolving the solution's small-scale structure. Errors for ground state He are larger than  $H^-$  because the exponential length scale for falloff of the He wave function is smaller than that of  $H^-$ ; errors for the excited state of He are larger than the ground state of He because the oscillatory length scale of the excited state is smaller than the exponential length scale of the ground state.

Figure 3.9 shows the impact on convergence of using a single numerical sub-domain,  $D_0$ , versus three,  $\{D_1, D_2, D_3\}$ . The single domain had one third as

many points as the computation with three domains. However, the resolution in the  $x$  direction dominates the convergence and in that dimension the resolution is identical. Domain  $D_0$  has radial-like coordinates near the electron-proton cusp but not near the electron-electron cusp. One anticipates slower convergence in the energy using  $D_0$ . Comparison shows that two interacting electrons on three domains (case A) or two noninteracting electrons on  $D_0$  (case F) have similar exponential rates of convergence. On the other hand, two interacting electrons on  $D_0$  (case E) converge more slowly. This result shows the multiple grids are essential for achieving superior convergence, and that the electron-electron cusp drives this requirement. If the single domain data were adjusted to account for the fact that they used fewer points, they would be shifted to the left by a factor of  $3^{1/3} \approx 1.44$ . This would not affect the conclusion that using three domains is more efficient because the single domain solution is only algebraically convergent starting at about  $n = 8$ . Using three subdomains is more efficient because the work involved in the calculation has the same scaling whether one or three subdomains is used.

Figure 3.10 presents a comparison of calculations having the full semi-infinite domain (case A) to those with a finite cutoff in  $\rho$  (case H). The scaling of the cutoff  $\rho_{\max} \propto \sqrt{n}$  imposed in case H is derived in Appendix A by balancing the error due to finite resolution from the numerical scheme with errors introduced by truncating the bound state. The figure shows that the semi-infinite calculation fairs better. This is a consequence of the two different sets of assumptions used to distribute the points. The grid points in the semi-infinite scheme are more often found where the wave function is large. Half the points have  $\rho < 1$  ( $x > 0$ ) because 0 is the center of the  $x$  dimension. By comparison, half the points have  $\rho < \rho_{\max}/2$  in the finite calculation. The number of points

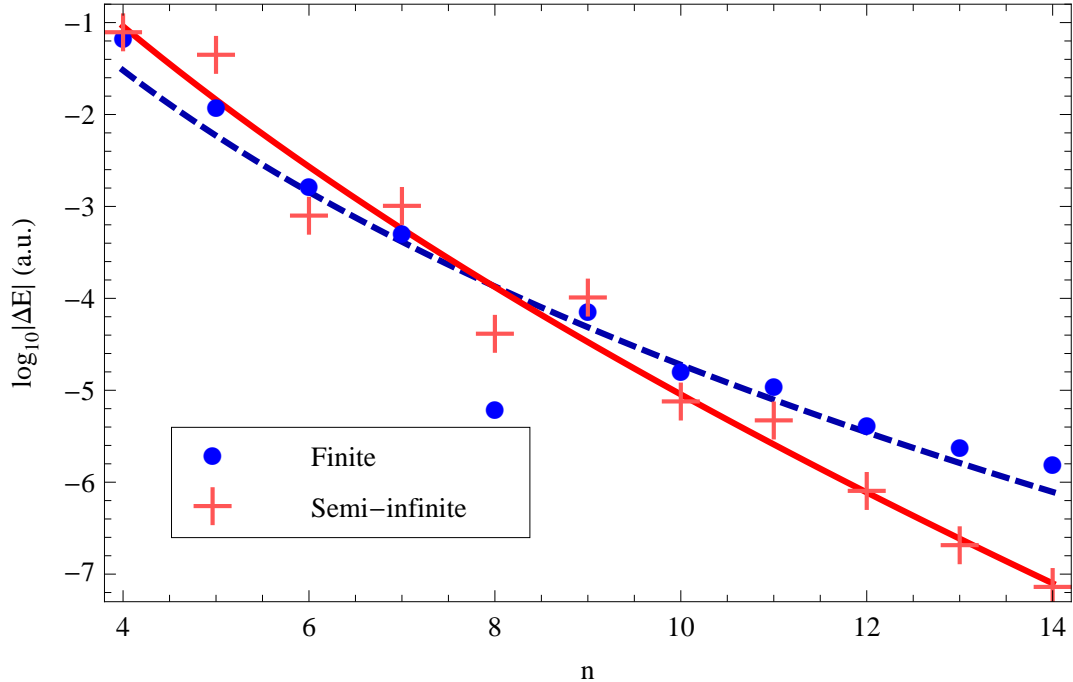


Figure 3.10: (Color online). The convergence of the energy of, case H,  $H^-$  doing the calculation on a finite domain (blue circles); and, case A, semi-infinite domain (red pluses) with dashed blue and solid red fits, respectively. See Appendix B for fitting functions and method.

where the wave function is large is smaller in this latter scheme. Although the semi-infinite strategy is more effective, nothing can be said about the optimal strategy because other distribution methods were not considered. The main advantage of the method is simplicity since there are no adjustable parameters.

Figure 3.11 presents a comparison of the different ways of handling the regularity of the wave function at the two-particle coalescence points. The simplest method, relying on the regularity of the Chebyshev polynomials (case A), does as well or better than the other methods (cases I and J).

Figure 3.12 compares two ways of handling the wave function at  $\rho = 0$ , case A, relying on the regularity of the Chebyshev polynomials (behavioral) and case

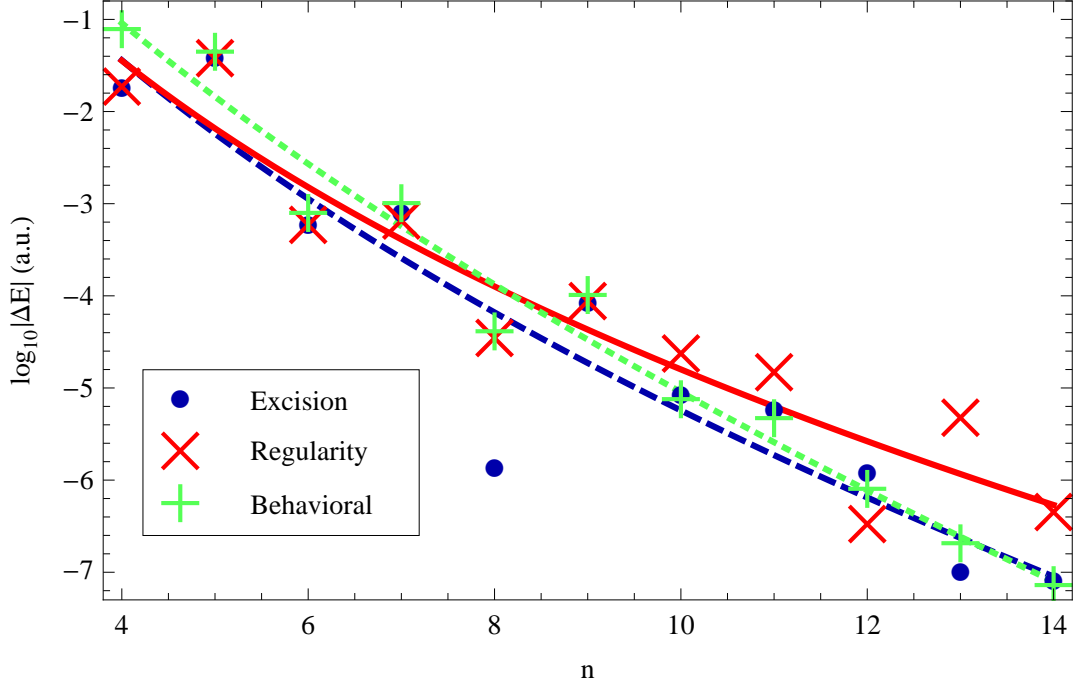


Figure 3.11: (Color online). The convergence of the energy of  $H^-$  using three different methods of ensuring regularity at the two-particle coalescence points: case A, relying on the regularity of the Chebyshev polynomials (green pluses); case I, using the Kato cusp condition as a regularity condition (red crosses); and case J, excising the singularity (blue circles) with green dotted, solid red, and dashed blue fits, respectively. See Appendix B for fitting functions.

G, directly specifying a logarithmic derivative (regularity). The latter method is slightly better but both have roughly the same convergence rate.

### 3.11.2 Convergence in local energy

Another useful measure of convergence is the local energy,

$$E_{\text{loc}} = \frac{\mathcal{H}\psi}{\psi}. \quad (3.106)$$

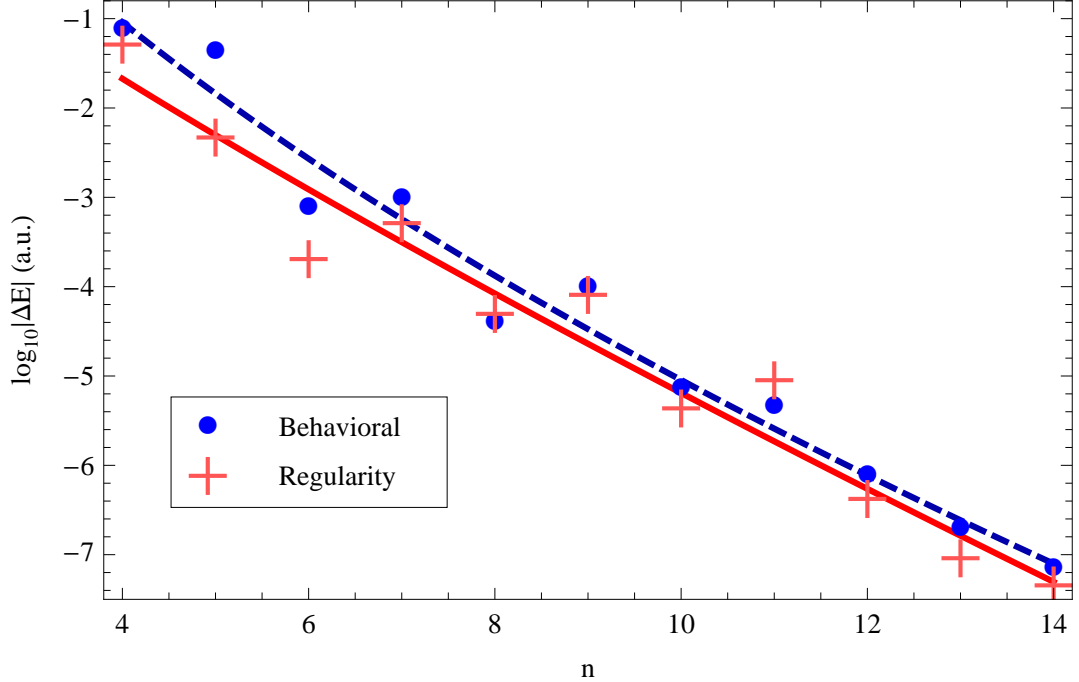


Figure 3.12: (Color online). The convergence of the energy of  $H^-$  using two different methods of ensuring regularity at the three-particle coalescence point: case A, relying on the regularity of the Chebyshev polynomials (blue circles); and case G, using the Fock condition to specify a logarithmic derivative (red pluses) with dashed blue and solid red fits, respectively. See Appendix B for fitting functions and method.

which is constant only for an exact eigenfunction  $\psi$  of Hamiltonian  $\mathcal{H}$ . Throughout this subsection all analysis and data refers to case A.

The difference between the local energy and the numerically evaluated eigenvalue  $E$  gives a local measure of the error in  $\psi$  in a particular calculation. Define

$$\Delta E_{\text{loc}} = E_{\text{loc}} - E. \quad (3.107)$$

For the PS method,  $\Delta E_{\text{loc}}$  is zero at all grid points (subject to limits of finite precision arithmetic). Nonzero differences exist between grid points. Figure 3.13 illustrates the convergence of local energy at four different points. Of the

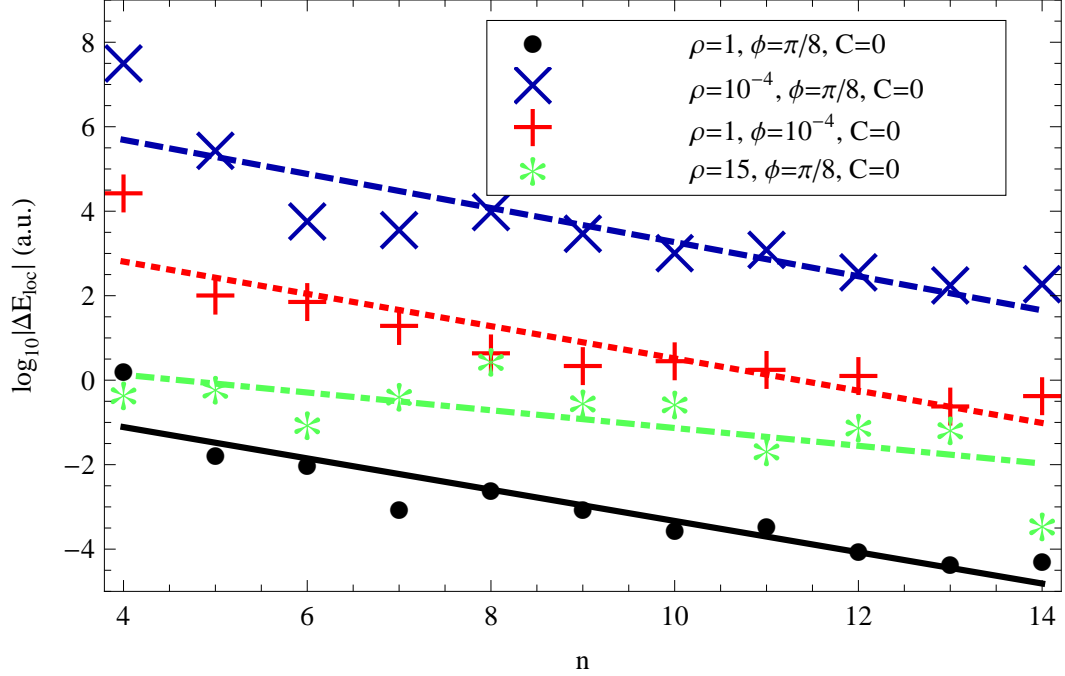


Figure 3.13: (Color online). The convergence of the local energy of  $H^-$  at a four points in the domain: the center of the computational domain (black circles), near the triple coalescence point (blue crosses), near the proton-electron coalescence point (red pluses), and at large  $\rho$  (green stars). Their geometric fits are given by the solid black, dashed blue, dotted red, and dot-dashed green lines, respectively. See Appendix B for fitting functions and method.

four points, the error in local energy is lowest at the point in the center of the computational domain ( $\{\rho, \phi, C\} = \{1, \pi/8, 0\}$ ). It is larger in magnitude near the singularities ( $\{\rho, \phi, C\} = \{10^{-4}, \pi/8, 0\}$  and  $\{1, 10^{-4}, 0\}$ ) because near these points  $E_{\text{loc}} \rightarrow \infty$  for any nonexact  $\psi$ . However, the geometric fits show that the rate of convergence is approximately the same at all three of those points. A different behavior is seen at  $\{\rho, \phi, C\} = \{15, \pi/8, 0\}$ . The error is roughly constant over much of the graph, but begins to decrease at high resolution. This is not surprising given the fact that there are only a few grid points at such large hyperradius.

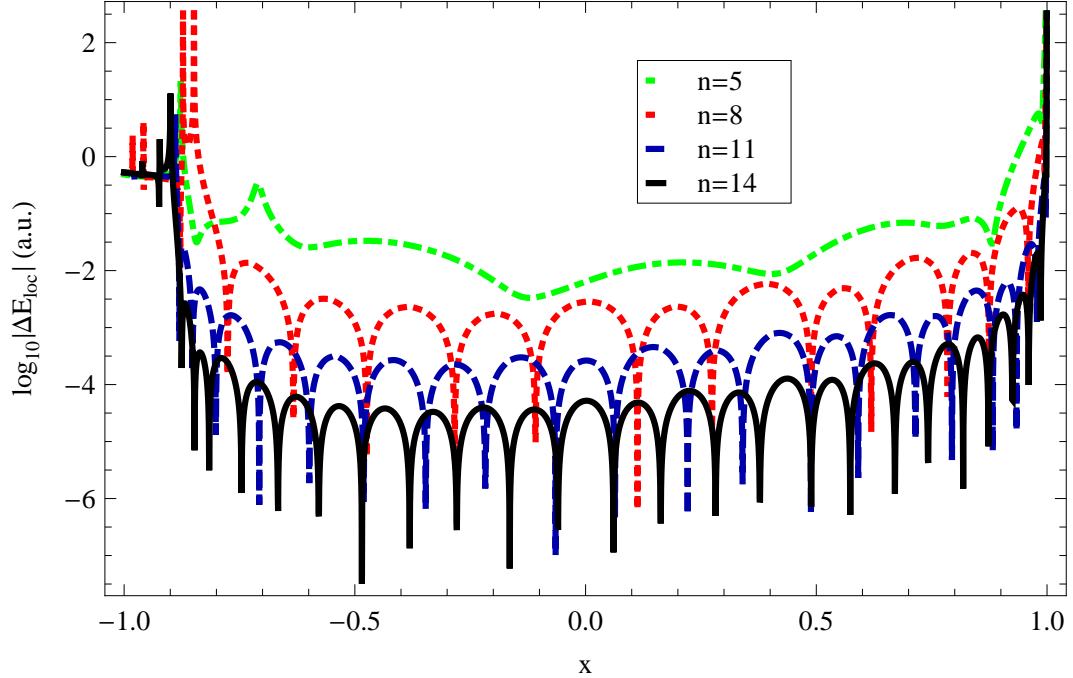


Figure 3.14: (Color online). The error in the local energy of  $\text{H}^-$  as a function of  $x$  with  $r_1 = 2r_2$ , and  $C = -1$  (the electrons are on the same side of the nucleus) at four different resolutions:  $n = 5$  green dot-dashed,  $n = 8$  red dotted,  $n = 11$  blue dashed,  $n = 14$  black solid.

Figure 3.14 displays the convergence of the local energy as a function of  $x$  at fixed angular coordinates. For a perfect exponential decrease in local energy error, the curves would be equidistant from each other. This is approximately true throughout the domain except near  $x = \pm 1$  (small and large  $\rho$ ).

If the numerical solution is considered to be trustworthy where the local energy error is less than some threshold (e.g.  $|\Delta E_{\text{loc}}| < 10^{-2}$ ), then the wave function is well represented in an intermediate range of  $\rho$  ( $10^{-2} < \rho < 10^{1.3}$ ) but not near the triple coalescence point nor at infinity<sup>10</sup>.

<sup>10</sup>The error in the function value is roughly constant everywhere in the domain, but the magnitude of derivatives and the wave function becomes large compared to the magnitude of the wave function at small and large  $\rho$ .

At large  $\rho$  ( $x \approx -1$ ), the true wave function falls off exponentially (in fact, with respect to the  $x$  coordinate it falls off even faster). The PS method represents the exponential in terms of a polynomial. When one extrapolates using the polynomial to  $x = -1$ , the wave function is small but nonzero (the exact value should be zero). However, the Hamiltonian acting on the polynomial is guaranteed to be zero because every coefficient in the Hamiltonian operator has a factor of  $(1 + x)$ . So

$$\lim_{\rho \rightarrow \infty} \frac{\mathcal{H}\psi}{\psi} = 0, \quad (3.108)$$

and  $\Delta E_{\text{loc}} \rightarrow -E$ , a constant at large  $\rho$  as seen in Fig. 3.14. Detailed inspection of the data near  $x = -1$  suggests that for any finite  $\rho$  there exists a resolution above which the solution becomes trustworthy.

The local energy behavior near the triple-coalescence point ( $\rho = 0$ ) is of special interest as a probe of the wave function's nonanalytic behavior. Figure 3.15 displays  $\Delta E_{\text{loc}}$  as a function of  $\theta_{12}$ , the angle between the two electrons, for fixed  $r_2/r_1$  and for a number of choices of  $\rho$ , following a similar figure from Myers *et al* [113]. In this small  $\rho$  regime, the terms that dominate the Hamiltonian are the kinetic energies in the various directions. Each of these, individually, scales as  $1/\rho^2$  [see Eq. (3.25)]. For the exact solution, these terms cancel each other, but for almost any solution which is not exact, the local energy scales as  $1/\rho^2$ . This scaling is shown in Figs. 3.14 and 3.15. Again detailed inspection of the data near  $x = 1$  suggests that for any finite nonzero  $\rho$  there exists a resolution above which the solution becomes trustworthy. Furthermore, Fig. 3.13 shows that there is no sign of the convergence rate being slowed due to the logarithmic terms at this resolution.

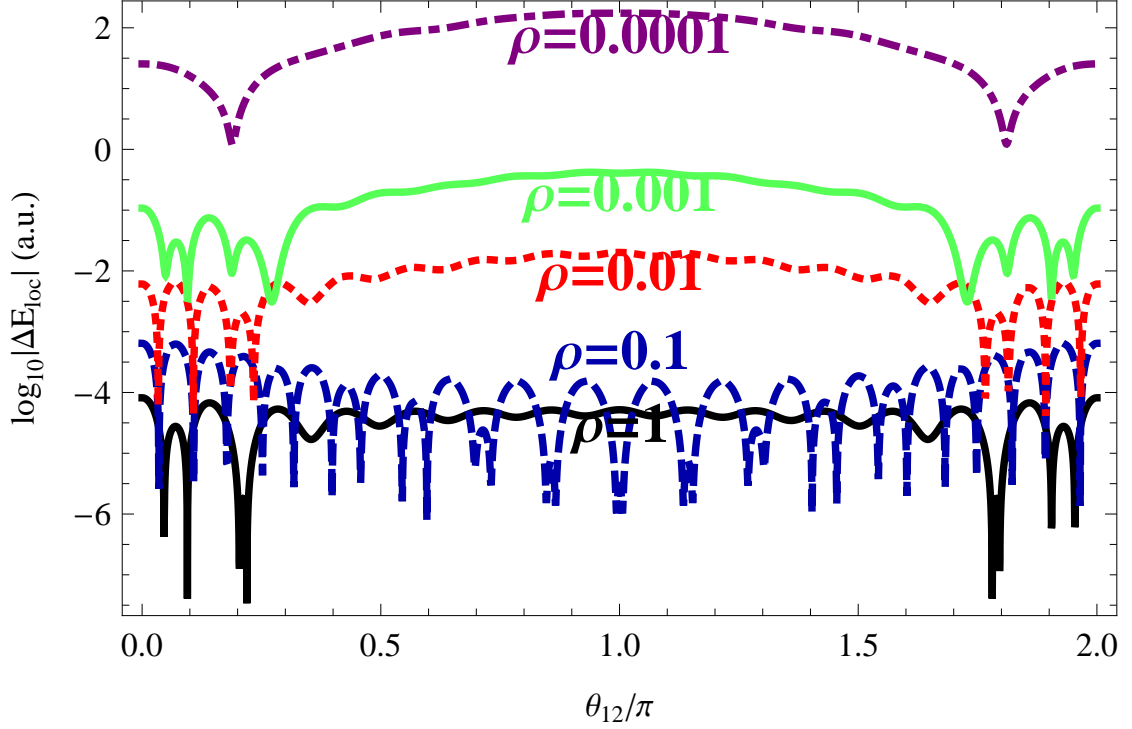


Figure 3.15: (Color online). The error in local energy of  $\text{H}^-$  plotted at different values of the angle  $\theta_{12}$  with  $r_1 = 2r_2$  and at resolution  $n = 14$  and at  $\rho = 1$  (solid black),  $\rho = 0.1$  (dashed blue),  $\rho = 0.01$  (dotted red),  $\rho = 0.001$  (solid green), and  $\rho = 0.0001$  (dot-dashed purple).

### 3.11.3 Cauchy errors

Throughout this subsection all data refers to cases A, B, and C. The Cauchy error is a measure of the difference between numerical solutions with different resolution. One such measure is the normed quantity

$$\Delta_n = \sqrt{\int d^3r_1 d^3r_2 (\psi_n - \psi_{n-1})^2}. \quad (3.109)$$

The true  $\psi$  satisfies

$$1 = \int d^3r_1 d^3r_2 \psi^2, \quad (3.110)$$

but integrating  $\psi_n$  all the way to  $\rho = \infty$  would diverge. This is a consequence of having small but nonzero errors at  $\rho = \infty$  in the value of  $\psi_n$ . An upper limit

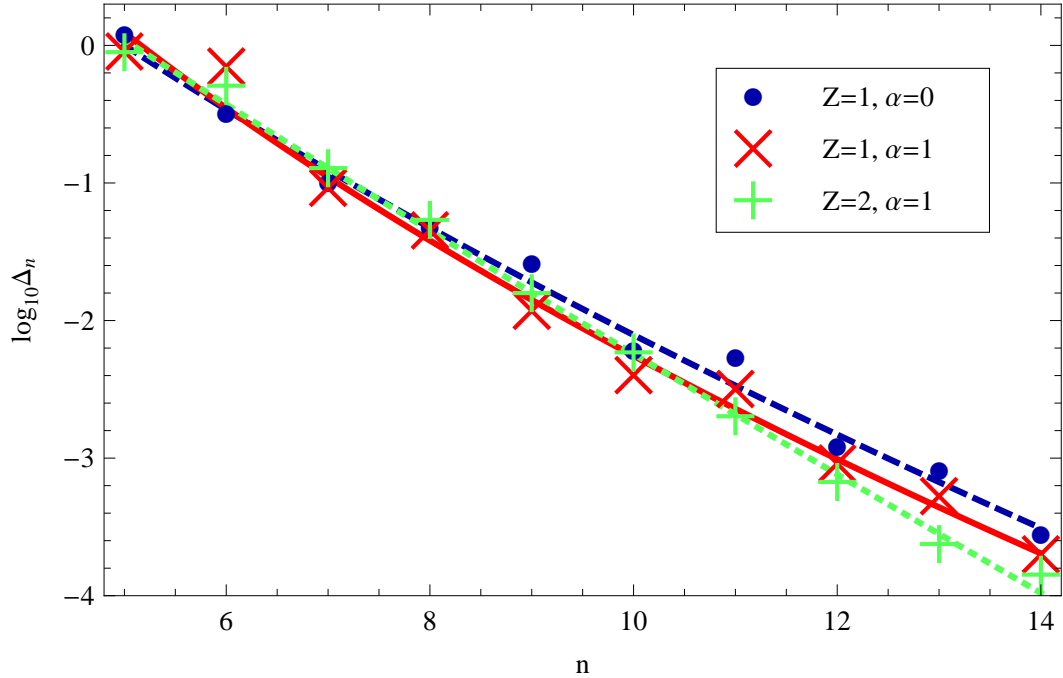


Figure 3.16: (Color online). The root-mean-square average Cauchy error is plotted with increasing resolution for three cases:  $H^-$  with noninteracting electrons (blue circles);  $H^-$  with interacting electrons (red crosses); and helium with interacting electrons (green pluses) with dashed blue, solid red, and dotted green fits, respectively. See Appendix B for fitting functions and method.

$\rho = 10$  is adopted in the normalization of  $\psi_n$  and calculation of  $\Delta_n$ . It is arbitrary but encompasses most of the physical extent of the solution. The Cauchy error in any subinterval of the full interval must converge. To the extent that the error in the interval calculated is dominant, the rate of convergence can be assessed.

Figure 3.16 gives  $\Delta_n$  as a function of resolution while Fig. 3.17 gives the pointwise difference at  $\rho = 0$  where the wave function is maximum. Both plots show that convergence is approximately exponential.

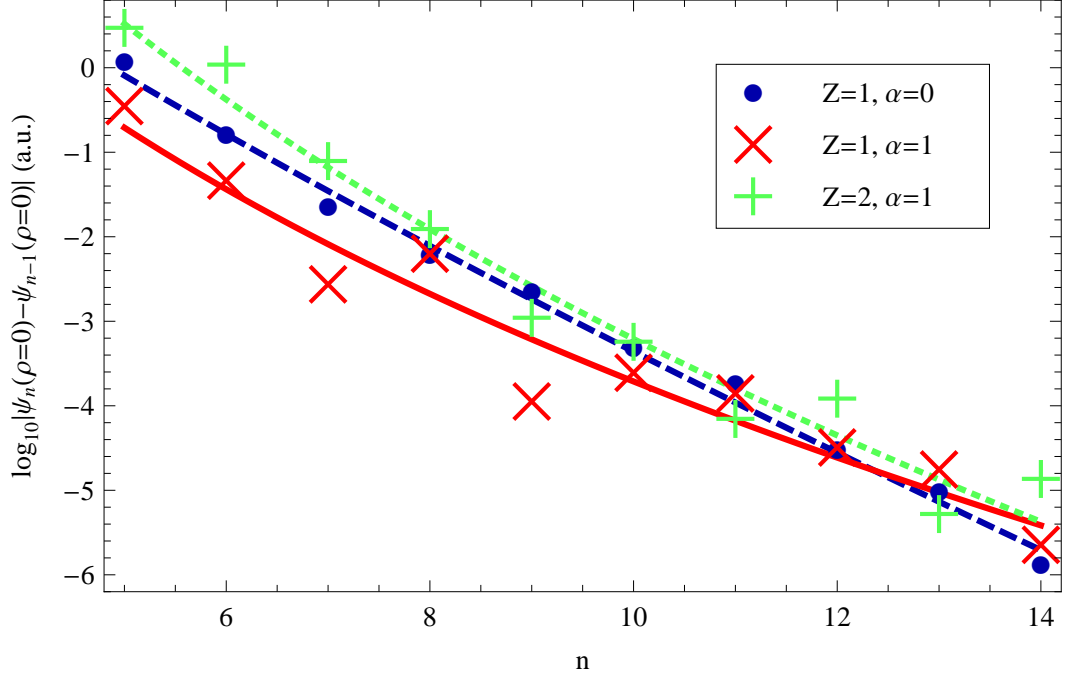


Figure 3.17: (Color online). Pointwise differences in the wave function evaluated at  $\rho = 0$  for increasing resolution for three cases:  $\text{H}^-$  with noninteracting electrons (blue circles);  $\text{H}^-$  with interacting electrons (red crosses); and helium with interacting electrons (green pluses) with dashed blue, solid red, and dotted green fits, respectively. See Appendix B for fitting functions and method.

### 3.11.4 The logarithmic derivative at the triple coalescence point

Throughout this subsection all data refers to cases A, B, and C. The only direct evidence that the convergence of the solutions is slowed by the logarithmic terms in the exact solution comes from evaluating the logarithmic derivative with respect to  $\rho$  at  $\rho = 0$ . The exact value is

$$\left. \frac{\partial_x \psi}{\psi} \right|_{x=1} = -\frac{1}{2} \left( -Z(\cos \phi + \sin \phi) + \frac{\alpha}{2} \sigma[C, \phi] \right). \quad (3.111)$$

The root-mean-square error is

$$\delta_{\text{RMS}} = \sqrt{\int d\Omega \left( \frac{\partial_x \psi}{\psi} - \frac{\partial_x \psi_n}{\psi_n} \right)_{x=1}^2}, \quad (3.112)$$

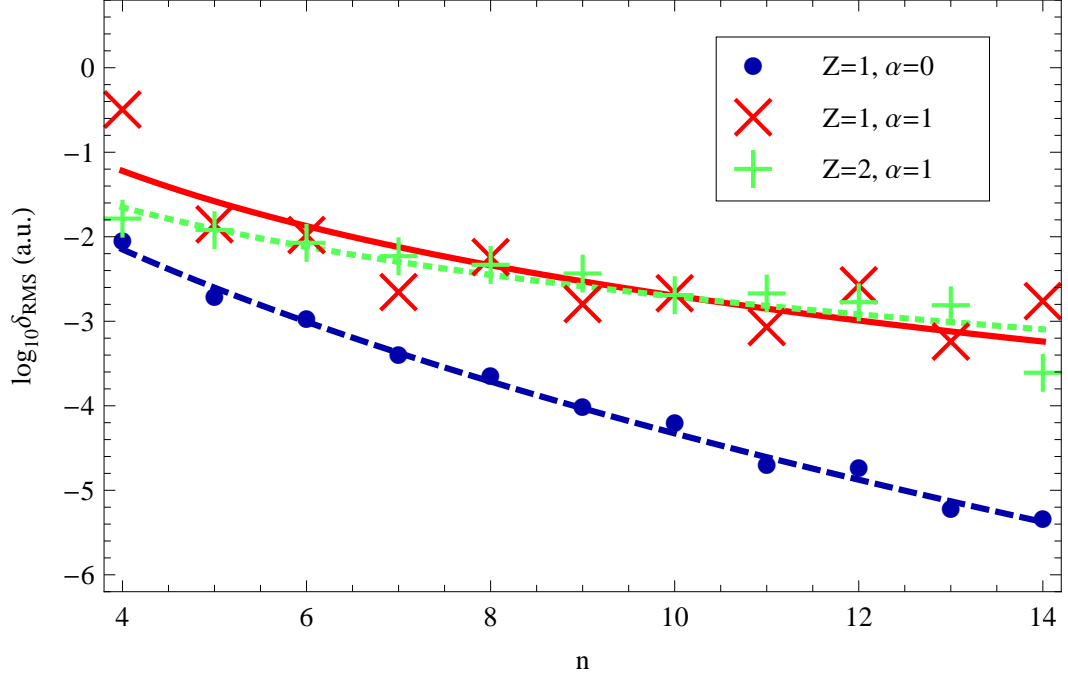


Figure 3.18: (Color online). The root-mean-square error in the logarithmic derivative evaluated at  $\rho = 0$  with increasing resolution for three cases:  $\text{H}^-$  with noninteracting electrons (blue circles);  $\text{H}^-$  with interacting electrons (red crosses); and helium with interacting electrons (green pluses) with dashed blue, solid red, and dotted green fits, respectively. See Appendix B for fitting functions and method.

where

$$\int d\Omega = \int_0^{\pi/4} d\phi \sin^2 2\phi \int_{-1}^1 dC. \quad (3.113)$$

Figure 3.18 displays  $\delta_{\text{RMS}}$ . Turning off the electron-electron interaction, the convergence is noticeably faster. The important conclusion is that the wave functions' convergence is indistinguishable from exponentially fast, while the convergence of its derivatives, at least near  $\rho = 0$  is slower. Of course, the second derivative with respect to  $\rho$  is infinitely wrong at  $\rho = 0$ . It converges to a finite value, and the exact value is infinite.

### 3.12 Conclusion

This article demonstrates the application of PS methods for solving the non-relativistic Schrödinger equation for a system with two electrons. The method successfully handled both ground and excited  $S$  states of heliumlike systems.

The rate of convergence for most properties measured was indistinguishable from being exponentially fast. Local errors decrease in the same manner.

The choice of variables in the vicinity of the two-particle coalescence and the use of multiple, overlapping domains are the critical requirements. These are important so the PS method can represent the analytic form of the solution near all the two-particle cusps and ensure a more efficient algorithm. In other respects the most straightforward choices work well. For example, grid points are determined by the roots of Chebyshev polynomials, which experience shows generally produce the best convergence in PS methods [62, 25]. Behavioral boundary conditions (no explicit regularity conditions) are sufficient to handle the wave function in the vicinity of the coalescence points and also produce convergence as good as or better than the other possibilities tested.

The energy eigenvalue found by the variational method converges most efficiently when basis functions which behave like the exact solution are included but this selection process can be time-consuming and problematic. Of course, much higher precision than reported here was obtained long ago by variational methods. The PS method has the advantage in new and possibly also in more complex applications of not needing the same sort of specialized tuning that has benefited variational calculations. Although this article does not attempt to reproduce the ultra-high-precision results achieved by variational methods

it strongly suggests that the PS method will ultimately prove to be a superior approach for reaching such results in systems with a small number of electrons.

The local energy is not directly controlled when total energy is minimized. Local energy minimization schemes exist and have the advantage that excited states are found at local minima of the variance in local energy instead of just the ground state as is true for the standard variational method [145]. However, they lead to nonlinear problems which may be difficult to handle numerically (minimization of the variance in local energy with respect to parameters in the trial wave function), but still tractable because one need not calculate the energy at each step. By contrast, the PS method controls local energy while the numerical solution remains a linear one. At the same time, the PS method is superior in terms of its convergence rate to other direct partial differential equation solvers (grid based methods) such as finite differencing and finite element which also control the local error.

We plan to extend the method to calculate non-S states and continuum two-electron states to compute the photoabsorption bound-free cross sections with both initial and final states evaluated with the same methodology.

CHAPTER 4  
**PSEUDOSPECTRAL CALCULATION OF HELIUM WAVE FUNCTIONS,  
EXPECTATION VALUES, AND OSCILLATOR STRENGTH**

This chapter is material which will be submitted to Physical Review A.

## 4.1 Abstract

We extend the pseudospectral formalism and the associated numerical methodology for solving Schrödinger's equation for two-electron atoms from S states to arbitrary angular momentum states. We use the calculated wave functions to evaluate the oscillator strength for the helium  $1^1S \rightarrow 2^1P$  transition. The result, 0.27616499(27) compares favorably to the best determination in the literature. We compare the length, velocity, and acceleration expressions for the oscillator strength and conclude that all have roughly the same accuracy in a pseudospectral treatment.

We also evaluate the leading order finite nuclear mass and relativistic corrections for the helium ground state. The pseudospectral method achieves state-of-the-art accuracy without requiring the implementation of any special-purpose numerical treatments. We find all the relevant quantities we tested – energy eigenvalues, S state expectation values and bound-bound dipole transitions for S and P states – converge exponentially with increasing resolution and at roughly the same rate. Expectation values, which depend most strongly on different parts of configuration space, converge to roughly the same accuracy. Quantum mechanical matrix elements are directly and reliably calculable with pseudospectral methods.

A general prescription is given for choosing subdomains needed for exponential convergence. With this prescription and the overall general applicability of the method, we conclude pseudospectral methods can be applied to general few-electron problems.

## 4.2 Introduction

The nonrelativistic helium atom problem has been studied extensively since quantum mechanics was first developed. The most widely used method to find the ground state is the variational method in which the expectation value of the Hamiltonian is minimized with respect to parameters in the trial wave function. The calculated energy provides an upper bound for the exact energy.<sup>1</sup> The method leads to accurate energies provided one starts with an appropriate trial wave function, *i.e.* one capable of representing the exact wave function to a good approximation. To achieve ever-more accurate answers, one must select a sequence of ever-better trial wave functions. There is more than a little art and intuition required for the selection, especially for a nonstandard problem where one may have only a vague idea what the wave function actually looks like. Exponentially small errors (*i.e.*  $e^{-an}$ ) with increasing basis size  $n$  can be achieved if the trial wave function reproduces the analytic properties of the exact wave function. Otherwise, convergence is algebraic (*i.e.*  $n^{-2}$ ).

Although achieving small errors in the value of the energy of a given state implies that the square of the wave function is correspondingly accurate in an average sense, it does not imply that local errors are as small. The variational approach optimizes the wave function weighted by its contributions to the total energy. At a fixed energy error, no bound exists for the error in the wave function at a specific point in configuration space.

A method which can be applied to many different problems (e.g. different interaction potentials, excitation levels, symmetries, etc.) without tinkering

---

<sup>1</sup>The method is not limited to ground states. A trial wave function, exactly orthonormal to all lower energy states, has calculated energy which is an upper bound to the exact result.

with or modifying the basis and which has direct, rigorous control of local errors can serve as a valuable alternative to variational methods and is the subject of the present work.

Recently, we applied pseudospectral methods to solve the nonrelativistic Schrödinger equation for helium and the negatively charged hydrogen ion with zero total angular momentum [73]. We found exponentially fast convergence of many measures of error, including the energy eigenvalues, local energy errors (*e.g.*  $(H\Psi)/\Psi - E$  as a function of position) and Cauchy wave function differences. Only the error in the logarithmic derivative at the triple coalescence point had discernably slower convergence, presumably due to the logarithmic singularity located there [14, 59, 60]. The key virtues were: no explicit assumptions had to be made about the asymptotic behavior of the wave function near cusps or at large distances, the Schrödinger equation was satisfied at all grid points, local errors decreased exponentially fast with increasing resolution, and the method required no fine tuning.

In this article, we extend our previous work to higher angular momentum calculations and utilize the results to evaluate matrix elements for combinations of states. To be systematic, we consider two sorts of matrix elements: the dipole absorption oscillator strength (between S and P states) and first-order mass polarization and  $\alpha^2$  relativistic corrections to the nonrelativistic finite-nuclear-mass Hamiltonian (for the S ground state). All have been the subject of much investigation. Our main focus is on testing the pseudospectral method's capabilities by comparing results to effectively "exact" solutions that others have previously calculated.

### 4.3 Review of pseudospectral methods

The application of pseudospectral methods has found success in fluid dynamics [34], numerical relativity [93, 122], and quantum chemistry [65, 66, 67, 127, 74, 112, 111, 96, 84]. Some problems in one-electron quantum mechanics [24, 26] have been treated but only recently has the method been applied to a fully correlated system with multiple electron atoms [73]. General background on pseudospectral methods can be found in Refs. [25, 62, 122, 124, 73].

The pseudospectral method is a grid-based finite difference method in which the order of the finite differencing is equal to the resolution of the grid in each direction. As the grid size increases it becomes more accurate than any fixed finite-order difference method. If a solution is smooth over an entire domain (or smooth in each subdomain) the pseudospectral method converges exponentially fast to the solution. A spectral basis expansion and a pseudospectral expansion of the same order are nearly equivalent with differences that are exponentially small.

The grid points in the pseudospectral method are located at the roots of Jacobi polynomials or their antinodes plus endpoints. They are clustered more closely near the boundary of a domain than in its center. Such an arrangement is essential for the method to limit numerical oscillations sourced by singularities beyond the numerical domain [62]. These singularities typically occur in the analytic continuation of solutions to non-physical regimes and in the extension of coordinates beyond the patches on which they are defined to be differentiable. The grid point arrangement facilitates a representation of a function and its derivative that is more uniformly accurate across the domain of interest than

is possible using an equal number of equidistant points. Finite difference methods typically use an equal-spaced grid and the derivatives are less accurate at the edge than at the center.

Consider the representation of the hamiltonian for a single domain problem in the pseudospectral method. Let  $\{\mathbf{x}_i^k\}_{k=1,2,\dots,N}$  be a set of grid points (also called collocation points) that lie on the roots of an  $N$ th order Jacobi polynomial in the  $i$ th dimension ( $x_i$ ) of the domain. Define the cardinal functions

$$C_j[x_i] = \prod_{\substack{k=1 \\ k \neq j}}^N \frac{x_i - x_i^k}{x_i^j - x_i^k} \quad (4.1)$$

with may easily be seen to satisfy the relation

$$C_j[x_i^k] = \delta_j^k. \quad (4.2)$$

For an  $n_d$  dimensional problem, one defines

$$\mathcal{C}_J[\mathbf{x}] = \prod_{i=1}^{n_d} C_{j_i}[x_i], \quad (4.3)$$

where the convention that capital letters represent  $n_d$  lowercase indices has been used and  $\mathbf{x} = \{x_1, x_2, \dots, x_{n_d}\}$ . The multidimensional cardinal functions also have the property

$$\mathcal{C}_J[\mathbf{x}^K] = \delta_J^K, \quad (4.4)$$

where  $\mathbf{x}^K$  is the grid point  $\{x_1^{k_1}, x_2^{k_2}, \dots, x_{n_d}^{k_{n_d}}\}$ . These functions are an effective basis, in the sense that a function  $f$  can be written

$$f[\mathbf{x}] = \sum_J f[\mathbf{x}^J] \mathcal{C}_J[\mathbf{x}], \quad (4.5)$$

where  $f[\mathbf{x}^J]$  is a pseudospectral coefficient (“pseudo” because it is more easily identified as the function value at the grid point).

In terms of bases constructed from position eigenstates  $\mathbf{x}^K$  and  $\mathcal{C}_J$ , the pseudospectral hamiltonian operator is

$$\hat{H}_{PS} = \sum_{JK} |\mathbf{x}^K\rangle \langle \mathbf{x}^K | \hat{H} | \mathcal{C}_J \rangle \langle \mathcal{C}_J|. \quad (4.6)$$

The operator  $\hat{H}_{PS}$  is non-Hermitian for any finite resolution. Complex eigenvalues are possible for  $\hat{H}_{PS}$ , but these eigenvalues do not converge with increasing resolution and so are easily discarded.

The pseudospectral matrix must be diagonalized to find the energy eigenvalues. In this representation the eigenvectors are simply the function values at the grid points. This contrasts with a spectral representation in which the eigenvectors are sums of basis functions. The latter is less efficient for determining local wave function values.

The pseudospectral method is not variational. Therefore, it is possible for pseudospectral energies to be too high or too low, and the energy convergence is not monotonic.

#### 4.4 The nonrelativistic two-electron atom

Two-electron atoms form a three-particle system requiring nine spatial coordinates for a full description. Three coordinates are eliminated by taking out the center-of-mass motion. In the infinite-nuclear-mass and nonrelativistic approximations the Hamiltonian is

$$\hat{H}_0 = -\frac{1}{2}(p_1^2 + p_2^2) + V, \quad (4.7)$$

where  $\mathbf{p}_{1,2}$  are the momenta of the two electrons and the potential is

$$V = -\frac{Z}{r_1} - \frac{Z}{r_2} + \frac{1}{r_{12}}. \quad (4.8)$$

Here and throughout this article, atomic units are used. Whenever the infinite-nuclear-mass approximation is not used, the reduced mass of the electron and nucleus is set to one instead of the electron mass. This form of Schrödinger's equation involves six-dimensional fully correlated wave functions.

A further reduction is possible for S states. Hylleraas [87] proposed the ansatz that the wave function be written in terms of three internal coordinates. Typical choices for these coordinates are  $r_1$ ,  $r_2$ , and  $r_{12}$ , the magnitudes of the vectors pointing from the nucleus to each electron and the vector pointing from one electron to the other, respectively. Alternatively,  $r_{12}$  may be replaced by  $\theta_{12}$ , the angle between the two electrons. The S state is independent of the remaining three coordinates that describe the orientation of the triangle with vertices at the two electrons and nucleus.

The situation for states of general angular momentum is more complicated. Bhatia and Temkin [21] introduced a particular set of Euler angles  $\{\Theta, \Phi, \Psi\}$  to describe the triangle's orientation. They defined<sup>2</sup> a set of generalized spherical harmonics which are eigenstates of the total angular momentum, its  $z$  component, parity, and exchange operators:

$$\hat{L}^2 D_{\kappa lm}^\nu = l(l+1) D_{\kappa lm}^\nu \quad (4.9)$$

$$\hat{L}_z D_{\kappa lm}^\nu = m D_{\kappa lm}^\nu \quad (4.10)$$

$$\hat{\Pi} D_{\kappa lm}^\nu = (-1)^\kappa D_{\kappa lm}^\nu \quad (4.11)$$

$$\hat{\mathcal{E}}_{12} D_{\kappa lm}^\nu = (-1)^{l+\kappa+\nu} D_{\kappa lm}^\nu. \quad (4.12)$$

---

<sup>2</sup>The notation used here is slightly different so that the equations can be written in a simplified form.

These four operators all commute with the Hamiltonian. Therefore, a stationary state wave function with total spin  $s$ , total angular momentum  $l$ ,  $z$  component of angular momentum  $m$ , and parity  $k$  obeys

$$\hat{L}^2 \psi_{klms}[\mathbf{r}_1, \mathbf{r}_2] = l(l+1) \psi_{klms}[\mathbf{r}_1, \mathbf{r}_2] \quad (4.13)$$

$$\hat{L}_z \psi_{klms}[\mathbf{r}_1, \mathbf{r}_2] = m \psi_{klms}[\mathbf{r}_1, \mathbf{r}_2] \quad (4.14)$$

$$\hat{\Pi} \psi_{klms}[\mathbf{r}_1, \mathbf{r}_2] = \pm \psi_{klms}[\mathbf{r}_1, \mathbf{r}_2] \quad (4.15)$$

$$\hat{\mathcal{E}}_{12} \psi_{klms}[\mathbf{r}_1, \mathbf{r}_2] = (-1)^s \psi_{klms}[\mathbf{r}_1, \mathbf{r}_2], \quad (4.16)$$

where in the third of the above equations the plus sign corresponds to even parity and the minus sign to odd. Equations 4.9-4.16 imply

$$\psi_{klms}[\mathbf{r}_1, \mathbf{r}_2] = \sum_{\nu=0}^1 \sum_{\substack{\kappa=0 \\ \kappa, \text{ even/odd}}}^l (1 - \delta_{1\nu} \delta_{0\kappa}) g_{\kappa ls}^\nu[r_1, r_2, \theta_{12}] D_{\kappa lm}^\nu[\Theta, \Phi, \Psi], \quad (4.17)$$

where the sum over  $\kappa$  is restricted to even or odd numbers if  $k$  is even or odd, respectively and  $g_{\kappa ls}^\nu$  is a real function of the internal coordinates. The convenience of the Bhatia and Temkin [21] coordinate choice is most evident in how one imposes total antisymmetry of the wave function. The spin singlet (triplet) must have a symmetric (antisymmetric) spatial wave function. The properties of the  $D_{\kappa lm}^\nu$  functions reduce this requirement to

$$\hat{\mathcal{E}}_{12} g_{\kappa ls}^\nu = (-1)^{\nu+\kappa+l+s} g_{\kappa ls}^\nu. \quad (4.18)$$

The full six-dimensional Schrödinger equation for given  $l$ ,  $s$ , even/odd parity, and any  $m$  yields  $l$  or  $l+1$  coupled three-dimensional equations

$$0 = (\hat{H}_S - E) g_{\kappa ls}^\gamma + \sum_{\nu=0}^1 \sum_{n=-1}^1 \hat{H}_{\nu \kappa n}^\gamma g_{\kappa+2n, s}^\nu. \quad (4.19)$$

Here,  $\gamma = 0$  or  $1$  and  $0 \leq \kappa \leq l$  (even or odd  $\kappa$  for even or odd parity). For explicit forms of the above Hamiltonian operators, see Appendix C.

## 4.5 Review of dipole radiative transitions

The absorption dipole oscillator strength measures the likelihood of a transition between two eigenstates of  $\hat{H}_0$  on account of interactions with a perturbing electromagnetic field. We review the derivation of the oscillator strength (see Baym [18] and Bethe and Salpeter [20] for details).

The nonrelativistic Hamiltonian of a two-electron atom in the presence of an electromagnetic field with the mass of the nucleus to infinity may be written

$$\hat{H}_{EM} = \hat{H}_0 + \hat{H}_{int}. \quad (4.20)$$

where  $\hat{H}_0$  describes the time-independent atom in the absence of radiation (Eq. 4.7) and  $\hat{H}_{int}$  describes the interaction of the atom with radiation,

$$\hat{H}_{int} = \sum_i \left( -\frac{\mathbf{p}_i \cdot \mathbf{A}_i + \mathbf{A}_i \cdot \mathbf{p}_i}{2c} - \frac{A_i^2}{2c^2} + \varphi_i \right), \quad (4.21)$$

where  $\mathbf{A}_i$  and  $\varphi_i$  are the vector and scalar potential, respectively, at the location of the  $i$ th electron (excluding the atomic Coulomb interactions included in  $V$ ), and  $c$  is the speed of light. When the density of photons is small the second term, corresponding to two-photon processes, is much smaller than the first. In the transverse gauge the third term is zero. With these assumptions only the terms linear in the vector potential contribute.

The oscillator strength is a measure of how strongly  $\hat{H}_{int}$  couples eigenstates of  $\hat{H}_0$ . Three distinct forms [85] for the oscillator strength in the dipole approximation are well-known. They are denoted as length, velocity, and acceleration

forms:

$$f_{ij}^l = \frac{2}{3}(E_j - E_i)|\langle j|\mathbf{R}|i\rangle|^2 \quad (4.22)$$

$$f_{ij}^v = \frac{2}{3}\frac{1}{E_j - E_i}|\langle j|\mathbf{P}|i\rangle|^2 \quad (4.23)$$

$$f_{ij}^a = \frac{2}{3}\frac{Z^2}{(E_j - E_i)^3}|\langle j|\mathbf{A}|i\rangle|^2. \quad (4.24)$$

Here  $E_i$  and  $E_j$  are the energies of the initial and final states. The two-particle operators are

$$\mathbf{R} = \mathbf{r}_1 + \mathbf{r}_2 \quad (4.25)$$

$$\mathbf{P} = \mathbf{p}_1 + \mathbf{p}_2 \quad (4.26)$$

$$\mathbf{A} = \frac{\mathbf{r}_1}{r_1^3} + \frac{\mathbf{r}_2}{r_2^3}, \quad (4.27)$$

i.e. the position, momentum and acceleration of the electrons. For the detailed forms used for calculating the oscillator strength in this article, see Appendix D.

If the wave functions, energies, and operators were exact, all three forms would give exactly the same result. However, in a numerical calculation the exact agreement may be destroyed whenever the commutator rule

$$\mathbf{P} = i[\hat{H}_0, \mathbf{R}] \quad (4.28)$$

is violated. This may occur due to approximations to  $\hat{H}_0$ ,  $\mathbf{P}$ , or  $\mathbf{R}$ , or approximations to their actions on the eigenstates. Agreement between the three forms is a necessary but not sufficient condition for convergence of the final answer [133, 85] because approximations made in constructing the wave function are identical for each form. A more stringent test for convergence is to check the convergence as a function of resolution or basis size, along with agreement between the three forms.

The oscillator strengths  $f_{0n}$  for transitions,  $1^1S \rightarrow n^1P$  of helium obey several sum rules [39]

$$S(-1) = \frac{2}{3} \langle (\mathbf{r}_1 + \mathbf{r}_2)^2 \rangle \quad (4.29)$$

$$S(0) = 2 \quad (4.30)$$

$$S(1) = -\frac{4}{3} \langle \hat{H}_0 - \mathbf{p}_1 \cdot \mathbf{p}_2 \rangle \quad (4.31)$$

$$S(2) = \frac{2\pi Z}{3} \langle \delta(\mathbf{r}_1) + \delta(\mathbf{r}_2) \rangle, \quad (4.32)$$

where

$$S(k) = \sum_n |\Delta E_{0n}|^k f_{0n}. \quad (4.33)$$

All the expectation values above are for the ground state, the summation is over all other states, including the continuum, and  $\Delta E_{0n}$  is the difference in energies between the ground state and the  $n^1P$  state. These sum rules provide checks that the theoretical values for the oscillator strengths are correct. Independent evaluation of  $S(k)$  involves using multiple methods to solve for all the final states, which include the low energy highly correlated states, countably infinite highly excited states, and uncountably many in the continuum. For a detailed discussion see Ref. [19], in which it is shown that the two sides of Eqs. 4.29-4.32 agree to about one percent using a combination of theoretical and experimental values for  $f_{0n}$ .

## 4.6 Methods for calculating oscillator strengths

Oscillator strength calculations have taken many forms over the last half century. The fundamental issue is the calculation of the initial and final wave functions. The preferred method depends on how large the electron correlation energy is. Historically, variational methods have been used when correlations are

important. Such methods are usually inapplicable to highly excited states because errors in the eigenproblem are cumulative as one goes to higher excitations. Other approximate methods may yield satisfactory results in such cases. We review the methodologies for determining the wave function.

### 4.6.1 Approximate methods

The central field approximation (see Ref. [20]) is a good approximation when electrons are nearly uncorrelated and exchange effects are negligible. Their wave function is then well represented by a single product of one-electron functions. Each electron experiences some potential which is only a function of its distance to the nucleus. This allows one to write the Schrödinger equation as a system of possibly coupled ordinary differential equations.

The Hamiltonian for a two-electron atom is approximated by

$$\hat{H}_0 \approx \hat{H}_1 + \hat{H}_2 \quad (4.34)$$

$$\hat{H}_i = \frac{p_i^2}{2} + U_i[r_i], \quad (4.35)$$

for some  $U_i$ , which takes into account the screening of the nucleus by the electron cloud. Green *et al.* [75] used this approximation, with wave functions of the configuration interaction form, to produce tables of S→P and P→S transitions. If the further approximation is made that the asymptotic form of the potential at large  $r_i$  is valid at all  $r_i$ , one arrives at the Coulomb approximation [17],

$$U_i[r_i] \approx -\frac{Z-1}{r_i}. \quad (4.36)$$

Because the regularity condition at  $r = 0$  no longer applies, one needs an alternate method of determining the discrete energy eigenvalues. These may be

borrowed from experimental measurements or other theoretical calculations. Wiese *et al.* [148, 149] used this approximation adding exchange effects to calculate oscillator strengths for hydrogen to calcium, Cameron *et al.* [32] tabulated 95 different transitions, and Theodosiou [144] produced extensive tables with errors better than 10% and used a more sophisticated form [41] of  $U_i$  to calculate the oscillator strength of the  $1^1\text{S} \rightarrow 2^1\text{P}$  transition to four decimal places. Runge and Valance [129] developed a similar approach which used the atomic Fues potential for the valance electron,

$$U[r] = \frac{Z}{r} + \sum_{l=0}^{\infty} \frac{B_l \hat{P}_l}{r^2}, \quad (4.37)$$

where  $B_l$  is an adjustable parameter and  $\hat{P}_l$  is the projection operator to a subspace defined by a given angular momentum  $l$ .

These methods greatly simplify the calculations and are advantageous if one is attempting to produce a large catalogue of values, especially for high angular momentum or highly excited states. However, the main limitation is for highly correlated states, which are not well-represented by any of these approximations.

Multiconfiguration Hartree-Fock [57] and coupled cluster methods [56] give much better results, but are more complicated.

## 4.6.2 Perturbation theory

Unlike the approximations above, perturbation theory can yield numerically exact results in the limit of large order. Sanders, Scherr, and Knight [131, 130] developed a  $1/Z$  expansion, in which the electron-electron interaction is the

perturbation. Even though  $Z$  is small, the perturbations can be carried out to high order to produce good convergence and their oscillator strengths were converged to three decimal places for the helium  $1^1\text{S} \rightarrow 2^1\text{P}$  transition. The accuracy improves with increasing  $Z$  and excitation.

Devine and Stewart [42, 43] divided the Hamiltonian as

$$\hat{H}_0 = \hat{H}_{HF} + \hat{H}_1, \quad (4.38)$$

where  $\hat{H}_{HF}$  is the Hamiltonian projected into the subspace spanned by solutions of the Hartree-Fock type and  $\hat{H}_1$  is the difference between this operator and the full nonrelativistic Hamiltonian  $H_0$ . They were able to produce results correct to three correct decimal places.

### 4.6.3 Variational methods

The main difference between various variational methods is the choice of basis. Some bases are able to represent parts of the wave function critical to oscillator strength calculations better than others. Configuration interaction (CI) calculations [134, 28, 29, 40, 36] can be precise but suffer from the absence of odd powers of the interelectronic distance [46]. One includes this value along with electron-proton distances (or linear combinations of these) in the bases using perimetric [118] coordinates [133, 45, 46, 48, 53, 50, 52] or Hylleraas [87] coordinates [146, 5, 97, 155], both of which have yielded some of the more accurate calculations to date. One can also use a large, simple exponential basis [33]. Of these, the most precise is Drake [45] who has calculated oscillator strengths to seven decimal places as well as some finite nuclear mass and relativistic corrections.

Higher precision is not warranted until higher order corrections are included.

#### 4.6.4 Miscellaneous

Some other works, which do not fit into the above categories, are notable. Anderson and Weinhold [5] calculated oscillator strengths with a Hylleraas basis and derived rigorous bounds on their values. Roginsky *et al.* [128] present a method to change the wave function so that the length and velocity forms agree, getting a better result. Abrashkevich *et al.* [2] used the hyperspherical adiabatic approach. The most complete tabulation of transitions is given by Wiese and Fuhr [147].

### 4.7 Variables and domains

To achieve exponentially fast convergence with a pseudospectral method, it is imperative that the solution be smooth for the choice of coordinates everywhere. This typically requires smooth representations on several computational subdomains. It is useful to have a guide for choosing coordinates.

If one has the ordinary differential equation

$$\left( \frac{d^2}{dx^2} + \frac{p_a[x]}{x-a} \frac{d}{dx} + \frac{q_a[x]}{(x-a)^2} \right) f = 0, \quad (4.39)$$

where both  $p_a[x]$  and  $q_a[x]$  are analytic at  $x = a$ , then  $x = a$  is a regular singular point and  $f$  has at least one Frobenius type solution about  $x = a$  of the form,

$$f[x] = (x-a)^{t_a} \sum_{n=0}^{\infty} c_n (x-a)^n, \quad (4.40)$$

where the coefficients  $c_n$  can be derived by directly plugging into Eq. 4.39 and  $t_a$  is the greatest of the solutions to the indicial equation

$$t_a(t_a - 1) + p_a[a]t_a + q_a[a] = 0. \quad (4.41)$$

For a proof, see Ref. [37]. Exponential convergence of the pseudospectral method for a differential equation of the form of Eq. 4.39 for all  $a$  in the computational domain requires  $t_a$  be a nonnegative integer for all  $a$  in the domain.<sup>3</sup>

A simple example is the radial Schrödinger equation for a hydrogenic atom

$$\left( \frac{d^2}{dr^2} + \frac{2}{r} \frac{d}{dr} - \frac{l(l+1) - 2Zr - 2Er^2}{r^2} \right) R_{nl} = 0, \quad (4.42)$$

where  $R_{nl}$  is the radial part of the full wave function. The only point at which the above condition is nontrivial is  $r = 0$ . A comparison with Eq. 4.39 yields  $p_0[0] = 2$  and  $q_0[0] = l(l+1)$ , which gives  $t_0 = l$ , the well known result for hydrogenic wave functions.

This result tells us that spherical coordinates are a good choice for solving hydrogenic wave functions using pseudospectral methods. A bad choice would be cartesian coordinates. For simplicity, restrict the Schrödinger equation to the  $z$  axis

$$\frac{d^2\psi}{dz^2} + \left( \frac{2Z}{|z|} + 2E \right) \psi = 0, \quad (4.43)$$

where  $\psi$  is the wave function. It is easy to see that at  $z = 0$ ,  $q_0[z]$  is not analytic. Therefore the Frobenius method fails. The ground state solution is

$$\psi = e^{-Z|z|}. \quad (4.44)$$

---

<sup>3</sup>The full class of one dimensional problems that would have exponentially fast convergence is larger because pseudospectral method just needs that the solution is smooth which is a slightly weaker statement than the function needs to be analytic. However, for all problem points discussed here, this distinction does not make any difference.

There is a cusp at  $z = 0$ , which the pseudospectral method would not handle well and convergence would be limited to being algebraic.

An arbitrary second order partial differential equation (PDE) may have singularities that occur on some convoluted hypersurface. Deriving the analytic properties of a solution near such a surface is a daunting task. A restriction is made to PDE's with singularities on a flat surface determined by  $x_i = a_i$  for some coordinate  $x_i$ . Focusing on this one coordinate and singularity, the PDE can be written in the form

$$\left( \frac{\partial^2}{\partial x_i^2} + \frac{\hat{P}_{a_i}^i[\mathbf{x}]}{x_i - a_i} \frac{\partial}{\partial x_i} + \frac{\hat{Q}_{a_i}^i[\mathbf{x}]}{(x_i - a_i)^2} \right) f = 0 \quad (4.45)$$

for each dimension  $x_i$ , where  $\hat{P}_{a_i}^i$  and  $\hat{Q}_{a_i}^i$  are linear second order differential operators that do not include derivatives with respect to  $x_i$  and only include functions that are analytic with respect to  $x_i$  at  $a$ . There is no generalization of the above theorem that allows one to conclude that  $f$  is analytic at  $x = a_i$ . The Schrödinger equation for two-electron atoms can be written in this form about the point  $\rho = \sqrt{r_1^2 + r_2^2} = 0$ . If such a theorem existed, the wave function could be expanded about  $\rho = 0$  as

$$\psi = \sum_{n=0}^{\infty} A_n \rho^n, \quad (4.46)$$

where  $A_n$  is an analytic function of the five remaining variables. However, Bartlett [14] proved that this cannot be the case. Instead, Fock [59, 60] suggested a solution of the form

$$\psi = \sum_{n=0}^{\infty} \sum_{m=0}^{\lfloor n/2 \rfloor} B_{nm} \rho^n (\log \rho)^m, \quad (4.47)$$

where  $B_{nm}$  is an analytic function of the remaining five variables. This solution has been shown to have a continuous value of the local energy  $\hat{H}\psi/\psi$  near  $\rho = 0$  by Myers *et al.* [113]. The logarithmic singularity has only a slight effect on

the convergence of variational energies [139] and for most measures of error does not affect pseudospectral calculations until very high resolutions [73], so we ignore it here.

In the absence of a definite theorem, we state as a rule of thumb, that one should require that the operators  $\hat{P}_{a_i}^i$  and  $\hat{Q}_{a_i}^i$  have forms in a neighborhood about  $a_i$  which satisfy

$$\hat{P}_{a_i}^i = \sum_{n=0}^{\infty} (x_i - a_i)^n \hat{p}_{a_i n}^i \quad (4.48)$$

$$\hat{Q}_{a_i}^i = \sum_{n=0}^{\infty} (x_i - a_i)^n \hat{q}_{a_i n}^i, \quad (4.49)$$

where  $\hat{p}_{a_i n}^i$  and  $\hat{q}_{a_i n}^i$  are linear differential operators not containing  $x_i$  or its derivatives, for all coordinates  $x_i$  and  $a_i$  within the domain of  $x_i$ .

The obvious places where Eqs. 4.48 and 4.49 might fail is where coefficients of the derivatives in the Hamiltonian (See Appendix C) are singular. These are  $r_1, r_2, r_{12} = 0$  and  $\theta_{12} = 0, \pi$ . The first three are physical singularities explored in detail in Ref. [73]. These cannot be treated separately until one changes variables because it is possible for  $r_1, r_2$ , and  $r_{12}$  to be zero simultaneously and so Eqs. 4.48 and 4.49 would be impossible to satisfy for all three coordinates at the same time. It is for this reason, the coordinate  $\rho$  is used. The point  $\rho = 0$  corresponds to both electrons being at the nucleus. The latter two are coordinate singularities corresponding to a colinear arrangement of the two electrons and the nucleus. These do not exist for S states, hence, the slight change in coordinate choice for the third variable used in each domain from Ref. [73] (*i.e.* from the coordinate  $C = -\cos \theta_{12}$  to just  $\theta_{12}$ ).

One choice of coordinates and subdomains which satisfy Eqs. 4.48 and 4.49

is given here. Let

$$r_1 = \rho \cos \phi \quad (4.50)$$

$$r_2 = \rho \sin \phi \quad (4.51)$$

$$r_{12} = \rho \sqrt{2} \sin \zeta \quad (4.52)$$

$$\sqrt{2} \sin \zeta = \sqrt{1 - \cos \theta_{12} \sin 2\phi} \quad (4.53)$$

$$\cos \beta_{12} = -\frac{\cos 2\phi}{\sqrt{1 - \cos^2 \theta_{12} \sin^2 2\phi}} \quad (4.54)$$

$$x = \frac{1 - \rho}{1 + \rho}. \quad (4.55)$$

The full ranges of these variables are given by:

$$\begin{aligned} 0 &\leq r_1, r_2, \rho < \infty \\ |r_1 - r_2| &\leq r_{12} \leq r_1 + r_2 \\ 0 &\leq \theta_{12}, \beta_{12} \leq \pi \\ 0 &\leq \phi, \zeta \leq \pi/2 \\ -1 &\leq x \leq 1. \end{aligned} \quad (4.56)$$

The coordinate  $x$  maps the semi-infinite domain to a finite domain. Two different sets of variables are used:  $\{x, \phi, \theta_{12}\}$  and  $\{x, \zeta, \beta_{12}\}$ , in three domains shown in Fig. 4.1 and given below.

$$\begin{aligned} D_1 : & -1 \leq x \leq 1, \quad 0 \leq \phi \leq \frac{1}{2}, \quad -1 \leq \cos \theta_{12} \leq 1 \\ D_2 : & -1 \leq x \leq 1, \quad \frac{1}{2} \leq \phi \leq \frac{\pi}{4}, \quad -1 \leq \cos \theta_{12} \leq \frac{2}{3} \\ D_3 : & -1 \leq x \leq 1, \quad 0 \leq \zeta \leq \frac{1}{2}, \quad -1 \leq \cos \beta_{12} \leq 0. \end{aligned} \quad (4.57)$$

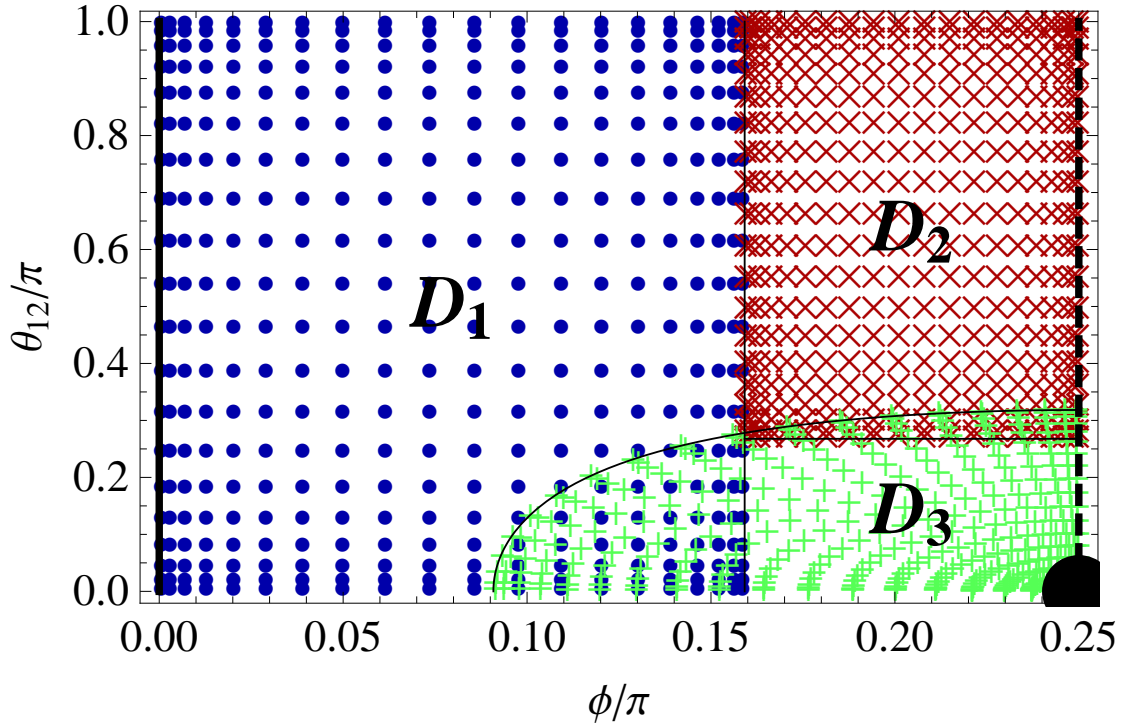


Figure 4.1: (Color online). This is the arrangement of grid points of the three domains at a constant value of  $\rho$  in  $\phi$  and  $\theta_{12}$  coordinates for  $n = 20$ . Note that the point density becomes larger at the boundary of each subdomain and that no grid points sit on the Coulomb singularities. The blue circles, red crosses, and green pluses belong to domains  $D_1$ ,  $D_2$ , and  $D_3$ , respectively.  $D_1$  and  $D_2$  are rectangular domains, while  $D_3$  has the curved boundary in  $\phi, \theta_{12}$  coordinates but is rectangular in  $\zeta, \beta_{12}$  coordinates. The electron-proton singularity occurs on the left side (solid line at  $\phi = 0$ ). The entire line corresponds to one physical point. The electron-electron singularity occurs at the lower right hand corner (solid disk at  $\phi = \pi/4, \theta_{12} = 0$ ). A line of symmetry falls on the right side (dashed line at  $\phi = \pi/4$  where  $r_1 = r_2$ ).

## 4.8 Boundary conditions

### 4.8.1 Internal boundary conditions

It is necessary to ensure continuity of the wavefunction and its normal derivative at internal boundaries. There are two ways in which the subdomains can touch: they can overlap or they can barely touch. For clarity, consider a one-dimensional problem with two domains. Let the first domain be domain 1 and the second be domain 2 with extrema  $x_{1,\min} < x_{2,\min} \leq x_{1,\max} < x_{2,\max}$ , where the 1 and 2 now refer to domain number. The first case corresponds to  $x_{2,\min} < x_{1,\max}$  and the second to  $x_{2,\min} = x_{1,\max} \equiv x_*$ . For both cases, exactly two conditions are needed to make the wavefunction and its derivative continuous. The simplest choice for the first case is

$$\psi_1[x_{1,\max}] = \psi_2[x_{1,\max}] \quad (4.58)$$

$$\psi_1[x_{2,\min}] = \psi_2[x_{2,\min}], \quad (4.59)$$

and for the second case is

$$\psi_1[x_*] = \psi_2[x_*] \quad (4.60)$$

$$\frac{d}{dx}\psi_1[x_*] = \frac{d}{dx}\psi_2[x_*]. \quad (4.61)$$

For multi-dimensional grids, the situation is analogous. The conditions are applied on surfaces of overlap. In this case the derivatives are surface normal derivatives. On a discrete grid, a finite number of conditions are given which, in the limit of an infinitely fine mesh, would cover the entire surface. Additional discussion and illustrations of the technique are in Ref. [73].

## 4.8.2 The symmetry condition

The Hamiltonian (see appendix C) is symmetric with respect to particle exchange. Therefore, there are two types of eigenstates: those with symmetric spatial wave functions (singlets) and those with antisymmetric spatial wave functions (triplets). The radial wave functions  $g_{\kappa ls}^\nu$  satisfying the appropriate symmetry must obey Eq. 4.18. This condition corresponds to setting the radial wave functions or their derivatives with respect to  $\phi$  or  $\beta_{12}$  equal to zero at  $\phi = \pi/4$  or  $\beta_{12} = \pi/2$ , respectively.

## 4.9 Matrix methods

To solve for the wave function, given  $k$ ,  $l$  and  $s$ , one must calculate the values of  $g_{\kappa ls}^\nu$  for each  $k$  and  $i$  that enters the summation in Eq. 4.17. There are two types of conditions which must be satisfied: the Schrödinger equation and the boundary conditions. The first can be represented in matrix form as

$$\begin{pmatrix} H_0^0 + (H_S - E)\mathbf{1} & H_1^0 \\ H_0^1 & H_1^1 + (H_S - E)\mathbf{1} \end{pmatrix} \begin{pmatrix} g^0 \\ g^1 \end{pmatrix} = 0, \quad (4.62)$$

where  $E$  is the energy,  $\mathbf{1}$  is the identity matrix,  $H_\nu^\gamma$  is the tridiagonal matrix

$$H_\nu^\gamma = \begin{pmatrix} H_{\nu P_\nu 0}^\gamma & H_{\nu P_\nu 1}^\gamma & 0 & \cdots & 0 \\ H_{\nu, P_\nu+2, -1}^\gamma & H_{\nu, P_\nu+2, 0}^\gamma & H_{\nu, P_\nu+2, 1}^\gamma & \ddots & \vdots \\ 0 & H_{\nu, P_\nu+4, -1}^\gamma & H_{\nu, P_\nu+4, 0}^\gamma & \ddots & 0 \\ \vdots & \ddots & \ddots & \ddots & H_{\nu, k_m-2, 1}^\gamma \\ 0 & \cdots & 0 & H_{\nu, k_m, -1}^\gamma & H_{\nu, k_m, 0}^\gamma \end{pmatrix}, \quad (4.63)$$

with  $P_0$  is zero (one) and  $P_1$  is two (one) for even (odd) parity states and  $k_m = 2\lfloor l/2 \rfloor + P_0$ , and

$$g^\nu = \begin{pmatrix} g_{P_\nu ls}^\nu \\ \vdots \\ g_{k_m ls}^\nu \end{pmatrix}, \quad (4.64)$$

with each  $g_{\kappa ls}^\nu$  being a vector containing all the values of the corresponding function on the grid points. The length of the vector  $g^\nu$  is either  $\lfloor l/2 \rfloor$  or  $\lceil l/2 \rceil$ , depending on the angular momentum, spin, and parity. For the S and P states calculated in this article,  $H_\nu^\gamma$  is only a one by one matrix. Each  $H_{\nu\kappa n}^\gamma$  and  $H_S$  are block diagonal matrices, where each block corresponds to a subdomain and is a pseudospectral matrix constructed from Eq. 4.6 with  $\hat{H}$  replaced by  $\hat{H}_{\nu\kappa n}^\gamma$  or  $\hat{H}_S$ , respectively (see appendix C) and using the grid points of that subdomain. So the number of columns and rows of  $H_{\nu\kappa n}^\gamma$  and  $H_S$  are both equal to the total number of grid points.

Similarly the boundary conditions can be written as

$$\begin{pmatrix} B_0 & 0 \\ 0 & B_1 \end{pmatrix} \begin{pmatrix} g^0 \\ g^1 \end{pmatrix} = 0, \quad (4.65)$$

where

$$B_\nu = \begin{pmatrix} B_\nu^{j_\nu} & 0 & \cdots & 0 \\ 0 & B_\nu^{j_\nu} & \ddots & \vdots \\ \vdots & \ddots & \ddots & 0 \\ 0 & \cdots & 0 & B_\nu^{j_\nu} \end{pmatrix}, \quad (4.66)$$

is a diagonal matrix of the same size as  $H_\nu^\gamma$ , and  $j_\nu = \nu + P_\nu + l + s$ ,  $B_\nu^{j_\nu}$  is a rectangular matrix of the same width as  $H_{\nu\kappa n}^\gamma$ , but a smaller height corresponding to the number of grid points near internal boundaries or where a symmetry condition holds. If  $\nu + P_\nu + l + s$  is even (odd)  $B_\nu^{\nu+P_\nu+l+s}$  enforces zero derivative (value) along the symmetry plane.

As in Ref. [73] each of the  $B_{\nu}^{j\nu}$  matrices can be split into two submatrices.

$$B_{\nu}^{j\nu} = (B_{\nu 1}^{j\nu} B_{\nu 2}^{j\nu}), \quad (4.67)$$

and similarly splitting the vector  $g_{\kappa ls}^{\nu}$

$$g_{\kappa ls}^{\nu} = \begin{pmatrix} g_{\kappa ls 1}^{\nu} \\ g_{\kappa ls 2}^{\nu} \end{pmatrix}, \quad (4.68)$$

yields the equation

$$B_{\nu 1}^{j\nu} g_{\kappa ls 1}^{\nu} + B_{\nu 2}^{j\nu} g_{\kappa ls 2}^{\nu} = 0, \quad (4.69)$$

where the vector and matrix have been ordered so that the index 1 refers to the  $n_b$  boundary points and the index 2 refers to the  $n_i$  interior points. The grid point nearest to the boundary, at which an explicit boundary condition is given is considered a boundary point.  $B_{\nu 1}^{j\nu}$  is an  $n_b$  by  $n_b$  matrix and  $B_{\nu 2}^{j\nu}$  is an  $n_b$  by  $n_i$  matrix. The total number of grid points is  $n_t = n_b + n_i$ .

Each  $n_t$  by  $n_t$  block of the Hamiltonian matrix  $H_{\nu}^{\gamma}$  (Eq. 4.63) can be split in a similar way,

$$H_{\nu\kappa n}^{\gamma} = \begin{matrix} n_b \{ \\ n_i \{ \end{matrix} \underbrace{\begin{pmatrix} H_{\nu\kappa n 11}^{\gamma} & H_{\nu\kappa n 12}^{\gamma} \\ H_{\nu\kappa n 21}^{\gamma} & H_{\nu\kappa n 22}^{\gamma} \end{pmatrix}}_{n_b + n_i}. \quad (4.70)$$

So there are  $n_t + n_b$  equations and  $n_t$  unknowns ( $g_1$  and  $g_2$ ) as well as the eigenvalue. One could approximately solve these equations with singular value decomposition [124], but it is much faster to simply discard the first  $n_b$  rows of each  $H_{\nu\kappa n}^{\gamma}$  (one should still check after finding a solution that it approximately satisfies those rows of the matrix equation) and incorporate the boundary conditions into the remaining eigenvalue problem by replacing each  $H_{\nu\kappa n}^{\gamma}$  with

$$H_{\nu\kappa n}^{\gamma} \rightarrow H_{\nu\kappa n 22}^{\gamma} - H_{\nu\kappa n 21}^{\gamma} (B_{\nu 1}^{j\nu})^{-1} B_{\nu 2}^{j\nu}, \quad (4.71)$$

where  $B_{\nu 1}^{j\nu}$  has an inverse because all of its rows are linearly independent (otherwise more than one boundary condition would have been specified for a given boundary point). Calculating the inverse is computationally inexpensive since  $n_b \ll n_t$ . One solves for  $g_{\kappa ls 1}^\nu$  afterwards with

$$g_{\kappa ls 1}^\nu = -(B_{\nu 1}^{j\nu})^{-1} B_{\nu 2}^{j\nu} g_{\kappa ls 2}^\nu. \quad (4.72)$$

The number of grid points in each subdomain was  $n_t = 2n \times n \times n$  (greater resolution is needed along the semi-infinite coordinate). This leads to a Hamiltonian matrix size of  $n_t \times n_t$  for S states and  $2n_t \times 2n_t$  for odd parity P states. After solving for boundary conditions with the above procedure, these are reduced to  $n_m \times n_m$ , where  $n_m = n_i = 6n^3 - 12n^2 + 6n$  and  $n_m = 2n_i$ , respectively. The number of nonzero elements  $n_{NZ}$  scales as  $n^4$ . For  $n = 20$ , this corresponds to 560 MB and 1.8 GB, respectively, of memory required to store the matrix<sup>4</sup>. The sizes of the matrices and the number of nonzero elements is given in Tab. 4.1.

The method of inverse iteration [124] was used to find eigenvalues with a shift equal to the known eigenvalues plus  $10^{-4}$  so that the matrix is not too singular. Each iteration requires a matrix solve. For the smaller matrices (up to  $17,000 \times 17,000$ ), these solves were performed using Mathematica's [153] multi-frontal matrix solve routine. This method is fast (eigenvalues can be calculated in about 10 minutes for that size) but 8 GB of RAM was not enough to do larger sizes. For larger matrices, the generalized *minimal residual* (GMRES) method of PETSc [10, 9, 11] was used. The GMRES method produces a solution with the Krylov space of the matrix and is more memory efficient.

---

<sup>4</sup>Note: some eigenvalue solvers do not require one to store this matrix and simply require a function which can calculate the matrix times a given vector.

Table 4.1: The matrix sizes  $n_m$  and number of nonzero elements  $n_{NZ}$  for each resolution  $n$ .

Resolution	<sup>1</sup> S States		<sup>1</sup> P States	
	$n_m$	$n_{NZ}$	$n_m$	$n_{NZ}$
7	1 512	182 952	3 024	573 720
8	2 352	381 024	4 704	1 204 448
9	3 456	722 304	6 912	2 297 276
10	4 860	1 273 320	9 720	4 069 800
11	6 600	2 118 600	13 200	6 798 440
12	8 712	3 362 832	17 424	10 826 640
13	11 232	5 133 024	22 464	16 571 568
14	14 196	7 580 664	28 392	24 531 416
15	17 640	10 883 880	35 280	35 292 600
16	21 600	15 249 600	43 200	49 536 960
17	26 112	20 915 712	52 224	68 048 960
18	31 212	28 153 224	62 424	91 722 888
19	36 936	37 268 424	73 872	121 570 056
20	43 320	48 605 040	86 640	158 726 000
21	50 400	62 546 400		
22	58 212	79 517 592		
23	66 792	99 987 624		

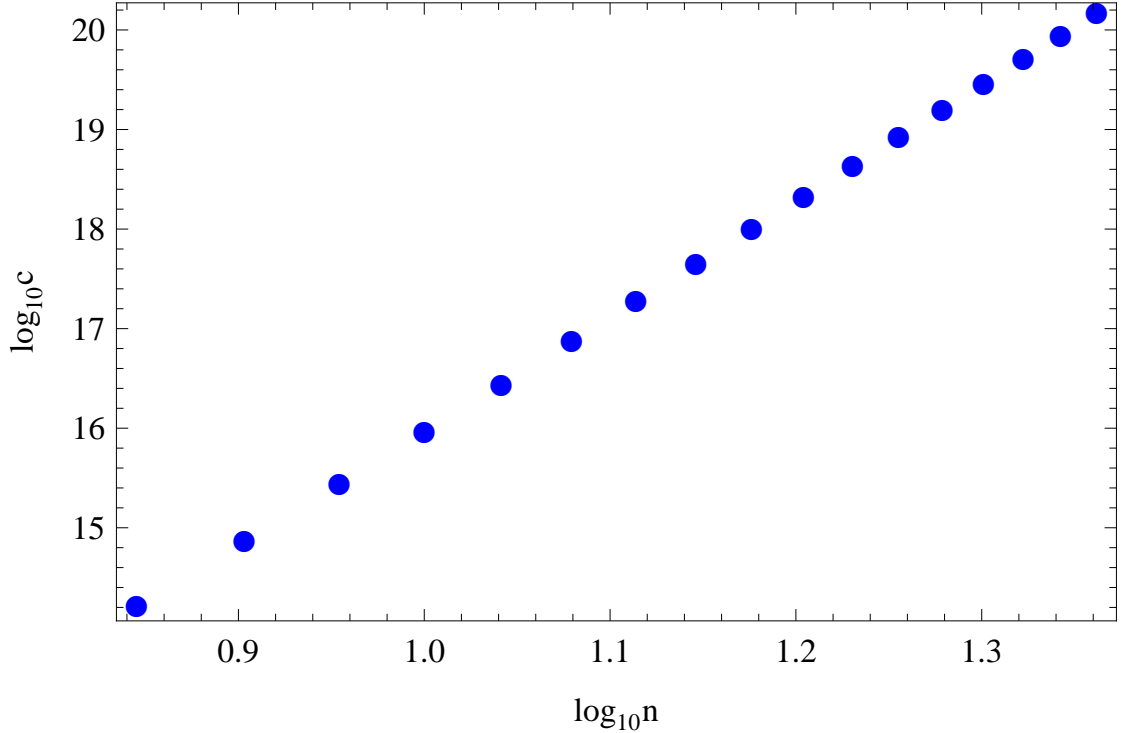


Figure 4.2: (Color online). A log-log plot of the approximate condition number  $c$  of the pseudospectral matrices as a function of resolution.

All calculations were done with double precision arithmetic. This gives a lower bound to the error in the calculated eigenstate. The effect is relatively big for the small exponential tail. We observe the wave functions to no longer follow their true asymptote at about the level of  $10^{-8.7}$  of their maximum value. This value is independent of resolution. Since a constant value for the wave function on a semi-infinite domain leads to divergent matrix elements,<sup>5</sup> we set any value of the eigenvector below this threshold to zero.

Condition numbers of pseudospectral matrices grow rather fast [121]. The matrices are not normal (the matrices and their transposes do not commute); nonetheless, we approximate the condition number by the ratio of the largest

---

<sup>5</sup>For a finite resolution, the quadrature still leads to a finite result with an error enhanced by at most  $10^4$ .

to smallest eigenvalues. This approximation is plotted versus resolution in Fig. 4.2. It starts out large and grows asymptotically as  $n^{12}$ . An ill-posed problem has a condition number which grows exponentially. This problem is well-posed but in order to solve this system of equations preconditioning is necessary. A reasonable preconditioner is a matrix produced by a second order finite differencing scheme on the same set of grid points. [121] The preconditioning matrix solves are further preconditioned with a block Jacobi preconditioner.

The modified Gram-Schmidt procedure was used to orthogonalize the Krylov subspace. Furthermore, the GMRES restart parameter,  $m$  needs to be very large for convergence, empirically,  $m = 1.3n_m^{3/4}$ , where  $n_m \times n_m$  is the matrix size. The computation time scales as  $n_m^3$ , which for  $n = 20$  was about a day running on six 2 GHz processors. The eigenvalue solver is the slowest part of the entire computation.

### 4.9.1 Quadrature

In this article, we calculate matrix elements of the form  $\langle i|\hat{O}|j\rangle$ , where  $|i\rangle$  and  $|j\rangle$  are two quantum states and  $\hat{O}$  is some operator. This calculation requires numerical integration. Pseudospectral methods, by design, use quadrature points as the grid points. A one dimensional function  $f[x]$  can be numerically integrated from  $x = -1$  to  $x = 1$  with weight function  $g[x]$  by

$$\int_{-1}^1 f[x]g[x]dx \approx \sum w_i f[x^i], \quad (4.73)$$

where  $w_i$  are the quadrature weights specific to the weighting function  $g$  at grid point  $x^i$ . This quadrature formula is exponentially accurate with increasing resolution if  $f$  is smooth over the domain  $-1 \leq x \leq 1$ . The problems solved in this

article are three-dimensional with three overlapping subdomains. A separate quadrature can be done in each domain. This is illustrated for domain  $D_1$ . The three coordinates used in this domain are  $x$ ,  $\phi$ , and  $\theta_{12}$  with ranges  $-1 \leq x \leq 1$ ,  $0 \leq \phi \leq 1$ , and  $0 \leq \theta_{12} \leq \pi$ . Define

$$x_1 = x \tag{4.74}$$

$$x_2 = 4\phi - 1 \tag{4.75}$$

$$x_3 = \frac{2\theta_{12}}{\pi} - 1, \tag{4.76}$$

so that  $-1 \leq x_1, x_2, x_3 \leq 1$ . Then integrals over  $D_1$  can be done with three quadratures like Eq. 4.73. To satisfy the requirement that  $f$  is smooth (up to the logarithmic singularity at  $\rho = 0$ ), we choose  $g = 1$ , which corresponds to Legendre quadrature points, which are used for all calculations in this article instead of Chebyshev which were used in Ref. [73].

If all the subdomains are nonoverlapping, then the above scheme is sufficient for all integrals. However, no set of nonoverlapping subdomains for which  $f$  is smooth could be found.<sup>6</sup> A method is needed for handling overlapping regions, which the above scheme double counts if a quadrature is performed in each subdomain. For these regions, an interpolation was performed to two new  $2n \times n \times n$  grids spanning the overlap regions, shown in Fig 4.3. For the pseudospectral method, interpolation is done to the same order as the grid size. A quadrature can then be done over the overlap region, which are used to correct the overall integration.

---

<sup>6</sup>Some do exist which are only nonanalytic on some edges, but these produce nonexponential convergence.

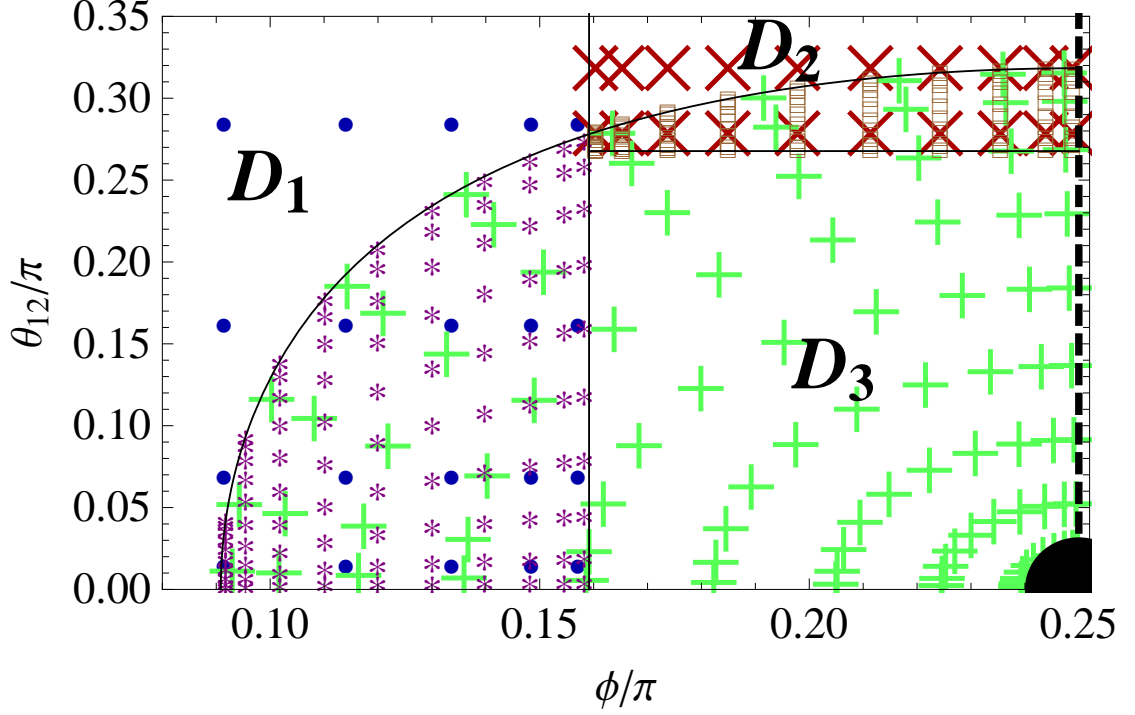


Figure 4.3: (Color online). This is the arrangement of grid points of the three domains at a constant value of  $\rho$  in  $\phi$  and  $\theta_{12}$  coordinates for  $n = 10$ . As in Fig. 4.1, the blue circles, red crosses, and green pluses belong to domains  $D_1$ ,  $D_2$ , and  $D_3$ , respectively. Also shown are the overlap grid points in  $D_1 \cap D_3$  (purple stars) and  $D_2 \cap D_3$  (brown squares). The electron-electron singularity is visible at the lower right hand corner (solid disk at  $\phi = \pi/4, \theta_{12} = 0$ ) as well as the line of symmetry on the right side (dashed line at  $\phi = \pi/4$  where  $r_1 = r_2$ ).

The overlap region is divided into two subdomains

$$D_{13} = D_1 \cap D_3 \quad (4.77)$$

$$D_{23} = D_2 \cap D_3 \quad (4.78)$$

These definitions are equivalent to

$$D_{13} : -1 \leq x \leq 1, \quad \phi_{\min} \leq \phi \leq \frac{1}{2}, \quad 0 \leq \theta_{12} \leq \theta_{12, \max}[\phi] \quad (4.79)$$

$$D_{23} : -1 \leq x \leq 1, \quad \frac{1}{2} \leq \phi \leq \frac{\pi}{4}, \quad \arccos \frac{2}{3} \leq \theta_{12} \leq \theta_{12, \max}[\phi],$$

where  $\phi_{\min} = \pi/4 - 1/2$  is determined by  $\zeta = 1/2$  and  $\theta_{12} = 0$  and  $\theta_{12, \max}[\phi] =$

$\arccos[\cos 1 \csc 2\phi]$  is determined by  $\zeta = 1/2$ . For these quadratures one must redefine  $x_1, x_2, x_3$ . For example, in  $D_{13}$

$$x_1 = x \quad (4.80)$$

$$x_2 = 2 \left( \frac{1}{2} - \phi_{\min} \right) (\phi - \phi_{\min}) - 1 \quad (4.81)$$

$$x_3 = 2\theta_{12,\max}[\phi]\theta_{12} - 1. \quad (4.82)$$

One proceeds by numerically integrating  $x_3$  first and then the others as normal.

The function values at the points necessary for the quadrature  $\{x^{i'}, \phi^{j'}, \theta_{12}^{j'k'}\}$  are calculated with interpolation

$$f[x^{j'_1}, \phi^{j'_2}, \theta_{12}^{j'_2j'_3}] \approx \sum_J f[x^{j_1}, \phi^{j_2}, \theta_{12}^{j_2j_3}] \mathcal{C}_J[x^{j'_1}, \phi^{j'_2}, \theta_{12}^{j'_2j'_3}]. \quad (4.83)$$

where  $\mathcal{C}_J$  refers to the effective basis defined in Eq. 4.3.

Sometimes  $f$  will include a Dirac delta function. In such a case, one integrates out the delta function analytically. One is left with a two dimensional integral on the surface where the argument of the delta function is zero. This entails first interpolating to that surface using Eq. 4.83. One can then proceed normally.

## 4.10 Energy and oscillator strength results

The purpose of this article is to generalize the pseudospectral methods we previously developed for S states to the general angular momentum case, calculate oscillator strengths, and test how local errors in the wave function vary with resolution. We study the convergence of the energies of S and P states and the absorption oscillator strength of the transition between them.

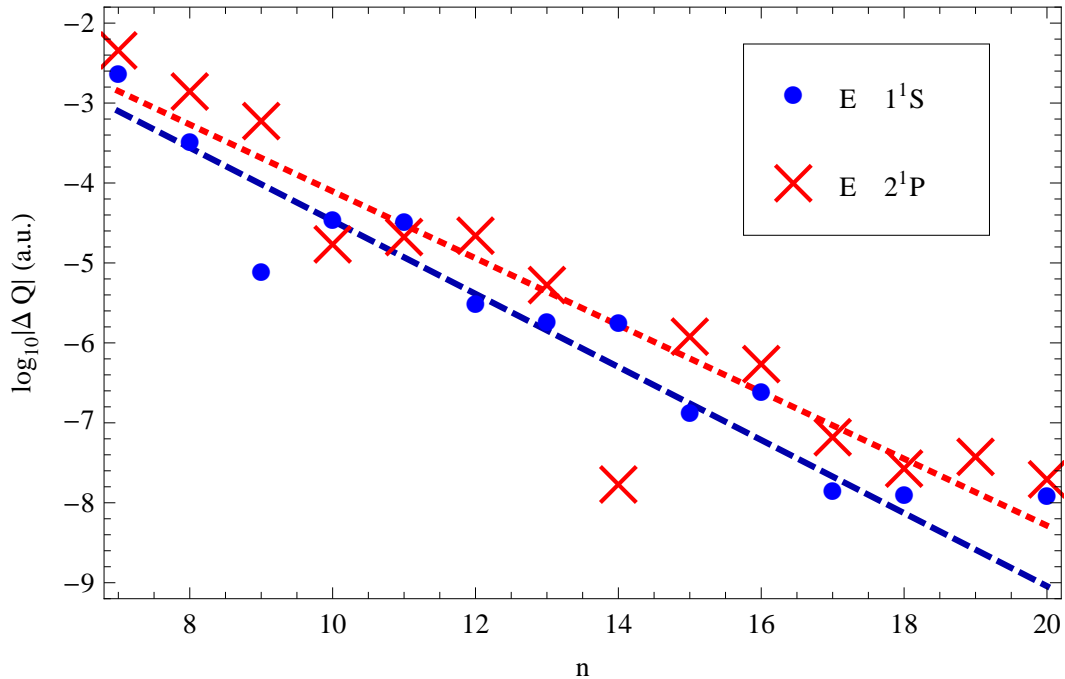


Figure 4.4: (Color online). The logarithm base 10 of the energy error of both the lowest energy S state and P state of helium. The dark blue circles are for the  $1^1\text{S}$  state and the light red crosses for the  $2^1\text{P}$  state with dashed blue and dotted red fits, respectively (see Tab. 4.2).

The most widely quoted number to ascertain convergence of a quantum method is the energy. This value gives a global measure of accuracy. Figure 4.4 shows the convergence rate of the energy of the  $1^1\text{S}$  and  $2^1\text{P}$  states of helium. Here and throughout the results section the high precision values of Drake [45] are taken to be exact. The energy error for both states decreases exponentially with resolution. Convergence for the S state is similar to that reported in Ref. [73] with slight differences related to a different choice of coordinates. The current calculation also goes to  $n = 20$  instead of  $n = 14$  in Ref. [73].

A common feature of the energy convergence and all other convergence plots in this article is nonmonotonic convergence. This method is not varia-

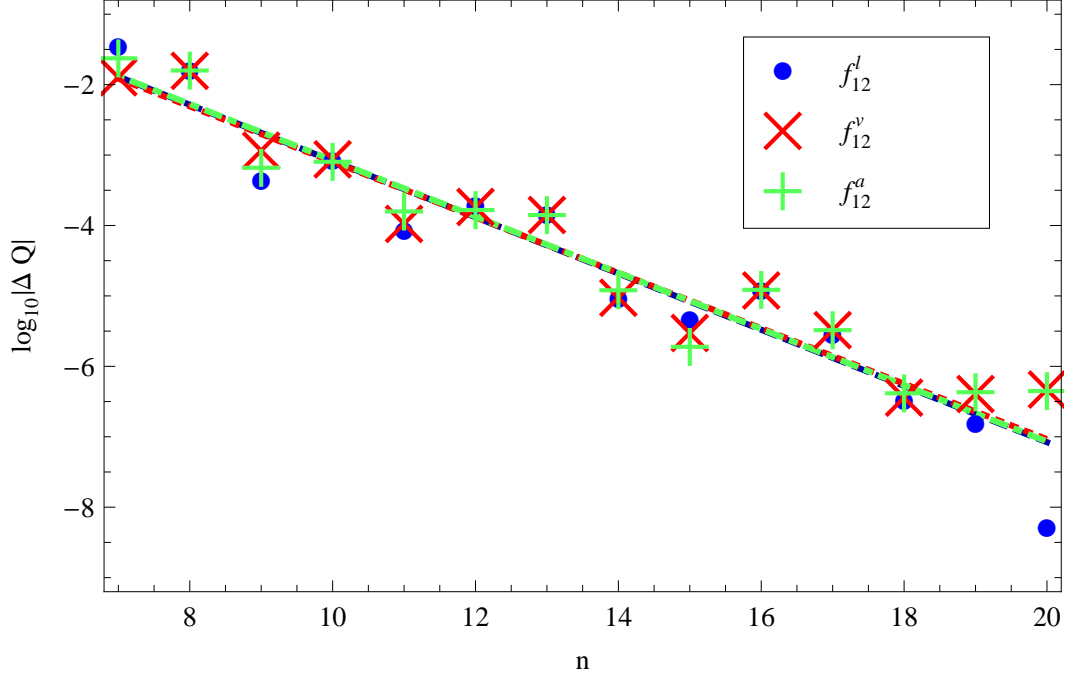


Figure 4.5: (Color online). The logarithm base 10 of the error in the oscillator strength of the  $1^1S \rightarrow 2^1P$  transition of helium. The dark blue circles are for the length form, the light red crosses are for the velocity form, and the green pluses for the acceleration form with dashed blue, dotted red, and dot-dashed green fits, respectively (see Tab. 4.2).

tional, so there is no reason to expect monotonic convergence. All quantities calculated can be above or below their actual value, with the error being quasirandomly determined by the exact positions of all the grid points. As is shown in these plots, the “random” jumps in error decrease in magnitude as the resolution is increased.

As described in Sec. 4.5, there are three commonly used forms for the oscillator strength. The length, velocity, and acceleration forms depend most strongly on the value of the wave function at positions in configuration space corresponding to large, medium, and small separations. Their relative errors can be

indicate where the wave function is more accurate. For most variational calculations, the acceleration form tends to be much less accurate than the other two forms, indicating errors in the wave function at small separation that have little effect on the variational energy. The length and velocity forms give roughly equally accurate results.

The oscillator strength of the  $1^1S \rightarrow 2^1P$  transition was calculated using all three forms with errors shown in Fig. 4.5. Here, all three forms give roughly the same results. At most resolutions the points are on top of one another and their fits are indistinguishable. One interpretation is that the wave function errors in the oscillator strength calculation are constant relative errors (excluding the part of space where the wave function is so small that roundoff error dominates).

It should be noted that the value used as the exact value [45] is given to seven decimal places. Consequently, the errors inferred for the highest resolution pseudospectral results in Fig. 4.5 are not too precise. There is little practical need for additional digits since a host of other effects including finite nuclear mass, relativistic, and quadrupole corrections would contribute to any hypothetical, high precision experimental measurement of the oscillator strength at greater levels.

As pointed out by Schiff *et al.* [133] and reviewed by Hibbert [85], the assumption that the differences between the values of the oscillator strength from the different forms give a measure of the accuracy of the method is not valid, and they suggest also checking the difference between the calculated value and the extrapolated value. This latter procedure is not possible to do for a pseudospectral method with nonmonotonic convergence. In Fig. 4.6 the error in the average of the three oscillator strength forms is plotted with the standard de-

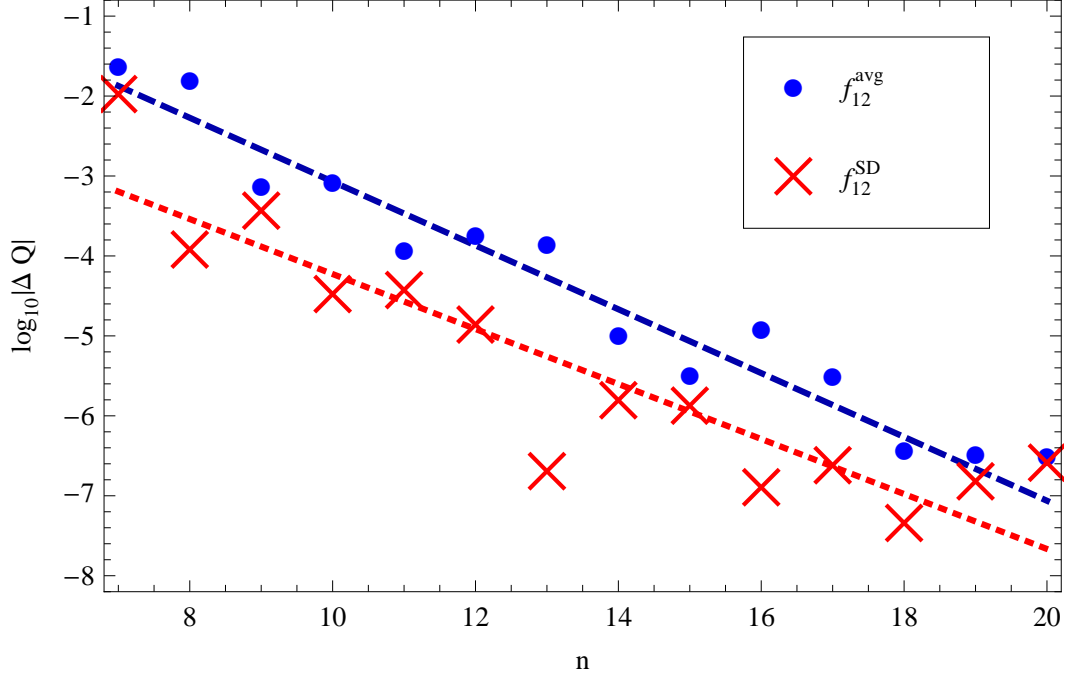


Figure 4.6: (Color online). The logarithm base 10 of the error in the average of the length, velocity, and acceleration forms of the oscillator strength (dark blue circles) and their standard deviation (light red crosses) for the  $1^1\text{S} \rightarrow 2^1\text{P}$  transition of helium, with dashed blue and dotted red fits, respectively (see Tab. 4.2).

viation. The standard deviation is about an order of magnitude less than the error in the average value of the oscillator strength. The trend lines suggest that the standard deviation is approaching the error. A possible explanation is that the calculation at the highest resolutions is starting to become sensitive to our truncation of the wave function when it is small (see Sec. 4.9) and so this error becomes the dominant contribution to both the standard deviation and the total error. So at  $n = 20$ , we assume the standard deviation and total error are equal and get a value for the oscillator strength of  $0.27616499(27)$  which compares favorably to Drake's [45]  $0.2761647$ .

All convergence data were fit to functions of the form  $A10^{-\beta(n-20)}$  using the

Table 4.2: The fit parameters to all the convergence plots of quantities  $Q$  in this section.

$Q$	Figure	$A$	$\beta$
$E(1^1\text{S})$	4.4	$9.0 \times 10^{-10}$	0.46
$E(2^1\text{P})$	4.4	$5.2 \times 10^{-9}$	0.42
$f_{12}^l$	4.5	$8.4 \times 10^{-8}$	0.40
$f_{12}^v$	4.5	$9.2 \times 10^{-8}$	0.39
$f_{12}^a$	4.5	$8.6 \times 10^{-8}$	0.40
$f_{12}^{avg}$	4.6	$8.7 \times 10^{-8}$	0.40
$f_{12}^{SD}$	4.6	$2.2 \times 10^{-8}$	0.34

same procedure as in Ref. [73]. Because of uncertainty in the errors for the largest resolutions ( $n = 19$  and  $n = 20$ ) these points were not used in the fits of  $f_{12}^l$ ,  $f_{12}^v$ ,  $f_{12}^a$ , and  $f_{12}^{avg}$ . All pairs of fit parameters are roughly the same, especially for the oscillator strength convergence fits.

#### 4.11 Corrections to the Hamiltonian

There are two small parameters in which the full Hamiltonian is often expanded: the ratio of the reduced mass of the electron-nucleus pair to the nuclear mass,  $\mu/M = 1.37074563559(58) \times 10^{-4}$  [107, 108] (for  $^4\text{He}$ ) and the fine structure constant  $\alpha = 7.2973525376(50) \times 10^{-3}$  [107, 108]. Here, the lowest order corrections in  $\mu/M$  and  $\alpha$  are considered. For very high-precision work, one needs the perturbative corrections in powers of each small quantity.

### 4.11.1 Finite nuclear mass correction

The nonrelativistic ( $\alpha^0$ ) Hamiltonian for two-electron atoms can be written

$$\hat{H}_{nr} = \hat{H}_0 + \hat{H}_{cm} + \hat{H}_{mp}, \quad (4.84)$$

where  $\hat{H}_0$  is the fixed nucleus approximation to the hamiltonian with the electron mass set to  $\mu$ ,  $\hat{H}_{cm}$  is the kinetic energy of the center of mass, and  $\hat{H}_{mp}$  is the mass polarization term:

$$\hat{H}_0 = \frac{1}{2}(p_1^2 + p_2^2) + \hat{V} \quad (4.85)$$

$$\hat{H}_{cm} = \frac{1}{2(M + 2m_e)}p_{cm}^2 \quad (4.86)$$

$$\hat{H}_{mp} = \frac{1}{M}\mathbf{p}_1 \cdot \mathbf{p}_2, \quad (4.87)$$

where  $\hat{V}$  is the potential energy operator,  $m_e$  is the electron mass,  $\mathbf{p}_{cm}$  is the momentum operator of the center of mass, and reduced mass atomic units ( $\mu = 1$ ) are being used. The second term is removed in center-of-mass coordinates and the last term provides the dominant nontrivial correction for finite nuclear mass (the trivial one being the scaling of the energy by  $m_e/\mu$ ).

### 4.11.2 Relativistic corrections

The Schrödinger equation is a nonrelativistic approximation to the true equation of motion. The lowest order relativistic corrections enter at order ( $Z\alpha^2$ ), as summarized in Ref. [58]. The Breit-Pauli Hamiltonian encapsulates the correction

$$\hat{H}_{BP} = \hat{H}_{nr} + \hat{H}_{rel}, \quad (4.88)$$

where  $\hat{H}_{nr}$  is the usual nonrelativistic Hamiltonian used in Schrödinger's equation and  $\hat{H}_{rel}$  is the lowest order relativistic correction. The latter can be further divided into nonfine-structure (NFS) and fine-structure (FS) contributions:

$$\hat{H}_{NFS} = \hat{H}_{mass} + \hat{H}_D + \hat{H}_{SSC} + \hat{H}_{OO} \quad (4.89)$$

$$\hat{H}_{FS} = \hat{H}_{SO} + \hat{H}_{SOO} + \hat{H}_{SS}. \quad (4.90)$$

The separate contributions to the Hamiltonian are the mass-velocity (mass), two-body Darwin (D), spin-spin contact (SSC), orbit-orbit (OO), spin-orbit (SO), spin-other-orbit (SOO), and the spin-spin (SS) terms. These are explicitly given by

$$\hat{H}_{mass} = -\frac{\alpha^2}{8} \sum_i p_i^4 \quad (4.91)$$

$$\hat{H}_D = -\frac{\alpha^2 Z}{8} \sum_i \nabla_i^2 r_i^{-1} + \frac{\alpha^2}{4} \sum_{i<j} \nabla_i^2 r_{ij}^{-1} \quad (4.92)$$

$$\hat{H}_{SSC} = -\frac{8\pi\alpha^2}{3} (\mathbf{s}_1 \cdot \mathbf{s}_2) \delta(\mathbf{r}_{12}) \quad (4.93)$$

$$\hat{H}_{OO} = -\frac{\alpha^2}{2} \left( \frac{\mathbf{p}_1 \cdot \mathbf{p}_2}{r_{12}} + \frac{\mathbf{r}_{12}(\mathbf{r}_{12} \cdot \mathbf{p}_1) \cdot \mathbf{p}_2}{r_{12}^3} \right) \quad (4.94)$$

$$\hat{H}_{SO} = \frac{\alpha^2 Z}{2} \sum_i \frac{\hat{\mathbf{l}}_i \cdot \hat{\mathbf{s}}_i}{r_i^3} \quad (4.95)$$

$$\hat{H}_{SOO} = -\frac{\alpha^2}{2} \sum_{i \neq j} \left( \frac{\mathbf{r}_{ij}}{r_{ij}^3} \times \mathbf{p}_i \right) \cdot (\mathbf{s}_i + 2\mathbf{s}_j) \quad (4.96)$$

$$\hat{H}_{SS} = \frac{\alpha^2}{r_{12}^3} \left( \mathbf{s}_1 \cdot \mathbf{s}_2 - \frac{3}{r_{12}^2} (\mathbf{s}_1 \cdot \mathbf{r}_{12})(\mathbf{s}_2 \cdot \mathbf{r}_{12}) \right), \quad (4.97)$$

where  $i$  and  $j$  can be 1 or 2,  $\mathbf{p}_i$  and  $\mathbf{r}_i$  are the momentum and position of the  $i$ th electron with respect to the nucleus, respectively,  $\mathbf{r}_{12}$  is the vector pointing from the first electron to the second, and  $\hat{\mathbf{s}}_i$  and  $\hat{\mathbf{l}}_i$  are the one-electron spin and angular momentum operators of the  $i$ th electron, respectively. The last three terms are zero for  $^1S$  states due to symmetry considerations.

There are many higher order terms (see Refs. [46, 50, 52]) but we do not

consider any of them.

## 4.12 Mass polarization and relativistic correction calculations

The mass polarization and low order relativistic corrections to the nonrelativistic Hamiltonian have been known for some time [20]. The main challenge in calculating these terms has been in numerical improvements to the wave functions. Early calculations [94, 89, 142, 6] were critical for comparing experimental and theoretical energies, confirming that Schrödinger's equation is correct in the nonrelativistic limit for helium.

The development of computers enabled Pekeris and coworkers [118, 119, 132] and others [136, 138, 82, 105, 40] to reach theoretical uncertainties in the energy of about  $10^{-2} \text{ cm}^{-1}$ . Such precision allowed Lewis and Serafino [105] to calculate the fine structure constant by comparing with experimental measurements of the  $2^3\text{P}$  splitting. They obtained  $\alpha^{-1} = 137.03608(13)$  only surpassed at the time by the measurements of the electron anomalous magnetic moment ( $g - 2$ ) by a factor of two in estimated uncertainty and the ac Josephson experiments by a factor of four.

Drake and collaborators [44, 51, 154, 49, 46, 47, 53] and Pachucki [116] have pushed relativistic corrections up to order  $\alpha^5$  and beyond. Drake [47] matched theoretical and observed energy differences in the  $J = 0, 1$  splitting of the  $2^3\text{P}$  state to determine  $\alpha^{-1} = 137.0359893(23)$ , which differs from the  $g - 2$  result  $137.0359996(8)$ , but agrees with the ac Josephson results  $137.0359872(43)$  [47]. However, the  $J = 1, 2$  splitting gives an unreasonable value, indicating that the helium fine structure needs to be understood better.

### 4.13 Expectation values

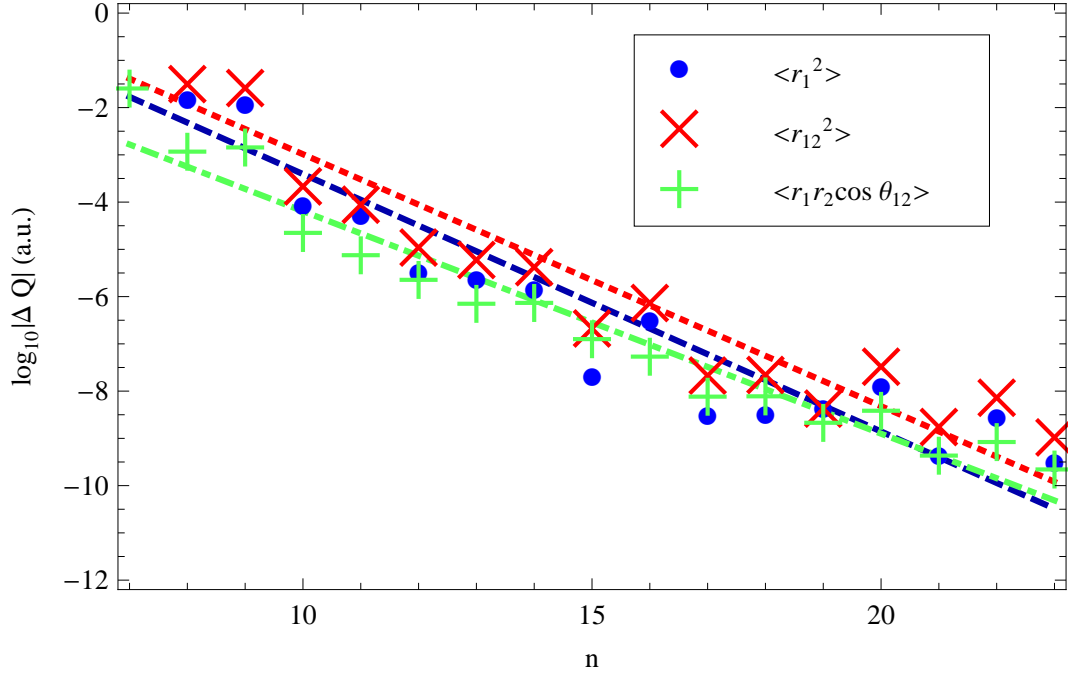


Figure 4.7: (Color online). The logarithm base 10 of the error in the expectation values of operators that scale as  $\rho^2$  for helium. The dark blue circles are for  $\langle r_1^2 \rangle$ , the light red crosses are for  $\langle r_{12}^2 \rangle$ , and the green pluses are for  $\langle r_1 r_2 \cos \theta_{12} \rangle$  with dashed blue, dotted red, and dot-dashed green fits, respectively (see Tab. 4.3).

This article does not attempt to compete with the above works, merely to test the pseudospectral method's ability to accurately represent the wave function in different parts of configuration space and to compare the convergence rates of the errors with that of the energies and oscillator strengths. To produce a representative set of calculations, the expectation values of all the operators needed for leading order relativistic (Sec. 4.11.2) and finite nuclear mass (Sec. 4.11.1) corrections, for the oscillator strength sum rules (Eqs. 4.29-4.32), and  $\langle V^2 \rangle$  are presented here. They are organized by type, which stress different parts of the wave function or different parts of the calculation.

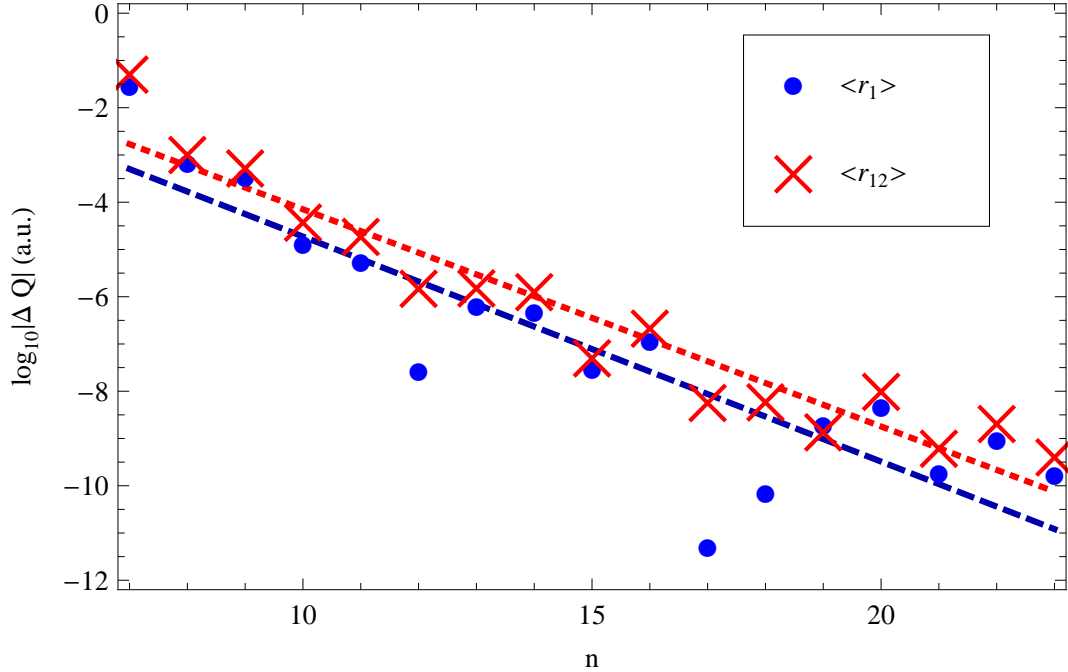


Figure 4.8: (Color online). The logarithm base 10 of the error in the expectation values of operators that scale as  $\rho$  for helium. The dark blue circles are for  $\langle r_1 \rangle$  and the light red crosses are for  $\langle r_{12} \rangle$  with dashed blue and dotted red fits, respectively (see Tab. 4.3).

One way to analyze local convergence is to look at the convergence of various operators that give different weights to different parts of the wave function. One can see that in all calculations of expectation values shown in Figs. 4.7, 4.8, 4.9, 4.10, 4.11, and 4.12, not only are the rates of convergence roughly the same, but also the magnitudes of the errors. These errors decrease exponentially until they reach roughly the level of error produced by truncating the wave function (see Sec. 4.9) at the highest resolutions. The differences that are seen in these plots are at low resolution, for which the representation of the wave function at large  $\rho$  is particularly poor and so the expectation values that scale as  $\rho^2$  and  $\rho$  have larger errors there. However, at high resolution the errors are about the same. This is reflected in the fits (see Tab. 4.3).

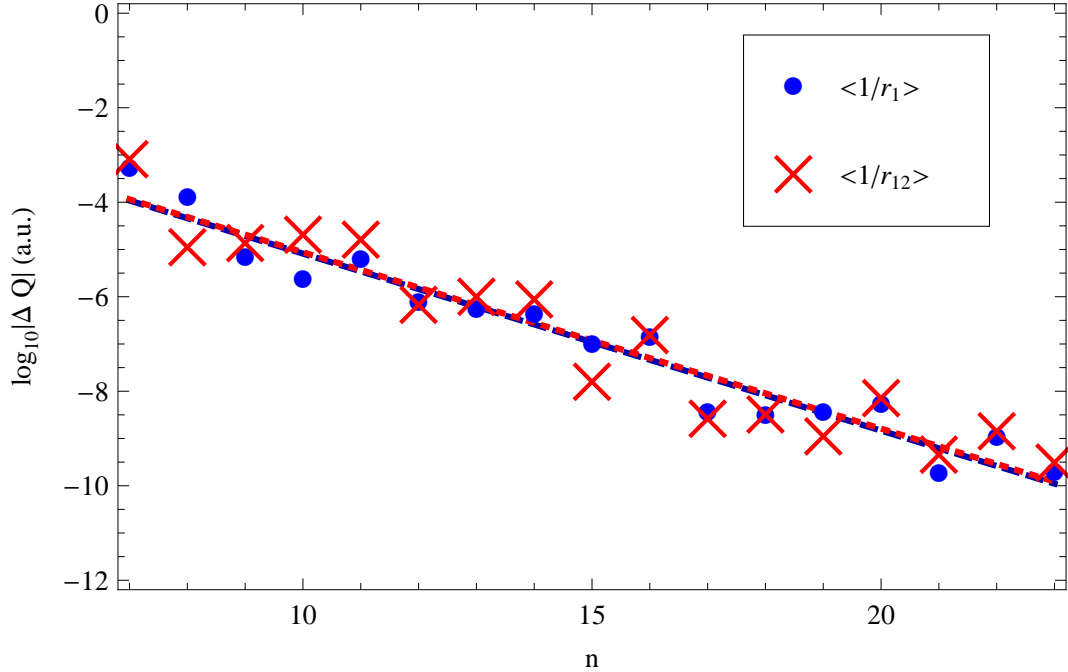


Figure 4.9: (Color online). The logarithm base 10 of the error in the expectation values of operators that scale as  $1/\rho$  for helium. The dark blue circles are for  $\langle 1/r_1 \rangle$  and the light red crosses are for  $\langle 1/r_{12} \rangle$  with dashed blue and dotted red fits, respectively (see Tab. 4.3).

Even the expectation values of delta functions (See Fig. 4.11) which are most sensitive to the Kato cusp conditions [92] have the same convergence properties. This provides evidence that our choices of coordinates allowed the pseudospectral method to infer the solution in the vicinity of a cusp.

The error in the mass polarization and orbit-orbit terms are also shown in Fig. 4.12. Again, the convergence rates are the same. Calculations of derivatives (needed to form the appropriate operators) appear to be just as accurate as the function values, even when they are most strongly weighted close to the electron-electron cusp, as is the case for the orbit-orbit interaction.

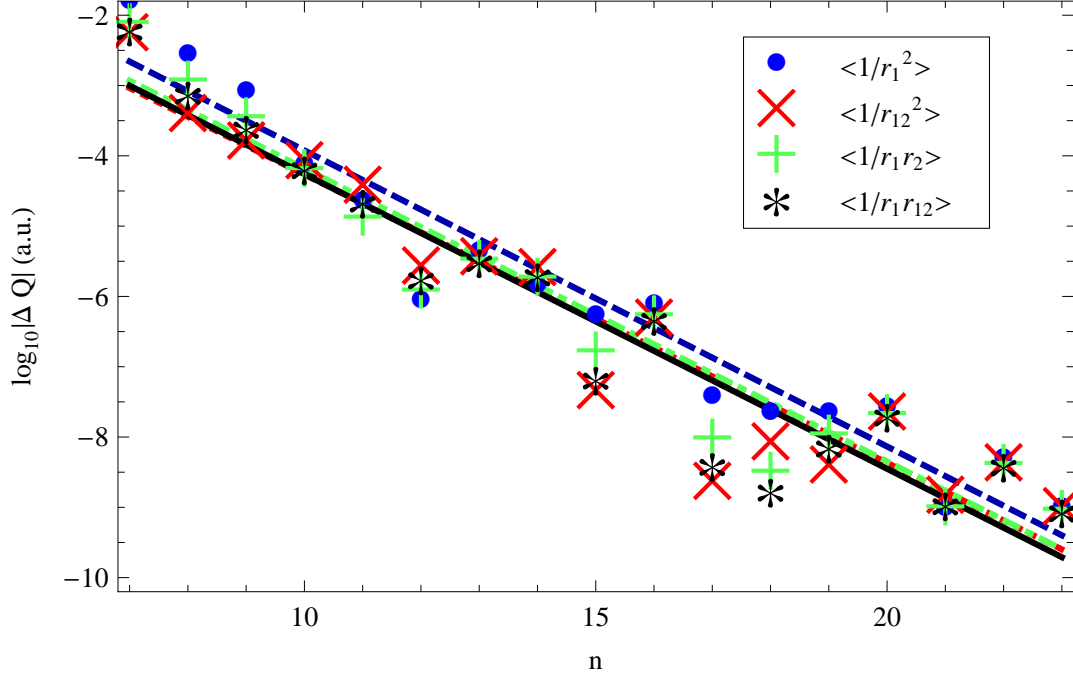


Figure 4.10: (Color online). The logarithm base 10 of the error in the expectation values of operators that scale as  $1/\rho^2$  for helium. The dark blue circles are for  $\langle 1/r_1^2 \rangle$ , the light red crosses are for  $\langle 1/r_{12}^2 \rangle$ , the green pluses are for  $\langle 1/r_1 r_2 \rangle$ , and the black stars are for  $\langle 1/r_1 r_{12} \rangle$  with dashed blue, dotted red, dot-dashed green, and solid black fits, respectively (see Tab. 4.3).

All convergence data were fit to functions of the form  $A10^{-\beta(n-23)}$  using the same procedure as in Ref. [73]. The fit parameters are shown in Tab. 4.3. The most striking feature is how similar the magnitudes of the errors are at  $n = 23$ . Also, the exponential parameter  $\beta$  is roughly the same for all expectation values and the energies and oscillator strengths (see Tab. 4.2) with the differences already discussed. So as one increases resolution, one increases the accuracy of all expectation values or oscillator strengths by roughly the same amount.

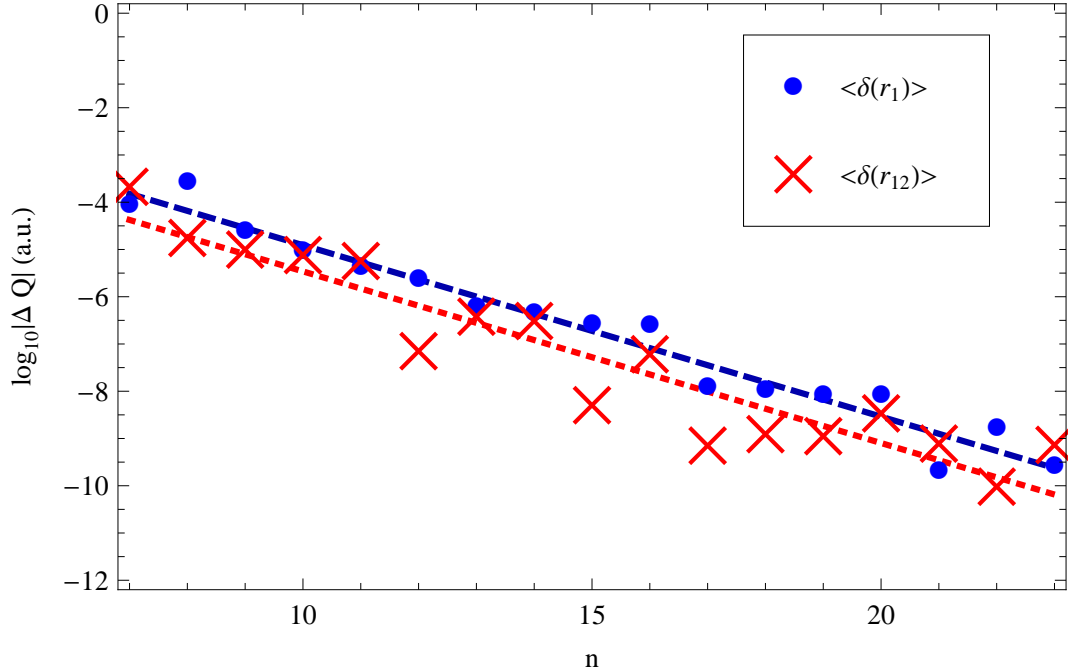


Figure 4.11: (Color online). The logarithm base 10 of the error in the expectation values of delta function operators for helium. The dark blue circles are for  $\langle\delta(r_1)\rangle$  and the light red crosses are for  $\langle\delta(r_{12})\rangle$  with dashed blue and dotted red fits, respectively (see Tab. 4.3).

## 4.14 Conclusions

A general prescription has been given for choosing subdomains for a pseudospectral method. This prescription has been applied to the helium problem with success.

The pseudospectral method provides exponentially fast convergence for many expectation values and the oscillator strength. The magnitudes of the errors and the convergence rates are roughly the same as that of the energy. The calculations were performed out to near the limits of double precision arithmetic. Higher precision will be necessary to improve these calculations. No fine

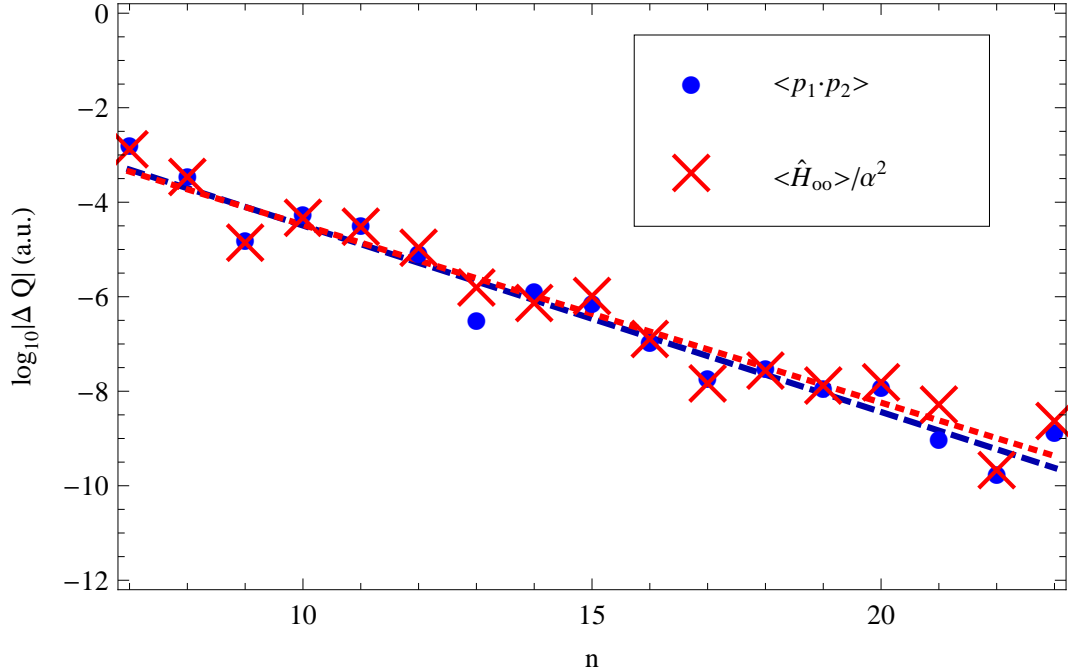


Figure 4.12: (Color online). The logarithm base 10 of the error in the expectation values of the mass polarization and the orbit-orbit interaction operators for helium. The dark blue circles are for  $\langle \mathbf{p}_1 \cdot \mathbf{p}_2 \rangle$  and the light red crosses are for  $\langle \hat{H}_{OO} \rangle / \alpha^2$  with dashed blue and dotted red fits, respectively (see Tab. 4.3).

tuning was done to improve convergence other than ensuring nonanalytic behavior was treated properly. This result means that the pseudospectral method should be widely applicable to many other calculations.

The method has been generalized to handle P states and can be trivially extended to higher angular momenta, albeit at larger computational cost. The GMRES method has been shown to be able to solve these large matrix problems with modest computational resources.

The oscillator strength of the helium  $1^1S \rightarrow 2^1P$  transition was calculated to about the same accuracy as the most accurate value in the literature [45] and

Table 4.3: The fit parameters to all the convergence plots of quantities  $Q$  in this section.

$Q$	Figure	$A$	$\beta$
$\langle r_1^2 \rangle$	4.7	$3.3 \times 10^{-11}$	0.54
$\langle r_{12}^2 \rangle$	4.7	$1.2 \times 10^{-10}$	0.53
$\langle \mathbf{r}_1 \cdot \mathbf{r}_2 \rangle$	4.7	$4.9 \times 10^{-11}$	0.47
$\langle r_1 \rangle$	4.8	$1.2 \times 10^{-11}$	0.48
$\langle r_{12} \rangle$	4.8	$7.5 \times 10^{-11}$	0.46
$\langle 1/r_1 \rangle$	4.9	$1.1 \times 10^{-10}$	0.37
$\langle 1/r_{12} \rangle$	4.9	$1.2 \times 10^{-10}$	0.37
$\langle 1/r_1^2 \rangle$	4.10	$7.1 \times 10^{-10}$	0.36
$\langle 1/r_{12}^2 \rangle$	4.10	$3.1 \times 10^{-10}$	0.38
$\langle 1/r_1 r_2 \rangle$	4.10	$3.9 \times 10^{-10}$	0.37
$\langle 1/r_1 r_{12} \rangle$	4.10	$2.6 \times 10^{-10}$	0.37
$\langle \delta(r_1) \rangle$	4.11	$2.4 \times 10^{-10}$	0.36
$\langle \delta(r_{12}) \rangle$	4.11	$6.5 \times 10^{-11}$	0.36
$\langle \mathbf{p}_1 \cdot \mathbf{p}_2 \rangle$	4.12	$2.4 \times 10^{-10}$	0.39
$\langle \hat{H}_{OO} \rangle / \alpha^2$	4.12	$4.3 \times 10^{-10}$	0.38

was found to agree to the expected precision.

## CHAPTER 5

### DISCUSSION

#### 5.1 Future work

##### 5.1.1 Continuum states

The most difficult problems in quantum mechanics involve continuum states. These are difficult to calculate because of the numerical problem of resolving an infinite number of oscillations with a finite computer. The main variational techniques employed are  $R$ -matrix [31], Schwinger variational [86], and the complex Kohn variational [126] methods. Accuracy for these methods lags far behind that of bound-state calculations. They are also limited by the understanding of the asymptotic form of the continuum state at large separation. For helium, this is still an active area of research (see Ref. [123]). For hydrogen, for which there is a known analytic solution, the asymptotic expansion is divergent. A way to bypass this problem is to use the complex rotation method [125]. In this method an oscillation  $e^{\pm ikr}$  is transformed to exponential growth or decay. This approach allows the entire method developed here to be extended to continuum states at only the cost of complexifying the Hamiltonian matrix and solution, which would double the memory requirements. A virtue of this method is it does not require knowledge of the precise asymptotic form.

New continuum state solutions can yield accurate photoabsorption cross sections, improving accuracies of results, currently known to about a percent [88]. This improvement seems feasible from extrapolation of our oscillator

strength calculations. At the cost of increasing the dimensionality of the system, and hence reducing accuracy, strong effects (*i.e.* large magnetic fields and densities) can be included nonperturbatively. The very general nature of the setup would lead to nonbiased wave functions in terms of where they are most accurate.

The pseudospectral method may prove to be particularly powerful in the energy regimes near thresholds and Fano resonances, energies at which the final state and cross section, rapidly change as a function of energy. In these regimes, it is particularly important not to be biased towards one outgoing channel over another.

### 5.1.2 Asymptotic forms

While the above scheme bypasses the need for the asymptotic form of the wave function at large distances, it is still interesting from a fundamental physics standpoint and for helping other methods. The pseudospectral method is ideal for checking theoretical forms because no explicit form has been given as input.

It is also possible to numerically solve Fock's expansion [59, 60], which gives the analytic form of the triple coalescence point. Such singularities are still poorly understood and often ignored.

## 5.2 Conclusion

We have established pseudospectral methods as a high precision numerical tool to calculate fully correlated few electron wave functions. The method produces exponential convergence for most measures of error, including local errors. We presented calculations of the absorption oscillator strength of the transition from the ground state to lowest energy P state. These calculations had a precision matching the best in the literature [45]. We also calculated all the expectation values required for the oscillator strength sum rules and leading order finite-nuclear-mass and relativistic corrections.

By using pseudospectral methods, we have confirmed the analytic structure of the two-electron atom wave function. Proper treatment of the Kato cusps [92] is necessary for exponential convergence. The logarithmic terms [14, 59, 60], in the expansion about the triple coalescence point, affect convergence of the logarithmic derivative about that singularity, thus confirming the nonanalytic structure there. However, no other error measures of physical quantities given here are affected.

The pseudospectral method can now be readily employed to solve many few-electron problems. It serves as a robust alternative to variational methods, having the advantage of local convergence and needing no explicit assumptions of the form of the wave function. The requirements for exponential convergence have been outlined and can be extended to many problems.

## APPENDIX A

### SETTING $\rho_{\text{MAX}}$ FOR THE TRUNCATED DOMAIN

When truncating the domain at a finite  $\rho$ , it is wise to balance the error produced by the cutoff with that given by the finite resolution. The former was studied by calculating the energy of case H as a function of  $\rho_{\text{max}}$ . Figure A.1 shows that difference between the truncated energy and the correct value of the  $\text{H}^-$  energy falls off as an exponential. The calculation was done with  $n = 14$ . We see at large values of  $\rho_{\text{max}}$  that this finite resolution ruins the exponential behavior. There is a minimum at  $\rho_{\text{max}} = 31$ . This is probably where the resolution error happens to cancel the truncation error. At larger  $\rho_{\text{max}}$ , the resolution error dominates. Therefore, only the points with  $15 \leq \rho_{\text{max}} \leq 25$  were used for the fit,  $\log_{10} |\Delta E| = A\rho_{\text{max}} + B$ .  $A$  and  $B$  were found to be  $-0.2089$  and  $-0.4313$ , respectively.

In order to measure the effect of finite resolution  $\rho_{\text{max}}$  was fixed at 20 and the difference between the energy at resolution  $n$  and 14 was plotted in Fig. A.2. The error from resolution effects should increase when  $\rho_{\text{max}}$  is increased because the density of points goes down. So the resolution error is assumed to be of the form  $\log_{10} |\Delta E| = Cn/\rho_{\text{max}} + D$ .  $C/20$  and  $D$  were found to be  $-0.6387$  and  $1.1344$ , respectively.

Setting the two errors equal to each other yields the formula

$$\rho_{\text{max}} = -3.7476 + 7.8100\sqrt{n + 0.2297}. \quad (\text{A.1})$$

It is technically possible to get better energies as was shown in Fig. A.1 (due to error cancellations), but taking advantage of that kind of effect is fine-tuning.

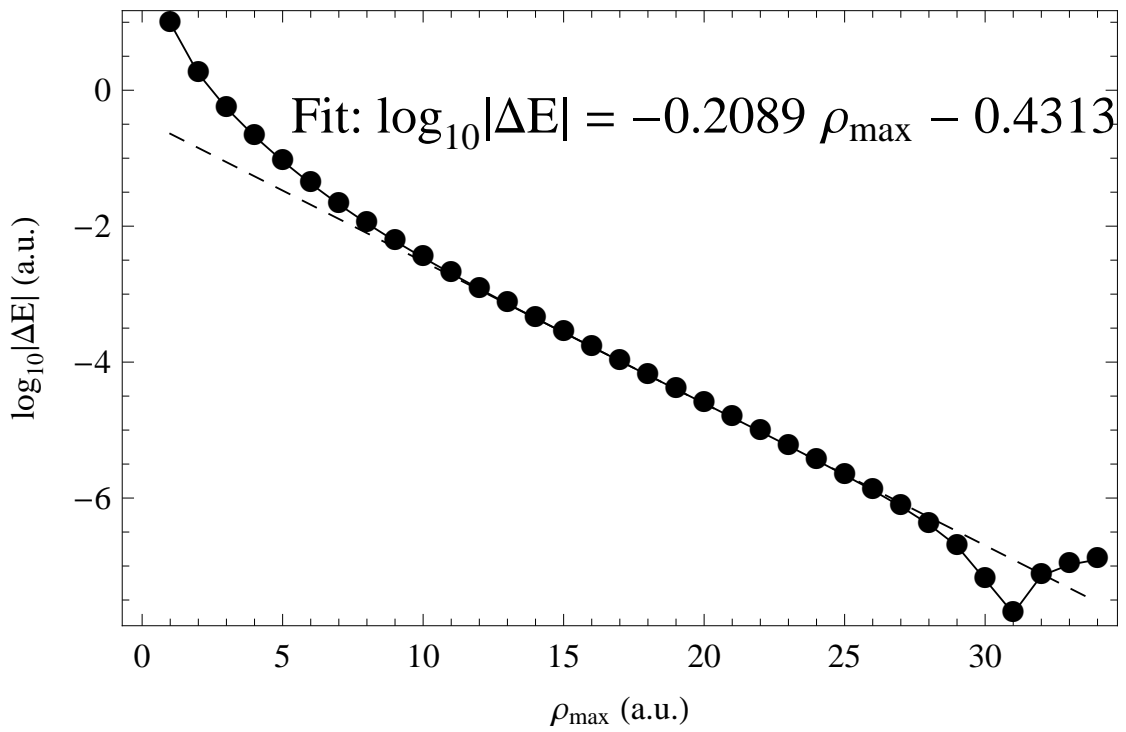


Figure A.1: Energy error from truncation as a function of  $\rho_{\max}$  with a fit to the points from  $\rho_{\max} = 15$  to  $\rho_{\max} = 25$ .

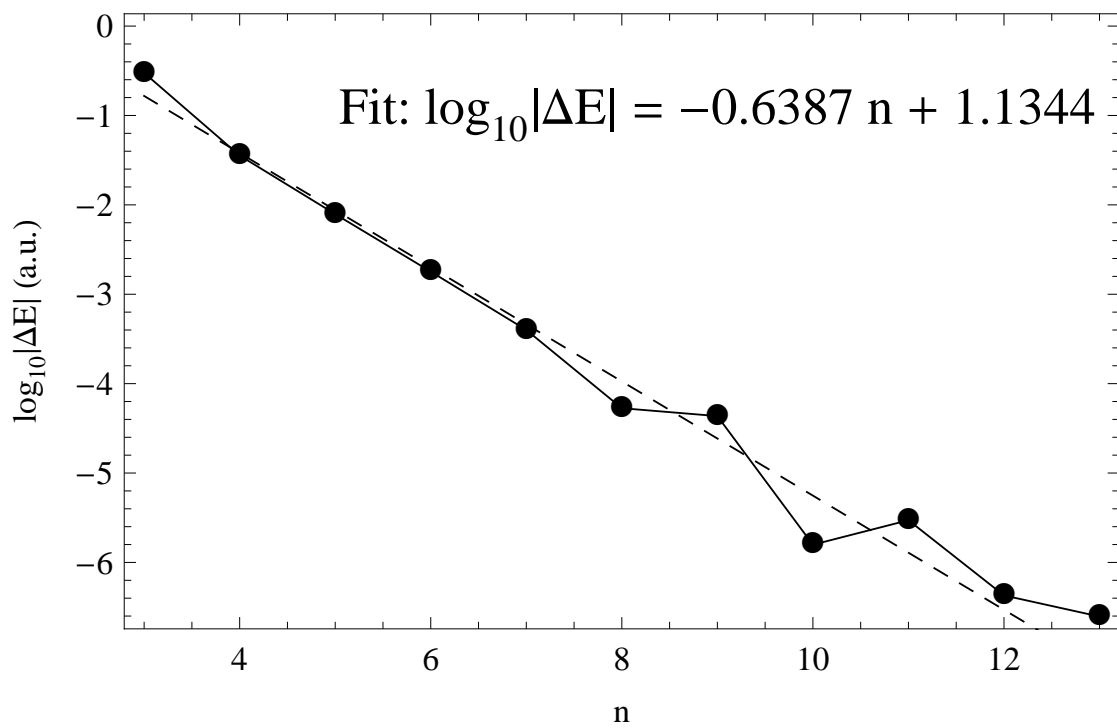


Figure A.2: Energy error from finite resolution as a function of resolution at  $\rho_{\max} = 20$  with a fit.

APPENDIX B

FITS

Table B.1: The convergence fits of quantities,  $Q$ , displayed in figures throughout chapter 3

$Q$	Figure(s)	Fitting Function			
		$a_1$	$a_2$	$a_3$	$a_4$
		$\Delta a_1$	$\Delta a_2$	$\Delta a_3$	$\Delta a_4$
$\delta_{\text{RMS}}^N[g_1]$	3.1	$a_1 n^{a_2}$			
0.470	-1.852				
0.189	0.206				
$\delta_{\text{RMS}}^N[g_1]$	3.1	$a_1(a_2)^{n^{a_3}}$			
0.895	0.4031	1.3846			
0.070	0.0015	0.0017			
$ \Delta f[\rho = 10^{-6}] $	3.2	$a_1(a_2)^n + a_3 n^{a_4}$			
0.0818	0.696	0.295	-3.822		
0.0487	0.022	0.113	0.092		
$ \Delta f[\rho = 10^{-1}] $	3.2	$a_1(a_2)^n + a_3 n^{a_4}$			
0.0264	0.725	0.472	-5.172		
0.0306	0.027	0.595	0.290		
$ \Delta f[\rho = 10^4] $	3.2	$a_1(a_2)^n + a_3 n^{a_4}$			
0.161	0.743	$1.29 \times 10^{-7}$	-2.460		
0.112	0.011	$2.16 \times 10^{-7}$	0.372		
$ \Delta H_N^{\max} (\alpha = 1)$	3.3	$a_1(a_2)^{n^{a_3}}$			
936.	0.5943	0.8348			
Continued on next page					

**Table B.1 – continued from previous page**

$Q$	Figure(s)	Fitting Function		
$a_1$	$a_2$	$a_3$	$a_4$	
$\Delta a_1$	$\Delta a_2$	$\Delta a_3$	$\Delta a_4$	
418.	0.0089	0.0067		
$ \Delta H_N^{\max} (\alpha = 0)$	3.3	$a_1(a_2)^{n^{a_3}}$		
14.6	0.3282	0.7209		
6.0	0.0073	0.0047		
$ (\Delta H_N)^{t^*} (\alpha = 1)$	3.4	$a_1(a_2)^n + a_3n^{a_4}$		
$1.96 \times 10^{-7}$	0.491	0.263	-10.358	
$1.36 \times 10^{-7}$	0.018	0.091	0.083	
$ (\Delta H_N)^{t^*} (\alpha = 0)$	3.4	$a_1(a_2)^{n^{a_3}}$		
181.	$2.90 \times 10^{-6}$	0.3733		
84.	$3.1 \times 10^{-7}$	0.0020		
$ \Delta E $ (Case A)	3.8, 3.9, 3.10 3.11, 3.12	$a_1(a_2)^{n^{a_3}}$		
121000.	0.00138	0.549		
64000.	0.00022	0.01		
$ \Delta E $ (Case B)	3.8	$a_1(a_2)^{n^{a_3}}$		
$1.17 \times 10^{11}$	$1.53 \times 10^{-8}$	0.3262		
$6.7 \times 10^{10}$	$4.3 \times 10^{-9}$	0.0070		
$ \Delta E $ (Case C)	3.8	$a_1(a_2)^{n^{a_3}}$		
$1.28 \times 10^{11}$	$5.71 \times 10^{-9}$	0.2796		
$5.7 \times 10^{10}$	$1.39 \times 10^{-9}$	0.0057		
$ \Delta E $ (Case D)	3.8	$a_1(a_2)^{n^{a_3}}$		
Continued on next page				

**Table B.1 – continued from previous page**

$Q$	Figure(s)		Fitting Function	
	$a_1$	$a_2$	$a_3$	$a_4$
$\Delta a_1$	$\Delta a_2$	$\Delta a_3$	$\Delta a_4$	
$1.62 \times 10^6$	0.000385		0.478	
880000.	0.000073		0.011	
$ \Delta E $ (Case E)	3.9		$a_1(a_2)^n + a_3n^{a_4}$	
193.	0.169		0.190	-3.39
140.	0.021		0.087	0.18
$ \Delta E $ (Case F)	3.9		$a_1(a_2)^{n^{a_3}}$	
286000.	0.00100		0.5604	
126000.	0.00012		0.0069	
$ \Delta E $ (Case G)	3.12		$a_1(a_2)^{n^{a_3}}$	
30.0	0.0972		0.819	
19.3	0.0100		0.019	
$ \Delta E $ (Case H)	3.10		$a_1(a_2)^{n^{a_3}}$	
$2.10 \times 10^{10}$	$5.73 \times 10^{-9}$		0.2614	
$1.52 \times 10^{10}$	$2.36 \times 10^{-9}$		0.0097	
$ \Delta E $ (Case I)	3.11		$a_1(a_2)^{n^{a_3}}$	
$3.89 \times 10^9$	$4.08 \times 10^{-8}$		0.289	
$3.10 \times 10^9$	$1.73 \times 10^{-8}$		0.011	
$ \Delta E $ (Case J)	3.11		$a_1(a_2)^{n^{a_3}}$	
$5.68 \times 10^6$	0.0000114		0.018	
$5.68 \times 10^6$	0.0000114		0.018	
Continued on next page				

**Table B.1 – continued from previous page**

$Q$	Figure(s)		Fitting Function	
	$a_1$	$a_2$	$a_3$	$a_4$
$\Delta a_1$	$\Delta a_2$	$\Delta a_3$	$\Delta a_4$	
$ \Delta E_{\text{loc}} ^1$	3.13		$a_1(a_2)^n$	
2.35	0.426			
1.97	0.037			
$ \Delta E_{\text{loc}} ^2$	3.13		$a_1(a_2)^n$	
$2.02 \times 10^7$	0.395			
$2.42 \times 10^7$	0.050			
$ \Delta E_{\text{loc}} ^3$	3.13		$a_1(a_2)^n$	
21700.	0.415			
21900.	0.044			
$ \Delta E_{\text{loc}} ^4$	3.13		$a_1(a_2)^n$	
9.33	0.616			
10.73	0.074			
$\Delta_n(Z = 1, \alpha = 0)$	3.16		$a_1(a_2)^{n^{a_3}}$	
7260.	0.0394		0.6282	
1200.	0.0016		0.0053	
$\Delta_n(Z = 1, \alpha = 1)$	3.16		$a_1(a_2)^{n^{a_3}}$	
$2.77 \times 10^6$	0.000876		0.4541	
590000.	0.000068		0.0047	
$\Delta_n(Z = 2, \alpha = 1)$	3.16		$a_1(a_2)^{n^{a_3}}$	

Continued on next page

<sup>1</sup> $\rho = 1, \phi = \pi/8, C = 0$

<sup>2</sup> $\rho = 10^{-4}, \phi = \pi/8, C = 0$

<sup>3</sup> $\rho = 1, \phi = 10^{-4}, C = 0$

<sup>4</sup> $\rho = 15, \phi = \pi/8, C = 0$

**Table B.1 – continued from previous page**

$Q$	Figure(s)	Fitting Function	
$a_1$	$a_2$	$a_3$	$a_4$
$\Delta a_1$	$\Delta a_2$	$\Delta a_3$	$\Delta a_4$
472.	0.2406	0.9001	
58.	0.0038	0.0047	
$ \psi_n(\rho = 0) - \psi_{n-1} ^5$	3.17	$a_1(a_2)^{n^{a_3}}$	
27300.	0.0520	0.7833	
5900.	0.0019	0.0052	
$ \psi_n(\rho = 0) - \psi_{n-1} ^6$	3.17	$a_1(a_2)^{n^{a_3}}$	
$1.17 \times 10^{12}$	$1.49 \times 10^{-8}$	0.3046	
$6.9 \times 10^{11}$	$4.5 \times 10^{-9}$	0.0073	
$ \psi_n(\rho = 0) - \psi_{n-1} ^7$	3.17	$a_1(a_2)^{n^{a_3}}$	
$1.63 \times 10^{14}$	$1.49 \times 10^{-8}$	0.3475	
$8.6 \times 10^{13}$	$3.6 \times 10^{-9}$	0.0059	
$\delta_{\text{RMS}}(Z = 1, \alpha = 0)$	3.18	$a_1(a_2)^{n^{a_3}}$	
170.	0.00418	0.4404	
23.	0.00022	0.0041	
$\delta_{\text{RMS}}(Z = 1, \alpha = 1)$	3.18	$a_1 n^{a_2}$	
10.3	-3.71		
6.1	0.27		
$\delta_{\text{RMS}}(Z = 2, \alpha = 1)$	3.18	$a_1 n^{a_2}$	
0.883	-2.65		
Continued on next page			

<sup>5</sup> $\rho = 0, (Z = 1, \alpha = 0)$

<sup>6</sup> $\rho = 0, (Z = 1, \alpha = 1)$

<sup>7</sup> $\rho = 0, (Z = 2, \alpha = 1)$

**Table B.1 – continued from previous page**

$Q$	Figure(s)	Fitting Function	
$a_1$	$a_2$	$a_3$	$a_4$
$\Delta a_1$	$\Delta a_2$	$\Delta a_3$	$\Delta a_4$
0.275	0.14		

Numerical rates for convergence are summarized in Table B.1. The method is as follows: let  $Q_n$  be the quantity converging to zero as  $n$  goes to infinity, consider fitting functions of the forms

$$f_{\text{geom}}[n] = a_1(a_2)^n \quad (\text{B.1})$$

$$f_{\text{alg}}[n] = a_1 n^{a_2} \quad (\text{B.2})$$

$$f_{\text{sup/sub}}[n] = a_1(a_2)^{n^{a_3}} \quad (\text{B.3})$$

$$f_{\text{geom/alg}}[n] = a_1(a_2)^n + a_3 n^{a_4}, \quad (\text{B.4})$$

which are geometric, algebraic, supergeometric ( $a_3 > 1$ ) or subgeometric ( $a_3 < 1$ ), and mixed geometric and algebraic fits, respectively. A  $\chi^2$  fitting method is used:

$$\chi^2 = \sum_n \left( \log_{10} \left| \frac{Q_n}{f[n]} \right| \right)^2, \quad (\text{B.5})$$

where  $Q_n$  is the quantity  $Q$  evaluated at resolution  $n$  and the sum over  $n$  goes from the even numbers from 8 to 100 for the one-dimensional models, 5 to 14 for the Cauchy errors, and from 4 to 14 for all others.  $\chi^2$  is minimized with respect to all  $a_i$  for the fit which is most reasonable on theoretical grounds. Errors in the  $a_i$  are estimated by calculating

$$\Delta a_i = \sqrt{\frac{\chi^2}{\partial_{a_i a_i} \chi^2}} \quad (\text{B.6})$$

at the minimum of  $\chi^2$ . Of course large error in the values of amplitudes  $a_1$  and  $a_3$  for the mixed geometric and algebraic fit imply that the other parameters that multiply that amplitude may be meaningless.

APPENDIX C

BHATIA AND TEMKIN HAMILTONIAN

Bhatia and Temkin [21] derived and we checked the following explicit expressions that make up the Hamiltonian

$$\hat{H}_S = -\frac{1}{2} \sum_{i=1}^2 \frac{1}{r_i^2} \left( \frac{\partial}{\partial r_i} r_i^2 \frac{\partial}{\partial r_i} + \frac{1}{\sin \theta_{12}} \frac{\partial}{\partial \theta_{12}} \sin \theta_{12} \frac{\partial}{\partial \theta_{12}} \right) + \hat{V} \quad (\text{C.1})$$

$$\hat{V} = -\frac{Z}{r_1} - \frac{Z}{r_2} + \frac{1}{r_{12}} \quad (\text{C.2})$$

$$\hat{H}_{\nu, \kappa, -1}^{\gamma} = (1 - \delta_{0\kappa} - \delta_{1\kappa} + (-1)^j \delta_{2\kappa}) h_{\nu}^{\gamma} B_{l\kappa, -1} \begin{cases} \cot \theta_{12} & \text{if } \nu = \gamma \\ (-1)^{\nu} & \text{if } \nu \neq \gamma \end{cases} \quad (\text{C.3})$$

$$\hat{H}_{\nu\kappa 0}^{\gamma} = h_{\nu}^{\gamma} \begin{cases} 2 \frac{l(l+1) - \kappa^2}{\sin \theta_{12}} + \kappa^2 \sin \theta_{12} - \gamma \cot \theta_{12} l(l+1) \delta_{1\kappa} & \text{if } \nu = \gamma \\ \nu \kappa (2 \cos \theta_{12} + 4 \sin \theta_{12} \frac{\partial}{\partial \theta_{12}}) - l(l+1) \delta_{1\kappa} & \text{if } \nu \neq \gamma \end{cases} \quad (\text{C.4})$$

$$\hat{H}_{\nu\kappa 1}^{\gamma} = (1 - \nu \delta_{0\kappa}) h_{\nu}^{\gamma} B_{l, \kappa+2, 1} \begin{cases} \cot \theta_{12} & \text{if } \nu = \gamma \\ (-1)^{\gamma} & \text{if } \nu \neq \gamma \end{cases} \quad (\text{C.5})$$

$$h_{\nu}^{\gamma} = \frac{1}{8 \sin \theta_{12}} \left( \frac{1}{r_2^2} + \frac{\nu \gamma}{r_1^2} \right) \quad (\text{C.6})$$

$$B_{l\kappa n} = (1 + \delta_{2\kappa} (\sqrt{2} - 1))^n \sqrt{(l - \kappa + 1)(l - \kappa + 2)(l + \kappa)(l + \kappa - 1)} \quad (\text{C.7})$$

APPENDIX D

CALCULATING THE OSCILLATOR STRENGTH WITH BHATIA AND  
TEMKIN'S RADIAL FUNCTIONS

In the Bhatia and Temkin three-three splitting [21], the matrix elements for an  $^1S \rightarrow ^1P$  oscillator strength transition are written:

$$\sum_m |\langle i|\hat{\mathbf{D}}|j\rangle|^2 = \left[ \int r_1^2 r_2^2 \sin \theta_{12} dr_1 dr_2 d\theta_{12} g_{000}^0 (d_D^0 g_{110}^0 + d_D^1 g_{110}^1) \right]^2, \quad (\text{D.1})$$

where  $D$  is one of the operators found inside the matrix elements of Eqs. 4.22 and the functions  $d_D^i$  are given by

$$d_{\mathbf{R}}^0 = (r_1 + r_2) \cos \frac{\theta_{12}}{2} \quad (\text{D.2})$$

$$d_{\mathbf{R}}^1 = (r_1 - r_2) \sin \frac{\theta_{12}}{2} \quad (\text{D.3})$$

$$d_{\mathbf{P}}^0 = \frac{(r_1 + r_2)(3 + \cos \theta_{12})}{4r_1 r_2 \cos \frac{\theta_{12}}{2}} + \cos \frac{\theta_{12}}{2} \left( \frac{\partial}{\partial r_1} + \frac{\partial}{\partial r_2} \right) - \frac{(r_1 + r_2) \sin \frac{\theta_{12}}{2}}{r_1 r_2} \frac{\partial}{\partial \theta_{12}} \quad (\text{D.4})$$

$$d_{\mathbf{P}}^1 = \frac{(r_1 - r_2)(-3 + \cos \theta_{12})}{4r_1 r_2 \sin \frac{\theta_{12}}{2}} + \sin \frac{\theta_{12}}{2} \left( \frac{\partial}{\partial r_1} - \frac{\partial}{\partial r_2} \right) - \frac{(r_1 - r_2) \cos \frac{\theta_{12}}{2}}{r_1 r_2} \frac{\partial}{\partial \theta_{12}} \quad (\text{D.5})$$

$$d_{\mathbf{A}}^0 = \frac{(r_1^2 + r_2^2) \cos \frac{\theta_{12}}{2}}{r_1^2 r_2^2} \quad (\text{D.6})$$

$$d_{\mathbf{A}}^1 = \frac{(r_1^2 - r_2^2) \sin \frac{\theta_{12}}{2}}{r_1^2 r_2^2}. \quad (\text{D.7})$$

## BIBLIOGRAPHY

- [1] P C Abbott and E N Maslen. Coordinate systems and analytic expansions for three-body atomic wavefunctions. i. partial summation for the fock expansion in hyperspherical coordinates. Journal of Physics A: Mathematical and General, 20(8):2043–2075, 1987.
- [2] A. G. Abrashkevich, D. G. Abrashkevich, M. I. Gaysak, V. I. L endyel, I. V. Puzynin, and S. I. Vinitzky. Multichannel calculation of the electric-dipole oscillator strengths fo r the discrete  $^1s_e \rightarrow ^1p_o$  transitions in helium within the hyperspherical adiabatic approach. Phys. Lett. A, 152(9):467 – 471, 1991.
- [3] Y. Accad, C. L. Pekeris, and B. Schiff.  $s$  and  $p$  states of the helium isoelectronic sequence up to  $z = 10$ . Phys. Rev. A, 4(2):516–536, Aug 1971.
- [4] J. Ackermann and J. Shertzer. Finite-element calculations for the three-body coulomb problem with two equal masses. Phys. Rev. A, 54(1):365–371, Jul 1996.
- [5] M. T. Anderson and F. Weinhold. Dipole oscillator strengths, with rigorous limits of error, for he and  $li^+$ . Phys. Rev. A, 9(1):118–128, Jan 1974.
- [6] Gentaro Araki, Masao Ohta, and Koichi Mano. Triplet intervals of helium. Phys. Rev., 116(3):651–653, Nov 1959.
- [7] George Arfken. Mathematical Methods for Physicists, chapter 9. Academic Press, 1970.
- [8] Jonathan D. Baker, David E. Freund, Robert Nyden Hill, and John D. Morgan. Radius of convergence and analytic behavior of the  $1z$  expansion. Phys. Rev. A, 41(3):1247–1273, Feb 1990.
- [9] Satish Balay, Kris Buschelman, Victor Eijkhout, William D. Gropp, Dinesh Kaushik, Matthew G. Knepley, Lois Curfman McInnes, Barry F. Smith, and Hong Zhang. PETSc users manual. Technical Report ANL-95/11 - Revision 3.0.0, Argonne National Laboratory, 2008.
- [10] Satish Balay, Kris Buschelman, William D. Gropp, Dinesh Kaushik, Matthew G. Knepley, Lois Curfman McInnes, Barry F. Smith, and Hong Zhang. PETSc Web page, 2009. <http://www.mcs.anl.gov/petsc>.

- [11] Satish Balay, William D. Gropp, Lois Curfman McInnes, and Barry F. Smith. Efficient management of parallelism in object oriented numerical software libraries. In E. Arge, A. M. Bruaset, and H. P. Langtangen, editors, Modern Software Tools in Scientific Computing, pages 163–202. Birkhäuser Press, 1997.
- [12] C. G. Barraclough and J. R. Mooney. Higher-order finite difference solutions of the schr[o-umlaut]ödinger equation for the helium atom. J. Chem. Phys., 54(1):35–44, 1971.
- [13] M. Barrett, M. Berry, T. F. Chan, J. Van der Horst, and H. Van der Horst. Templates for the Solution of Linear Systems: Building Blocks for Iterative Methods. SIAM, Philadelphia, PA, 1994.
- [14] J. H. Bartlett. The helium wave equation. Phys. Rev., 51(8):661–669, Apr 1937.
- [15] J. H. Bartlett, J. J. Gibbons, and C. G. Dunn. The normal helium atom. Phys. Rev., 47(9):679–680, May 1935.
- [16] James H. Bartlett. Helium wave equation. Phys. Rev., 98(4):1067–1070, May 1955.
- [17] D. R. Bates and Agnete Damgaard. The calculation of the absolute strengths of spectral lines. Phil. Trans. Roy. Soc. Lond. A, 242(842):101–122, 1949.
- [18] Gordon Baym. Lectures on Quantum Mechanics. W. A. Benjamin, Inc., Reading, MA, 1969.
- [19] J Berkowitz. Sum rules and the oscillator strength distribution in helium. J. Phys. B, 30(4):881, 1997.
- [20] Hans Bethe and Edwin Salpeter. Quantum Mechanics of One- and Two-Electron Atoms. Academic Press Inc., Berlin, 1957.
- [21] A. K. Bhatia and A. Temkin. Symmetric euler-angle decomposition of the two-electron fixed-nucleus problem. Rev. Mod. Phys., 36(4):1050–1064, Oct 1964.
- [22] A. K. Bhatia and A. Temkin. Decomposition of the schrödinger equation

- for two identical particles and a third particle of finite mass. Phys. Rev., 137(5A):A1335–A1343, Mar 1965.
- [23] S. Bonazzola, E. Gourgoulhon, and J. A. Marck. Spectral methods in general relativistic astrophysics. J. Comput. Appl. Math., 109(1-2):433 – 473, 1999.
- [24] A. G. Borisov. Solution of the radial schrödinger equation in cylindrical and spherical coordinates by mapped fourier transform algorithms. J. Chem. Phys., 114(18):7770–7777, 2001.
- [25] John P. Boyd. Chebyshev and Fourier Spectral Methods. Dover, Mineola, New York 11501, 2nd edition, 2000.
- [26] John P. Boyd, C. Rangan, and P. H. Bucksbaum. Pseudospectral methods on a semi-infinite interval with application to the hydrogen atom: a comparison of the mapped fourier-sine method with laguerre series and rational chebyshev expansions. J. Comput. Phys., 188(1):56 – 74, 2003.
- [27] M. Braun, W. Schweizer, and H. Herold. Finite-element calculations for the s states of helium. Phys. Rev. A, 48(3):1916–1920, Sep 1993.
- [28] R. T. Brown. Ultraviolet Wavelengths and Oscillator Strengths for 3d-nf Transitions in the Helium Isoelectronic Sequence. Astrophys. J., 158:829, November 1969.
- [29] RT Brown and JLM Cortez. Oscillator Strengths for Allowed nD-n’F Transitions in Helium Isoelectronic Sequence. Astrophys. J., 176(1):267, 1972.
- [30] W. Byers Brown and Ronald J. White. Analytic power-series solution of the schrödinger equation for the helium atom. Phys. Rev. Lett., 18(24):1037–1038, Jun 1967.
- [31] P. G. Burke and K. A. Berrington. Atomic and Molecular Processes: an R-Matrix Approach. IOP, Bristol, 1993.
- [32] S. Cameron, McEachran. R. P., and M. Cohen. Can. J. Phys., 48:211–215, 1970.
- [33] Natalie Mary Cann and Ajit J. Thakkar. Oscillator strengths for s-p and p-d transitions in heliumlike ions. Phys. Rev. A, 46(9):5397–5405, Nov 1992.

- [34] C. Canuto, M.Y. Hussaini, A. Quarteroni, and T.A. Zang. Spectral Methods in Fluid Dynamics. Springer, Berlin, 1988.
- [35] W. F. Chan, G. Cooper, and C. E. Brion. Absolute optical oscillator strengths for the electronic excitation of atoms at high resolution: Experimental methods and measurements for helium. Phys. Rev. A, 44(1):186–204, Jul 1991.
- [36] Ming-Keh Chen. Accurate oscillator strengths for s-p transitions in the helium atom. J. Phys. B, 27(5):865, 1994.
- [37] Earl A. Coddington. An Introduction to Ordinary Differential Equations, chapter 4. General Publishing Company, Ltd., Toronto, Ontario, 1961.
- [38] Robert Lynn Coldwell. Zero monte carlo error or quantum mechanics is easier. Int. J. Quant. Chem., 12(S11):215–222, Jan 1977.
- [39] A Dalgarno and N Lynn. Properties of the helium atom. Proc. Phys. Soc. A, 70(11):802, 1957.
- [40] Brian F. Davis and Kwong T. Chung. Mass-polarization effect and oscillator strengths for  $s, p, d$  states of helium. Phys. Rev. A, 25(3):1328–1333, Mar 1982.
- [41] J. P. Desclaux. Hartree fock Slater self consistent field calculations. Comp. Phys. Commun., 1(3):216 – 222, 1970.
- [42] K R Devine and A L Stewart. A perturbation calculation on helium. J. Phys. B, 5(3):432, 1972.
- [43] K R Devine and A L Stewart. Perturbation corrections to hartree-fock oscillator strengths for helium. J. Phys. B, 5(12):2182, 1972.
- [44] G. W. F. Drake. New variational techniques for the 1s states of helium. Phys. Rev. Lett., 59(14):1549–1552, Oct 1987.
- [45] G. W. F. Drake. High precision calculations for helium. In G. W. F. Drake, editor, Atomic, Molecular, and Optical Physics Handbook. American Institute of Physics, 1996.
- [46] G W F Drake. High precision theory of atomic helium. Phys. Scr., T83:83–92, 1999.

- [47] G. W. F. Drake. Progress in helium fine-structure calculations and the fine-structure constant. Can. J. Phys., 80(11):1195–1212, 2002.
- [48] G. W. F. Drake, Mark M. Cassar, and Razvan A. Nistor. Ground-state energies for helium,  $h^-$ , and  $ps^-$ . Phys. Rev. A, 65(5):054501, Apr 2002.
- [49] G. W. F. Drake and S. P. Goldman. Can. J. Phys., 77(11):835–845, 1999.
- [50] G. W. F. Drake and Donald C. Morton. A multiplet table for neutral helium with transition rates. Astrophys. J. Supplementary Series, 170(1):251, 2007.
- [51] G. W. F. Drake and Zong-Chao Yan. Energies and relativistic corrections for the rydberg states of helium: Variational results and asymptotic analysis. Phys. Rev. A, 46(5):2378–2409, Sep 1992.
- [52] G. W. F. Drake and Zong-Chao Yan. High-precision spectroscopy as a test of quantum electrodynamics in light atomic systems. Can. J. Phys., 86(1):45–54, JAN 2008.
- [53] G.W.F. Drake. Helium, relativity, and qed. Nuc. Phys. A, 737:25 – 33, 2004.
- [54] Sverker Edvardsson, Daniel Aberg, and Per Uddholm. A program for accurate solutions of two-electron atoms. Comput. Phys. Commun., 165(3):260 – 270, 2005.
- [55] Eyal Fattal, Roi Baer, and Ronnie Kosloff. Phase space approach for optimizing grid representations: The mapped fourier method. Phys. Rev. E, 53(1):1217–1227, Jan 1996.
- [56] J A Fernley, K T Taylor, and M J Seaton. Atomic data for opacity calculations. vii. energy levels, f values and photoionisation cross sections for he-like ions. J. Phys. B, 20(23):6457, 1987.
- [57] C F Fischer. Correlation effects important for accurate oscillator strengths. J. Phys. B, 7(4):L91, 1974.
- [58] Charlott F. Fischer. Atomic structure: Multiconfiguration hartree-fock theories. In G. W. F. Drake, editor, Atomic, Molecular, and Optical Physics Handbook. American Institute of Physics, 1996.
- [59] V. A. Fock. Izv. Akad. Nauk. SSSR, Ser. Fiz, 18:161, 1954.

- [60] V. A. Fock. K. Nor. Vidensk. Selsk. Forh., 31:145, 1958.
- [61] B. Fornberg and D. Merrill. Comparison of finite difference and pseudospectral methods for convective flow over a sphere. Geophys. Res. Lett., 24(24):3245–3248, 1997.
- [62] Bengt Fornberg. A Practical Guide to Pseudospectral Methods. Cambridge University Press, 40 West 20th Street, New York, NY 10011-4211, 1996.
- [63] Robert C. Forrey. Compact representation of helium wave functions in perimetric and hyperspherical coordinates. Phys. Rev. A, 69(2):022504, Feb 2004.
- [64] K. Frankowski and C. L. Pekeris. Logarithmic terms in the wave functions of the ground state of two-electron atoms. Phys. Rev., 146(1):46–49, Jun 1966.
- [65] Richard A. Friesner. Solution of self-consistent field electronic structure equations by a pseudospectral method. Chem. Phys. Lett., 116(1):39 – 43, 1985.
- [66] Richard A. Friesner. Solution of the hartree–fock equations by a pseudospectral method: Application to diatomic molecules. J. Chem. Phys., 85(3):1462–1468, 1986.
- [67] Richard A. Friesner. Solution of the hartree–fock equations for polyatomic molecules by a pseudospectral method. J. Chem. Phys., 86(6):3522–3531, 1987.
- [68] Alexei M. Frolov. High-precision, variational, bound-state calculations in coulomb three-body systems. Phys. Rev. E, 62(6):8740–8745, Dec 2000.
- [69] Alexei M. Frolov. Optimization of nonlinear parameters in trial wave functions with a very large number of terms. Phys. Rev. E (Statistical, Nonlinear, and Soft Matter Physics), 74(2):027702, 2006.
- [70] Alexei M Frolov. Highly accurate evaluation of the singular properties for the positronium and hydrogen negative ions. J. of Phys. A, 40(23):6175–6181, 2007.
- [71] J E Gottschalk, P C Abbott, and E N Maslen. Coordinate systems and

- analytic expansions for three-body atomic wavefunctions. ii. closed form wavefunction to second order in  $r$ . J. Phys. A: Gen. Phys., 20(8):2077–2103, 1987.
- [72] J E Gottschalk and E N Maslen. Coordinate systems and analytic expansions for three-body atomic wavefunctions. iii. derivative continuity via solutions to laplace's equation. J. Phys. A: Gen. Phys., 20(10):2781–2803, 1987.
- [73] Paul E. Grabowski and David F. Chernoff. Pseudospectral calculation of the wave function of helium and the negative hydrogen ion. Phys. Rev. A, 81(3):032508, Mar 2010.
- [74] Burnham H. Greeley, Thomas V. Russo, Daniel T. Mainz, Richard A. Friesner, Jean-Marc Langlois, William A. Goddard, III, Jr. Robert E. Donnelly, and Murco N. Ringnalda. New pseudospectral algorithms for electronic structure calculations: Length scale separation and analytical two-electron integral corrections. J. Chem. Phys., 101(5):4028–4041, 1994.
- [75] L. C. Green, N. C. Johnson, and E. K. Kolchin. Astrophys. J., 144:369–75, 1966.
- [76] M. Griebel and J. Hamaekers. Sparse grids for the Schrödinger equation. Mathematical Modelling and Numerical Analysis, 41(2):215–247, 2007.
- [77] M. I. Haftel and V. B. Mandelzweig. Exact solution of coupled equations and the hyperspherical formalism: Calculation of expectation values and wavefunctions of three coulomb-bound particles. Ann. Phys., 150(1):48 – 91, 1983.
- [78] M. I. Haftel and V. B. Mandelzweig. A fast convergent hyperspherical expansion for the helium ground state. Phys. Lett. A, 120(5):232 – 236, 1987.
- [79] M. I. Haftel and V. B. Mandelzweig. Precise nonvariational calculations on the helium atom. Phys. Rev. A, 38(12):5995–5999, Dec 1988.
- [80] M. I. Haftel and V. B. Mandelzweig. Fast convergent hyperspherical harmonic expansion for three-body systems. Ann. of Phys., 189(1):29 – 52, 1989.
- [81] M. I. Haftel and V. B. Mandelzweig. Accuracy of three-body wave func-

- tions obtained with the correlation-function hyperspherical-harmonic method. Phys. Rev. A, 42(11):6324–6332, Dec 1990.
- [82] Lars Hambro. Second-order corrections to the fine structure of helium. Phys. Rev. A, 5(5):2027–2045, May 1972.
- [83] I. L. Hawk and D. L. Hardcastle. Finite-difference solution to the schrodinger equation for the helium isoelectronic sequence. Comput. Phys. Commun., 16(2):159 – 166, 1979.
- [84] J. S. Heyl and A. Thirumalai. Pseudospectral methods for atoms in strong magnetic fields. arXiv e-prints, February 2009.
- [85] A. Hibbert. Developments in atomic-structure calculations. Rep. Prog. Phys., 38(11):1217–1338, 1975.
- [86] W. M. Huo. In W. M. Huo and F. Gianturco, editors, Computational Methods for Electron-Molecule Collisions, chapter 15. Plenum, New York, 1995.
- [87] Von Egil A. Hylleraas. Neue berechnung der energie des heliums im grundzustande, sowie des tiefsten terms von ortho-helium. Z. Phys., 54:347–366, 1929.
- [88] T. L. John. Continuous absorption by the negative hydrogen ion reconsidered. Astron. Astrophys., 193:189–192, March 1988.
- [89] P. K. Kabir and E. E. Salpeter. Radiative corrections to the ground-state energy of the helium atom. Phys. Rev., 108(5):1256–1263, Dec 1957.
- [90] Tosio Kato. Fundamental properties of hamiltonian operators of schrodinger type. Transactions of the American Mathematical Society, 70(2):195–211, 1951.
- [91] Tosio Kato. On the existence of solutions of the helium wave equation. Transactions of the American Mathematical Society, 70(2):212–218, 1951.
- [92] Tosio Kato. On the eigenfunctions of many-particle systems in quantum mechanics. Commun. Pure Appl. Math., 10(2):151–177, 1957.
- [93] Lawrence E. Kidder and Lee Samuel Finn. Spectral methods for numerical relativity: The initial data problem. Phys Rev. D, 62(8):084026, Sep 2000.

- [94] Toichiro Kinoshita. Ground state of the helium atom. Phys. Rev., 105(5):1490–1502, Mar 1957.
- [95] Bruno Klahn and John D. Morgan, III. Rates of convergence of variational calculations and of expectation values. J. Chem. Phys., 81(1):410–433, 1984.
- [96] Chaehyuk Ko, David K. Malick, Dale A. Braden, Richard A. Friesner, and Todd J. Martínez. Pseudospectral time-dependent density functional theory. J. Chem. Phys., 128(10):104103, 2008.
- [97] Akihiro Kono and Shuzo Hattori. Accurate oscillator strengths for neutral helium. Phys. Rev. A, 29(6):2981–2988, Jun 1984.
- [98] Akihiro Kono and Shuzo Hattori. Variational calculations for excited states in he i: Improved estimation of the ionization energy from accurate energies for the n 3s, n 1d, n 3d series. Phys. Rev. A, 31(2):1199–1202, Feb 1985.
- [99] V. I. Korobov. Coulomb three-body bound-state problem: Variational calculations of nonrelativistic energies. Phys. Rev. A, 61(6):064503, May 2000.
- [100] Vladimir I. Korobov. Nonrelativistic ionization energy for the helium ground state. Phys. Rev. A, 66(2):024501, Aug 2002.
- [101] R. Krivec, M. I. Haftel, and V. B. Mandelzweig. Precise nonvariational calculation of excited states of helium with the correlation-function hyperspherical-harmonic method. Phys. Rev. A, 44(11):7158–7164, Dec 1991.
- [102] R. Krivec, V. B. Mandelzweig, and K. Varga. Local properties of three-body atomic wave functions. Phys. Rev. A, 61(6):062503, May 2000.
- [103] Yusaku I. Kurokawa, Hiroyuki Nakashima, and Hiroshi Nakatsuji. Solving the schrodinger equation of helium and its isoelectronic ions with the exponential integral (ei) function in the free iterative complement interaction method. Phys. Chem. Chem. Phys., 10:4486–4494, 2008.
- [104] F. S. Levin and J. Shertzer. Finite-element solution of the schrödinger equation for the helium ground state. Phys. Rev. A, 32(6):3285–3290, Dec 1985.

- [105] Michael L. Lewis and Paul H. Serafino. Second-order contributions to the fine structure of helium from all intermediate states. Phys. Rev. A, 18(3):867–888, Sep 1978.
- [106] K. McIsaac and E. N. Maslen. Exact wave functions for few-particle systems: The choice of expansion for coulomb potentials. Int. J. Quant. Chem., 31:361, 1987.
- [107] P. J. Mohr, B. N. Taylor, and D. B. Newell. Rev. Mod. Phys., 80(2):633–730, 2008.
- [108] P. J. Mohr, B. N. Taylor, and D. B. Newell. J. Phys. Chem. Ref. Data, 37(3):1187–1284, 2008.
- [109] John D. Morgan. Convergence properties of fock’s expansion for s-state eigenfunctions of the helium atom. Theor Chim Acta, 69:181–223, 1986.
- [110] Donald C. Morton, Qixue Wu, and G. W. F. Drake. Energy levels for the stable isotopes of atomic helium ( $^4\text{he}$  i and  $^3\text{he}$  i). Can. J. Phys., 84(2):83–105, 2006.
- [111] R. B. Murphy, Y. Cao, M. D. Beachy, M. N. Ringnalda, and R. A. Friesner. Efficient pseudospectral methods for density functional calculations. J. Chem. Phys., 112(23):10131–10141, 2000.
- [112] Robert B. Murphy, Michael D. Beachy, Richard A. Friesner, and Murco N. Ringnalda. Pseudospectral localized moller–plesset methods: Theory and calculation of conformational energies. J. Chem. Phys., 103(4):1481–1490, 1995.
- [113] Christopher R. Myers, Cyrus J. Umrigar, James P. Sethna, and John D. Morgan. Fock’s expansion, kato’s cusp conditions, and the exponential ansatz. Phys. Rev. A, 44(9):5537–5546, Nov 1991.
- [114] Hiroyuki Nakashima and Hiroshi Nakatsuji. Solving the schr[ö]dinger equation for helium atom and its isoelectronic ions with the free iterative complement interaction (ici) method. J. Chem. Phys., 127(22):224104, 2007.
- [115] Hiroyuki Nakashima and Hiroshi Nakatsuji. Solving the electron-nuclear schrödinger equation of helium atom and its isoelectronic ions

- with the free iterative-complement-interaction method. J. Chem. Phys., 128(15):154107, 2008.
- [116] Krzysztof Pachucki. Quantum electrodynamics effects on singlet s-states of helium of order  $m\alpha^6$ . J. Phys. B, 31(16):3547, 1998.
- [117] Russell T Pack and W. Byers Brown. Cusp conditions for molecular wavefunctions. J. Chem. Phys., 45(2):556–559, 1966.
- [118] C. L. Pekeris. Ground state of two-electron atoms. Phys. Rev., 112(5):1649–1658, Dec 1958.
- [119] C. L. Pekeris.  $1s1$  and  $2s3$  states of helium. Phys. Rev., 115(5):1216–1221, Sep 1959.
- [120] C. L. Pekeris.  $1s^1$ ,  $2s^1$ , and  $2s^3$  states of  $h^-$  and of he. Phys. Rev., 126(4):1470–1476, May 1962.
- [121] Harald P. Pfeiffer. personal communication, April 2010.
- [122] Harald P. Pfeiffer, Lawrence E. Kidder, Mark A. Scheel, and Saul A. Teukolsky. A multidomain spectral method for solving elliptic equations. Comput. Phys. Commun., 152(3):253 – 273, 2003.
- [123] Yu. V. Popov and L. U. Ancarani. Rigorous mathematical study of the he bound states. Phys. Rev. A, 62(4):042702, Sep 2000.
- [124] William H. Press, Saul A. Teukolsky, William T. Vetterling, and Brian P. Flannery. Numerical Recipes: The Art of Scientific Computing. Cambridge University Press, 32 Avenue of the Americas, New York, NY 10013-2473, USA, third edition edition, 2007.
- [125] T. N. Rescigno, C. W. McCurdy, and V McKoy. Photoabsorption cross sections of two-electron atoms by the coordinate rotation method: Application to  $h^-$  and several states of he. J. Chem. Phys., 64(2):477, 1976.
- [126] T. N. Rescigno, C. W. McCurdy, A. E. Orel, and B. H. Lengsfeld, III. The complex kohn variational method. In W. M. Huo and F. Gianturco, editors, Computational Methods for Electron-Molecule Collisions, chapter 1. Plenum, New York, 1995.

- [127] Murco N. Ringnalda, Mahfoud Belhadj, and Richard A. Friesner. Pseudospectral hartree–fock theory: Applications and algorithmic improvements. J. Chem. Phys., 93(5):3397–3407, 1990.
- [128] D. V. I. Roginsky, M. Klapisch, and M. Cohen. Electric dipole oscillator strengths: length and velocity! Chem. Phys. Lett., 95(6):568 – 572, 1983.
- [129] S. Runge and A. Valance. Use of the atomic fues potential for the excited states of he: energies and oscillator strengths. Chem. Phys. Lett., 95(6):564 – 567, 1983.
- [130] Frank C. Sanders and Robert E. Knight. Oscillator strengths for s-p and p-d transitions for singly excited states of two-electron ions via z-dependent perturbation theory. Phys. Rev. A, 39(9):4387–4399, May 1989.
- [131] Frank C. Sanders and Charles W. Scherr. Perturbation study of some excited states of two-electron atoms. Phys. Rev., 181(1):84–97, May 1969.
- [132] B. Schiff, H. Lifson, C. L. Pekeris, and P. Rabinowitz.  $2p^{1,3}$ ,  $3p^{1,3}$ , and  $4p^{1,3}$  states of he and the  $2p^1$  state of  $li^+$ . Phys. Rev., 140(4A):A1104–A1121, Nov 1965.
- [133] B. Schiff, C. L. Pekeris, and Y. Accad.  $f$  values for transitions between the low-lying  $s$  and  $p$  states of the helium isoelectronic sequence up to  $z = 10$ . Phys. Rev. A, 4(3):885–893, Sep 1971.
- [134] B Schiff and CL Pekeris. Phys. Rev. A, 134(3A):A638, 1964.
- [135] C. Schwartz. Further Computations of the He Atom Ground State. ArXiv Mathematical Physics e-prints, May 2006.
- [136] Charles Schwartz. Lamb shift in the helium atom. Phys. Rev., 123(5):1700–1705, Sep 1961.
- [137] Charles Schwartz. Ground state of the helium atom. Phys. Rev., 128(3):1146–1148, Nov 1962.
- [138] Charles Schwartz. Fine structure of helium. Phys. Rev., 134(5A):A1181–A1187, Jun 1964.
- [139] Charles Schwartz. Experiment and theory in computations of the he atom ground state. Int. J. of Mod. Phys. E, 15(4):877–888, 2006.

- [140] H. M. Schwartz. Ritz-hylleraas solutions of the ground state of two-electron atoms involving fractional powers. Phys. Rev., 120(2):483–487, Oct 1960.
- [141] W. Schweizer, P. Fabinder, R. Gonzalez-Ferez, M. Braun, S. Kulla, and M. Stehle. Discrete variable and finite element techniques applied to simple atomic systems. J. Comput. Appl. Math., 109(1-2):95 – 122, 1999.
- [142] J. Sucher. Energy levels of the two-electron atom to order  $\alpha^3$  ry; ionization energy of helium. Phys. Rev., 109(3):1010–1011, Feb 1958.
- [143] Ajit J. Thakkar and Toshikatsu Koga. Variational calculations for helium-like ions using generalized kinoshita-type expansions. Theor. Chim. Acta, 109(1):36, Feb 2003.
- [144] Constantine E. Theodosiou. Transition probabilities for the helium singly excited states  $1snl^{1,3}l$  with  $n=2-21$  and  $l=0-5$ . Atom. Data and Nucl. Data Tab., 36(1):97–127, Jan 1987.
- [145] C. J. Umrigar, K. G. Wilson, and J. W. Wilkins. Optimized trial wave functions for quantum monte carlo calculations. Phys. Rev. Lett., 60(17):1719–1722, Apr 1988.
- [146] A. W. Weiss. J. Res. NBSS A, 71(163), 1967.
- [147] W. L. Wiese and J. R. Fuhr. Accurate atomic transition probabilities for hydrogen, helium, and lithium. J. Phys. Chem. Ref. Data, 38(4):564, Dec 2009.
- [148] W. L. Wiese, M. W. Smith, and B. M. Glennon. Atomic Transition Probabilities, volume 1. US Govt Printing Office, Washington, D.C., 1966.
- [149] W. L. Wiese, M. W. Smith, and B. M. Miles. Atomic Transition Probabilities, volume 2. US Govt Printing Office, Washington, D.C., 1969.
- [150] R. Wildt. Astrophys. J., 190:611, 1939.
- [151] N. W. Winter, Dennis Diestler, and Vincent McKoy. Numerical solution of the s-limit schr[ö]dinger equation. J. Chem. Phys., 48(5):1879–1882, 1968.

- [152] Inc. Wolfram Research. Mathematica, version 6.0. Wolfram Research, Inc., Champaign, Illinois, 2007.
- [153] Inc. Wolfram Research. Mathematica, version 7.0. Wolfram Research, Inc., Champaign, Illinois, 2008.
- [154] Zong-Chao Yan and G. W. F. Drake. High precision calculation of fine structure splittings in helium and he-like ions. Phys. Rev. Lett., 74(24):4791–4794, Jun 1995.
- [155] Binwei Yang. Study of two-electron systems in a radiation field using interparticle coordinates. PhD thesis, University of Southern California, Los Angeles, Dec. 1997.
- [156] Weiyang Zheng and Lung an Ying. Finite element approximations to the discrete spectrum of the schr[o-umlaut]dinger operator with the coulomb potential. SIAM J. Numer. Anal., 42(1):49–74, 2004.
- [157] Weiyang Zheng and Lung-An Ying. Finite-element calculations for the helium atom. Int. J. Quant. Chem., 97:659–669, 2004.